

Mechanism of Allosteric Regulation of Dnmt1's Processivity[†]Željko M. Svedružić[#] and Norbert O. Reich^{*}

Department of Chemistry and Biochemistry and Program in Biomolecular Science and Engineering, University of California, Santa Barbara, California 93106

Received May 26, 2005; Revised Manuscript Received August 11, 2005

ABSTRACT: We have analyzed the relationship between the allosteric regulation and processive catalysis of DNA methyltransferase 1 (Dnmt1). Processivity is described quantitatively in terms of turnover rate, DNA dissociation rate, and processivity probability. Our results provide further evidence that the active site and the allosteric sites on Dnmt1 can bind DNA independently. Dnmt1's processive catalysis on unmethylated DNA is partially inhibited when the allosteric site binds unmethylated DNA and fully inhibited when the allosteric site binds a single-stranded oligonucleotide inhibitor. The partial inhibition by unmethylated DNA is caused by a decrease in the turnover rate and an increase in the substrate DNA dissociation rate. Processive catalysis with premethylated DNA is not affected if the allosteric site is exposed to premethylated DNA but is fully inhibited if the allosteric site binds unmethylated DNA or poly(dA-dT). In sum, the occupancy of the allosteric site modulates the enzyme's commitment to catalysis, which reflects the nature of the substrate and the DNA bound at the allosteric site. Our *in vitro* results are consistent with the possibility that the processive action of Dnmt1 may be regulated *in vivo* by specific regulatory nucleic acids such as DNA, RNA, or poly(ADP-ribose).

Mammalian DNA methylation is an essential component of epigenetic chromatin reorganization processes that regulate gene silencing, oncogene activation, tumor suppressor inactivation, DNA repair, viral infection, early development, cell differentiation, and DNA recombination (1–3). Several mammalian DNA methyltransferases have been identified (4–6) yet remain poorly characterized due to their complex kinetic properties and exceptionally slow catalytic turnover rates (6–8). The large, 1620-residue DNA methyltransferase 1 (Dnmt1)¹ enzyme is the best characterized (7, 9–14) and is composed of a small C-terminal catalytic domain (residues 1102–1620) and a large regulatory domain (residues 1–1101) (10, 15, 16). The catalytic domain shows structural similarities with the small bacterial DNA cytosine methyltransferases, while the regulatory domain is in many aspects unique and less understood.

The sequence homology with pyrimidine methyltransferases indicates that the small catalytic domain includes the AdoMet binding domain and the active site (17). Inhibition by the mechanism-based inactivator 5-fluoro-cytosine (18)

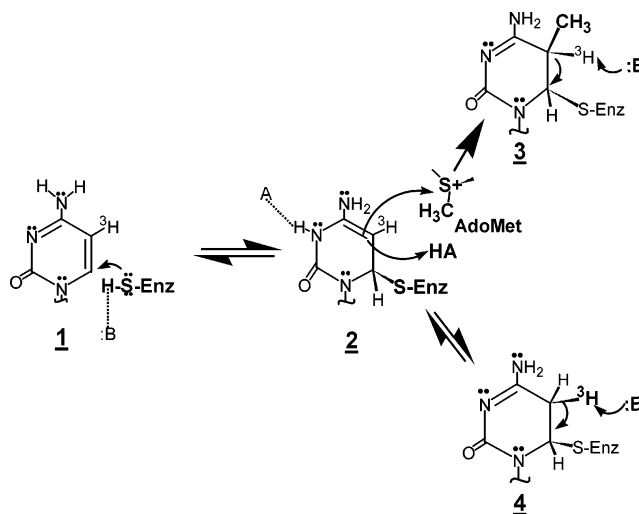


FIGURE 1: Enzyme activity assays for Dnmt1 (19). Methylation (as in Figure 8) is followed using radiolabeled AdoMet. A slight variation is the ³H release assay (as in Figures 3–7), where unlabeled AdoMet is used with DNA tritiated at the cytosine C⁵ position, and tritium release is followed (2 → 3). This allows the enzymes activity to be followed with labeled and unlabeled DNA mixtures (depicted in Figure 2 and given in Figures 4–7). The ³H exchange assay (2 → 4) is similar to the release assay but done without AdoMet or in the presence of AdoMet analogues; this separates product formation (5-methylcytosine) steps from the enzyme's attack onto the target base (1 → 2, see data in Figure 9).

and the ability to catalyze the exchange of the cytosine C⁵ hydrogen (19) suggest that Dnmt1 and other pyrimidine methyltransferases share a common catalytic mechanism (Figure 1 and ref 20). Dnmt1 activates the target base prior to the methyltransfer step by reversible formation of a covalent intermediate with the target base (Figure 1 and ref

[†] This work was supported by NIH GM56289 to N.O.R.

^{*} To whom correspondence should be addressed. Tel: 805-893-8368. FAX 805-893-4120. E-mail reich@chem.ucsb.edu.

[#] Current address: School of Molecular Biosciences, Department of Biophysics and Biochemistry, Washington State University, Pullman, WA 99164.

¹ Abbreviations: AdoMet, S-adenosyl-L-methionine; bp, base pair; C⁵, C², C⁴ etc., carbon five, carbon two, etc. of the target base; ^{5m}C, 5-methyl-2'-deoxycytosine; dCTP, deoxycytosine triphosphate; poly(dG-dC), double-stranded alternating polymer of deoxyguanine and deoxycytosine; dITP, deoxyinosine triphosphate; Dnmt1, DNA methyltransferase 1; *k*_{off}, rate constant for the enzyme–DNA dissociation; poly(dI-dC), double-stranded alternating polymer of deoxyinosine and deoxycytosine; pm-poly(dG-dC) or pm-poly(dI-dC), premethylated poly(dG-dC) or poly(dI-dC); sin, sinefungin.

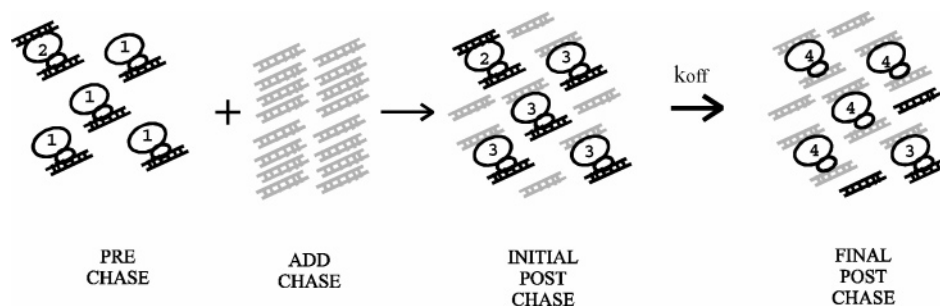


FIGURE 2: Schematic showing the chase experiments following tritium release. At the start of the chase experiments (PRE CHASE), the hot reaction is prepared by adding Dnmt1 (oval shapes) and ^3H -labeled DNA (black rail) in a concentration ratio that gives only a mild substrate inhibition (19). This ensures the presence of a mixture of Dnmt1 with only the active site occupied (1) and with both the active and allosteric sites occupied (2). The reaction is initiated by adding AdoMet, and the measured ^3H release rates derive from the combined activity of forms 1 and 2. The chase reaction is started after the first few turnovers by adding a large excess (n -fold) of unlabeled DNA (gray rail) to an aliquot of the labeled reaction mixture. Unlabeled DNA can have the same or different sequence than the substrate DNA. Adding an excess of unlabeled DNA results in the immediate occupancy of unoccupied DNA binding sites (transition between forms 1 \rightarrow 3, INITIAL POST CHASE). If Dnmt1 is processive, the turnover rates (k , eq 6) will be much faster than the dissociation rate constant for the labeled DNA (k_{off} , eq 6). Thus, the labeled DNA will stay bound at the active site through the subsequent turnovers and the ^3H release rates will reflect the combined catalytic activity from forms 2 and 3. If Dnmt1 is not processive, the dissociation rate for the labeled DNA at the active site (k_{off} , eq 6) is faster than the turnover rates (k , eq 6), and the labeled DNA will dissociate from the active site before the next turnover. Thus, the measured ^3H release rates will be only n th fraction of the original rates since most of the Dnmt1 molecules will be in ^3H exchange silent form (4, FINAL POST CHASE). Further details about the assay design are presented at the start of the results section.

20). Dnmt1 and the bacterial enzyme M•HhaI share catalytic intermediates, the rate-limiting step, and some key features that ensure stability of the activated target base (19).

The N-terminal regulatory domain is unique for Dnmt1. It contains part of a sequence that binds the methylation target site (21), an allosteric site that binds nucleic acids (10, 22), and sequence motifs that support interaction with other proteins (4, 23). There is also a phosphorylation site at Ser 514 (24) within the sequence that targets Dnmt1 to the DNA replication foci (25). Dnmt1 mutants lacking portions of the N-terminal regulatory domain show faster rates than the wild-type Dnmt1 with all DNA substrates (10). Thus, the N-terminal regulatory domain inhibits Dnmt1 activity, and the mechanism and extent of inhibition depend on DNA sequence, methylation state, and structure (10, 13, 26). Unmethylated DNA substrates show partial inhibition at higher substrate concentrations consistent with a gradual occupancy of the active site and allosteric site (13, 19). In contrast, no distinct inhibition is observed with premethylated substrates, which have at least one ^5mC positioned within the enzyme's footprint from the target cytosine (14, 19, 26). A GC-rich 30-nucleotide single-stranded sequence (13) fully inhibits Dnmt1 in vitro (K_i close to 30 nM) and DNA methylation in cells (13). Interestingly, the inhibitor's potency is 2 orders of magnitude lower if its single ^5mC site is replaced with cytosine (13). This methylation-dependent inhibition may be unique for *single-stranded* DNA because no such methylation-dependent enhancement of inhibition is observed with *double-stranded* DNA (7, 13, 19, 26). Dnmt1 function is modulated by RNA and DNA, both in vitro and in vivo, as first reported by Bolden and co-workers working with HeLa cell extracts (27). We made similar observations during the enzyme purification from MEL cells (28). Recent studies showed that noncoding RNA molecules regulate DNA methylation in human cells (29, 30) and other organisms (31). Dnmt1 binds RNA polymerase II in vivo (32) and interacts with several RNA binding proteins (33).

Recent results further implicate Dnmt1 in interactions involving multiple proteins and nucleic acids (34–39). A full understanding of how Dnmt1 and other mammalian DNA

cytosine methyltransferases determine and maintain the developmentally orchestrated patterns of DNA methylation demands that we understand the functional consequences of such higher order assemblies. The functional consequences of Dnmt1 forming ternary complexes involving its substrate DNA and a second nucleic acid bound at the allosteric site remain poorly understood (10, 13, 15, 22). We investigated DNA binding at the active site and allosteric site (Figure 2) by measuring Dnmt1 processivity on its DNA substrate (40). We show how DNA binding at the allosteric site partially or fully inhibits the enzyme, depending on the DNA molecules that are bound at the active site and the allosteric site.

MATERIALS AND METHODS

Materials. *S*-Adenosyl-L-[methyl ^3H] methionine (66–82 Ci/mmol or 5900–7200 cpm/pmol), deoxy[5- ^3H] cytidine 5' triphosphate (19.0 Ci/mmol) ammonium salt, and Sequenase 2.0 were purchased from Amersham Corp. Poly(dI-dC) (1960 bp), poly(dG-dC) (850 bp), dITP, and dCTP were purchased from Pharmacia Biotech. DTT, Trizma, sinefungin, and activated charcoal were purchased from Sigma Chemical Co. BSA was purchased from Roche (Indianapolis, IN). BSA did not cause Dnmt1 inhibition in the concentration range from 0.2 to 0.8 mg/mL. DE81 filters were purchased from Whatman, Inc. AdoMet (85% pure) was purchased from Sigma Chemical Co. Dnmt1 was prepared from mouse erythroleukemia cells as previously described (41), and protein concentration was determined using pre-steady-state burst measurements as previously described and a potent oligo inhibitor (13, 19). The single-stranded 30-base oligonucleotide inhibitor d(CTG GAT CCT TGC CC ^5mCG CC CCT TGA ATT CCC) was prepared by solid-phase synthesis as earlier described (13). The methylation sequence is underlined and shown in bold. The concentrations of AdoMet, sinefungin, poly(dI-dC), poly(dG-dC), and the oligonucleotide inhibitor were determined by the absorbance at 260 nm. The respective molar absorptivity coefficients are $15.0 \times 10^3 \text{ M}^{-1} \text{ cm}^{-1}$ for AdoMet and

sinefungin (Merck Index), $6.9 \times 10^3 \text{ M}^{-1} \text{ cm}^{-1}$ for poly(dI-dC) bp, $8.4 \times 10^3 \text{ M}^{-1} \text{ cm}^{-1}$ for poly(dG-dC) bp (Pharmacia technical information sheet).

Preparation of [^3H] Cytosine-poly(dG-dC) and Poly(dI-dC). ^3H -labeled substrates were prepared as earlier described (42). Briefly, the labeling reaction was prepared as 500 μM bp of poly(dI-dC) [or poly(dG-dC)] with 100 μM [^3H] dCTP, 1 mM dCTP, 10 mM dITP (or 1 mM dGTP) with 0.62 U/ μL of Sequenase 2.0 in 40 mM Tris/HCl (pH 7.5), 10 mM MgCl_2 , 50 mM NaCl, 10 mM DTT, and 1.0 mg/mL BSA. The labeling gives 13–40 cpm/pmol of base pairs for poly(dI-dC) and 60–105 cpm/pmol of base pairs for poly(dG-dC).

Preparation of Premethylated Poly(dG-dC) and Poly(dI-dC). The premethylated substrates were prepared with excess AdoMet and M·HhaI as earlier described (19). Briefly, M·HhaI (30–40 μM) and [methyl- ^{14}C] AdoMet (100 μM) were incubated with 300 μM bp DNA. The labeling reaction was run for only one or two turnovers (~ 1.0 min) to limit the number of methylated cytosines (^{14}C) to the number of initially bound M·HhaI molecules. The substrates prepared by this procedure contain an average of one ^{14}C every 7 to 20 bp, depending on the length of the labeling reaction and the ratio between total M·HhaI and DNA. All substrates prepared in this fashion showed a characteristic pre-steady-state burst (7, 19) and do not show allosteric inhibition (19, 26).

Preparation of [^3H] Cytosine Pm-poly(dG-dC) and Pm-poly(dI-dC). ^3H -labeled premethylated DNA was prepared from ^3H -labeled poly(dI-dC) and poly(dG-dC) using the procedure described for the preparation of unlabeled premethylated substrates.

Methylation Reactions. Incorporation of tritiated methyl groups into DNA was determined as previously described (7). Briefly, Dnmt1, DNA substrate, and radioactive AdoMet (15 μM) were incubated in 100 mM Tris/HCl (pH, 8.0), 10 mM EDTA, 10 mM DTT, and 0.5 mg/mL BSA at 37 °C. The enzyme and DNA concentrations are specific for each assay and described in the figure legends. The reaction was followed by placing reaction aliquots onto DE81 paper that was subsequently washed and dried.

Tritium Exchange Reactions. The tritium exchange reaction was followed essentially as previously described (42, 43). Briefly, tritium exchange is measured by quenching reaction aliquots in an acid suspension of activated charcoal (HCl, pH = 2.0–2.5). The enzyme concentration, DNA concentration, and cofactor concentration are specific for each assay and described in the figure legends. All reactions were saturated with the cofactor. The reaction buffer was 100 mM Tris/HCl (pH, 8.0), 10 mM EDTA, 10 mM DTT, and 0.5 mg/mL BSA.

Data Analysis. All processivity profiles were analyzed using nonlinear regression analysis according to eqs 5 or 8 using the Levenberg–Marquardt algorithm and the nonlinear regression package in *Mathematica* (Wolfram Inc.). All linear profiles were analyzed by linear least squares using the Microcal Origin program. The results were reported as the best fit values \pm standard error. Each experiment was repeated with different enzyme and substrate concentrations to test for the consistency in the observed phenomena; shown are representative examples.

RESULTS

Strategy using Chase Experiments in Studies of Processivity and Allosteric Regulation by Dnmt1 (Figures 1 and 2). In the chase experiments, Dnmt1 activity is measured in parallel in three different assays: *hot*, *dilute*, and *chase* (Figure 2). The hot reaction has only ^3H -labeled DNA (Figure 2). The dilute reaction is prepared by adding an n -fold excess (usually $n = 10$) of unlabeled DNA to the hot reaction aliquot with negligible changes in reaction volume. The hot and dilute reactions are started simultaneously by adding equal amounts of enzyme and the cofactor (Figure 2, prechase). The tritium release rate in the hot reaction is expected to be n -fold higher than in the dilute reaction because only a fraction (one n th) of DNA molecules in the dilute reaction are labeled. After the first few turnovers the chase reaction is prepared from the hot reaction aliquot by adding an n -fold excess of unlabeled DNA as in the dilute reaction (Figure 2) with negligible changes in the reaction volume. If the Dnmt1 is fully processive during the course of the measurements, adding an excess of unlabeled DNA will not affect the initial tritium release rates in the chase reaction relative to the hot reaction (Figure 2, initial post chase). If the enzyme is not processive, the tritium release rates in the chase reaction will be immediately identical to the release rates in the dilute reaction (Figure 2). For a partially processive enzyme (in which case after each turnover only a fraction of the enzyme molecules remain on the original substrate) the initial tritium release rates in the chase reaction will be between the tritium release rates for the hot and dilute reaction. The rate will gradually decrease with each turnover until the chase and dilute reactions become identical (Figure 2, final post chase). The unlabeled DNA used as the chase can be the same or different from the labeled DNA that is used as the original substrate. A combination of unlabeled and labeled DNA allows us to track which DNA binds at the active and allosteric sites (Figure 2, forms **1** \rightarrow **3**). The whole process can be described quantitatively (see appendix).

We used poly(dI-dC), poly(dG-dC), and different chase substrates (7, 10, 13, 14, 19, 22, 26, 44). Poly(dI-dC) and poly(dG-dC) substrates allow unambiguous quantitative analyses since every Dnmt1 molecule can bind the same sequence at the active site and the allosteric site (19). We previously showed that unmethylated poly(dI-dC) and poly(dG-dC) substrates have a maximum rate when 30–50 bp of DNA are present per Dnmt1 molecule (7, 13, 14, 19, 44), in which case Dnmt1 is mostly present in form **1** and partially present in form **2** (Figure 2 and ref 19). A combination of premethylated and unmethylated substrates is attractive since the two substrate forms differ in allosteric inhibition (19).

Chase Experiments with ^3H -Poly(dI-dC) as the Substrate and Unlabeled Poly(dI-dC) as the Chase (Figure 3, Table 1). Dnmt1 shows the highest catalytic rates with poly(dI-dC) substrates and allosteric inhibition (7, 9, 10, 13, 14, 26, 44) which greatly facilitates processivity measurements. In chase experiments, the ^3H release reaction (Figure 1) on labeled poly(dI-dC) was challenged by a saturating concentration of unlabeled poly(dI-dC) (19). The hot reaction had 181 nM Dnmt1 and 10 μM bp poly(dI-dC), or 55 bp per each Dnmt1 molecule. This molar ratio gives the highest rates with poly(dI-dC) substrates, with the majority of Dnmt1

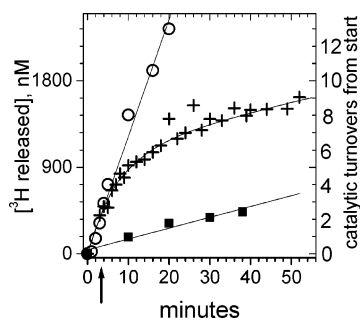


FIGURE 3: ^3H -poly(dI-dC) as the substrate and unlabeled poly(dI-dC) as the chase. The hot (O) reaction (10 μM bp ^3H -poly(dI-dC) (18 cpm/pmol) and 12.5 μM of unlabeled AdoMet) and the dilute reaction (■) were prepared from a hot reaction aliquot by adding 9-fold excess of unlabeled poly(dI-dC). Both reactions were started simultaneously by adding 181 nM Dnmt1. The chase reaction (+) was started 3 min later by mixing a hot reaction aliquot with 100 μM bp of unlabeled poly(dI-dC) (arrow). Reaction profiles were analyzed with eqs 6–8; the calculated values are summarized in Table 1.

Table 1: Processivity Rate Constants from Chase Experiments (Figures 3 and 4)^a

	poly(dI-dC) chase with poly(dI-dC)	pm-poly(dI-dC) chase with pm-poly(dI-dC)
k_{ss} , h^{-1}	3.6 ± 0.6	not measured
CI	[2.3, 4.8]	
Ccf, (k , k_{off})	(0.46, 0.88)	
k , h^{-1}	45 ± 2	205 ± 4
CI	[40, 49]	[198, 211]
ccf, (k_{ss} , k_{off})	(0.46, 0.82)	(0.955)
k_{off} , h^{-1}	7.8 ± 0.8	5 ± 0.4
CI	[6.0, 9.0]	[4.4, 6]
ccf, (k_{ss} , k)	(0.88, 0.47)	(0.955)
p (eq 6)	0.88	0.97
$n_{1/2}$ (eq 7)	5.5	22
hot reaction h^{-1}	43 ± 1.4	211 ± 8
dilute reaction h^{-1}	3.2 ± 0.3	25.4 ± 0.45

^a Best fit values for turnover rates (k), substrate dissociation rates (k_{off}), and late linear phase rates (k_{ss}) were determined using eq 6. The ability of the applied equation to resolve the best fit parameters is indicated by a narrow 2σ -confidence interval (CI) and low correlation coefficient between the rates i and j ($ccf_i(j)$). The processivity probability p was calculated according to eq 6. The “ $n_{1/2}$ ” values (eq 7) represent a number of processive steps for the given reaction before 50% of the enzyme is dissociated of the DNA.

molecules in form **1** (Figure 2) and a smaller fraction in form **2** (19). The hot reaction was started by adding unlabeled AdoMet and the chase reaction was started 3 min later by adding a 9-fold excess of unlabeled poly(dI-dC) to an aliquot of the hot reaction (arrow Figure 3). The tritium release rates in the chase reaction immediately following addition of an excess of unlabeled DNA are similar to the tritium release rates in the hot reaction (Figure 3). Thus, Dnmt1 is processive on poly(dI-dC) substrate when challenged with an excess of unmethylated poly(dI-dC) (Figure 2).

The chase profiles were analyzed numerically (Table 1) to calculate the turnover rate constant (k , eq 5), the substrate DNA off rate constant (k_{off} , eq 5), and the processivity probability (eqs 6 and 7, Table 1). On the basis of this, there is an 88% chance that at the end of each catalytic turnover the next catalytic turnover will be on the same DNA molecule (eq 6, Table 1). Thus, 50% of all Dnmt1 molecules catalyze at least 5.5 turnovers on the initially bound, labeled DNA substrate before the first dissociation (eq 7, Table 1, Figure

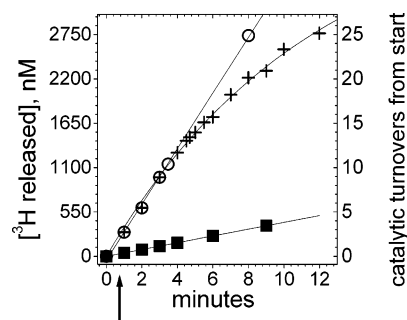


FIGURE 4: ^3H -pm-poly(dI-dC) as the substrate and unlabeled pm-poly(dI-dC) as the chase. The hot (O) reaction had 10 μM bp ^3H -pm-poly(dI-dC) (18 cpm/pmol) and ^5mC to C ratio was 1:15) and of unlabeled AdoMet (12.5 μM). Dilute reaction (■) was prepared from a hot reaction aliquot by adding 10-fold excess of unlabeled pm-poly(dI-dC). Both reactions were started simultaneously by adding 110 nM Dnmt1. The chase reaction (+) was started 1.5 min later by adding 100 μM bp of unlabeled pm-poly(dI-dC) in the hot reaction aliquot (arrow). Profiles were analyzed using eqs 5–7; the calculated values are summarized in the Table 1.

3). The calculated rate constants are consistent with the data. The figure shows that the tritium release rate in the chase reaction becomes equal to the tritium release rate in the dilute reaction at ~ 24 min. Thus, 21 min after adding unlabeled DNA almost all of the Dnmt1 molecules have dissociated from the original labeled DNA substrate (Figure 2, transition **3** \rightarrow **4**). The calculated half-life for dissociation of the labeled DNA from the active site is 5.3 min (Table 1), so 21 min corresponds to 4 half-lives or 94% of dissociation.

Chase Experiments with Premethylated ^3H -Poly(dI-dC) as the Substrate and Unlabeled Premethylated Poly(dI-dC) as the Chase (Figure 4, Table 1). Premethylated poly(dI-dC) (pm-poly(dI-dC)) has approximately one or two methylated cytosines per one Dnmt1 footprint on its DNA substrate (19). In comparison to unmethylated poly(dI-dC), premethylated poly(dI-dC) shows higher catalytic rates and no allosteric inhibition at high substrate concentration (19, 26). In the chase experiments with tritiated pm-poly(dI-dC) ($^5\text{mC}/\text{C} = 1/18$), a 10-fold excess of unlabeled pm-poly(dI-dC) ($^5\text{mC}/\text{C} = 1/15$) was added as the chase 3 min after the start of the hot reaction (Figure 3B, arrow). The tritium release rates in the chase reaction immediately following addition of unlabeled pm-poly(dI-dC) are similar to the release rates in the hot reaction (Figure 4). Thus, Dnmt1 is processive on pm-poly(dI-dC) substrate when challenged with an excess of pm-poly(dI-dC). By numerical analysis, each catalytic turnover is followed by another turnover on the same substrate with a 95% probability and 22.8 turnovers occur before 50% of all enzyme molecules dissociate from the original substrate (eqs 5–7 and Tables 1 and 2). This high level of processivity results in the release rates never reaching the rates that were observed in the control dilute reaction. In summary, Dnmt1 is processive on pm-(dI-dC) substrate when challenged by an excess of unlabeled pm-poly(dI-dC) substrate. Also Dnmt1 is more processive on pm-poly(dI-dC) relative to poly(dI-dC) (Table 2).

Processivity Analysis with Tritiated Poly(dI-dC) as the Substrate and Unlabeled Single-Stranded Oligonucleotide Inhibitor as the Chase (Figure 5). A previously identified GC-rich 30-base-long, single-stranded oligonucleotide with a single 5-methylcytosine acts as a potent inhibitor of Dnmt1

Table 2: Processivity Rate Constants for Methylation and Exchange with Poly(dI-dC) and Poly(dG-dC) (Figures 8 and 9)

A. Methylation and ^3H Exchange Reaction with Poly(dI-dC) and Pm-poly(dI-dC)				
	methylation with poly(dI-dC)	methylation with pm-poly(dI-dC)	methylation at high poly(dI-dC)	^3H exchange with sinefungin (Figure 4B)
k_{ss} , h^{-1}	6.0 ± 0.8	4.2 ± 0.4	4.2 ± 0.24	21 ± 2
CI	[4.2, 7.8]	[3.2, 5.1]	[3.7, 4.2]	[17.4, 25]
ccf (k , k_{off})	(0.14, 0.92)	(0.41, 0.87)	(0.59, 0.71)	(0.38, 0.88)
k , h^{-1}	29 ± 1	47 ± 2	20 ± 3	50 ± 5
CI	[26, 31]	[43, 50]	[19, 21]	[40, 60]
ccf (k_{ss} , k_{off})	(0.14, 0.48)	(0.41, 0.78)	(0.59, 0.84)	(0.38, 0.73)
k_{off} , h^{-1}	1.6 ± 0.2	2.8 ± 0.2	7.2 ± 0.8	2.9 ± 0.7
CI	[1.1, 2.2]	[2.3, 3.3]	[4.1, 7.7]	[1.4, 4.4]
ccf (k_{ss} , k)	(0.92, 0.48)	(0.87, 0.78)	(0.71, 0.84)	(0.88, 0.73)
p (eq 6)	0.96	0.94	0.74	0.95
$n_{1/2}$ (eq 7)	17	11	2	14

B. Methylation and ^3H Exchange Reaction with Pm-poly(dG-dC)		
	methylation with pm-poly(dG-dC) (Figure 8B)	exchange with sinefungin and pm-poly(dG-dC) (Figure 9 inset)
k_{ss} , h^{-1}	0.018 ± 0.010	0.2 ± 0.1
CI	[0.001, 0.022]	[0.45, 0.05]
ccf (k , k_{off})	(0.33, 0.87)	(0.06, 0.91)
k , h^{-1}	7 ± 0.2	10.5 ± 0.2
CI	[6.6, 7.2]	[10.07, 10.9]
ccf (k_{ss} , k_{off})	(0.33, 0.74)	(0.06, 0.44)
k_{off} , h^{-1}	3 ± 0.2	4.6 ± 0.3
CI	[2.4, 3.2]	[4.1, 5.5]
ccf (k_{ss} , k)	(0.87, 0.74)	(0.91, 0.44)
p (eq 6)	0.70	0.69
$n_{1/2}$ (eq 7)	1.9	1.87

^a Best fit values for turnover rates (k), substrate dissociation rates (k_{off}), and late linear rates (k_{ss}) as indicated in the text (eq 5). All rates are given as the best fit value \pm asymptotic standard error. The ability of applied equation to resolve the best fit parameters is indicated by a narrow 2 σ -confidence interval (CI) and low correlation coefficient between the rates i and j ($ccf(i,j)$). The processivity probability p was calculated according to eq 6. The " $n_{1/2}$ " values (eq 7) represent a number of processive steps for the given reaction before 50% of the enzyme is dissociated of the substrate DNA.

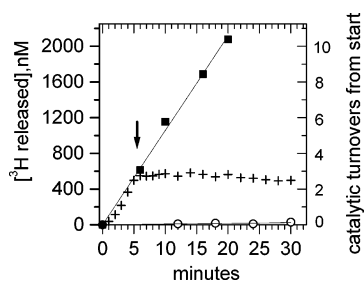


FIGURE 5: ^3H -poly(dI-dC) as the substrate and single-stranded oligo inhibitor as the chase. The hot (\blacksquare) reaction had $10 \mu\text{M}$ bp ^3H -poly(dI-dC) and $12.5 \mu\text{M}$ AdoMet and 200 nM Dnmt1. Dilute reaction (\circ) was started 5 min after the hot reaction by adding 250 nM of the single-stranded inhibitor. The chase reaction (+) was started 5 min after the hot and dilute reactions by adding 250 nM of the oligo inhibitor in a hot reaction aliquot. Measured ^3H release rate constants are $46 \pm 0.8 \text{ h}^{-1}$ for the hot reaction, while the dilute reaction was at the background level. The chase reaction profile clearly shows complete Dnmt1 inhibition immediately following addition of the oligo inhibitor.

($K_i \sim 30 \text{ nM}$), and DNA methylation in vivo (13). This inhibitor appears to bind to the allosteric site through the formation of an inhibitory ternary complex (enzyme/substrate/inhibitor) (13). Here we used chase experiments to further define this inhibitor's mechanism of action. The hot reaction was prepared using 200 nM Dnmt1 and $10 \mu\text{M}$ bp tritiated poly(dI-dC), or 50 bp per one Dnmt1 molecule, in which case Dnmt1 is largely in form 1 (Figure 2), and a small fraction is in form 2 (Figure 2). The hot reaction was started by adding unlabeled AdoMet ($12.5 \mu\text{M}$), and 5 min later

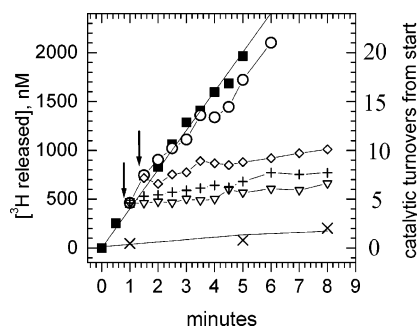


FIGURE 6: ^3H -pm-poly(dI-dC) as the substrate and unlabeled poly(dI-dC), poly(dG-dC), pm-poly(dG-dC), and poly(dA-dT) as the chase. The hot (\blacksquare) reaction had $10 \mu\text{M}$ bp ^3H -pm-poly(dI-dC), $12.5 \mu\text{M}$ AdoMet, and 90 nM Dnmt1. The chase reaction was started 1 to 1.5 min after the hot reaction by adding to a hot reaction aliquot: $100 \mu\text{M}$ bp of cold poly(dI-dC) (∇), $100 \mu\text{M}$ bp of cold poly(dG-dC) (+), $100 \mu\text{M}$ bp of cold poly(dA-dT) (\diamond), or $100 \mu\text{M}$ bp of pm-poly(dG-dC) (\circ). For clarity, only the dilute reaction (\times) with poly(dI-dC) is shown.

(arrow Figure 5), the chase reaction was started by adding a saturating concentration (250 nM) of the inhibitor as the chase. Interestingly, adding the inhibitor led to the immediate cessation of catalysis (Figure 6), in contrast to the delayed impact observed with excess poly(dI-dC) as the chase (Figure 3). This instant inhibition of processive catalysis must be caused by the formation of the ternary complex (enzyme/substrate/inhibitor) (Figure 2, form 3), since Dnmt1 is processive on poly(dI-dC) substrate (Figure 3, Table 1, $k_{off} = 7.8 \pm 0.8 \text{ h}^{-1}$) and its active site is not readily available

for interaction with DNA that was added as the chase (Figure 2., transition **1** → **4**).

In summary, we found that the allosteric site on Dnmt1 can bind a second DNA molecule when the active site is involved in processive catalysis (Figure 2, transition **1** → **3**). The difference between the chase reaction with poly(dI-dC) (Figure 3) and inhibitor (Figure 5) indicates how different DNA molecules can lead to full or partial inhibition of catalytic activity. Finally, the chase experiments confirm the original proposal (13) that the potent Dnmt1 inhibitor binds allosterically through the formation of a ternary complex (enzyme/substrate/inhibitor) (Figure 2, form **3**).

Processivity Analysis with ³H-pm-poly(dI-dC) as the Substrate and Unlabeled Poly(dI-dC), Poly(dG-dC), Pm-poly(dG-dC), and Poly(dA-dT) as the Chase (Figure 6). We used chase experiments to test how unmethylated DNA affects the catalytic activity on premethylated DNA. In comparison to premethylated DNA, unmethylated DNA led to Dnmt1 inhibition at the high substrate concentration that is associated with allosteric site (7, 10, 13, 14, 19, 22, 26, 44). Here we use the chase experiments to analyze how saturation with unmethylated poly(dG-dC), poly(dI-dC), and premethylated poly(dG-dC) impact Dnmt1's processive catalysis with pm-poly(dI-dC) (Figure 6). Since Dnmt1 is processive with ³H-pm-poly(dI-dC) (Figure 4, Table 1, $k_{off} = 5 \pm 0.4 \text{ h}^{-1}$), its active site is not readily accessible for interaction with chase molecules.

The hot reaction was prepared by incubating 90 nM Dnmt1 with 10 μM bp ³H-pm-poly(dI-dC) (110 bp per each Dnmt1 molecule); thus, there is an excess of ³H-pm-poly(dI-dC) relative to Dnmt1 (Figure 2), and both the active and the allosteric sites have access to DNA (Figure 2, form **2**) (19). Hot and dilute reactions were started simultaneously by adding unlabeled AdoMet (12.5 μM). The chase reaction was initiated 30–45 s after the start of the hot reaction by adding 100 μM bp poly(dI-dC), poly(dG-dC), or pm-poly(dG-dC) to separate aliquots of the hot reaction. The slope of the chase reaction immediately following the addition of unlabeled poly(dI-dC) and poly(dG-dC) is identical to the slope in dilute reaction (Figure 3B). Thus, by forming a heterocomplex (Figure 2, form **3**) unmethylated poly(dI-dC) interrupts processive catalysis on premethylated ³H-poly(dI-dC) but not on unmethylated ³H-poly(dI-dC) (Figure 3). In contrast, premethylated poly(dG-dC) and poly(dI-dC) do not interrupt processive catalysis on ³H-pm-poly(dI-dC) (Figures 4 and 6).

A recent study showed that Dnmt1 is inhibited by poly(ADP-ribose) in vivo as a part of the poly(ADP-ribose)-polymerase-1 (PARP-1) response to DNA damage (45). This provides a plausible explanation for the previous surprising observation that Dnmt1 is inhibited by poly(dA)-poly(dT) and poly(dA-dT) (27). In Figure 6, we show that saturation with poly(dA-dT) stops Dnmt1's processive catalysis on pm-poly(dI-dC) by binding at the allosteric site (Figure 2., transition **1** → **3**).

Chase Experiments with Premethylated ³H-poly(dG-dC) as the Substrate and Unlabeled Premethylated Poly(dG-dC) as the Chase (Figure 7, Table 1). Dnmt1 has exceptionally slow catalytic rates with DNA molecules that have CpG target sites (19). We wanted to analyze how slow turnover rates are affected by Dnmt1–DNA interactions. With pm-poly(dG-dC), the hot reaction was prepared as ³H-pm-

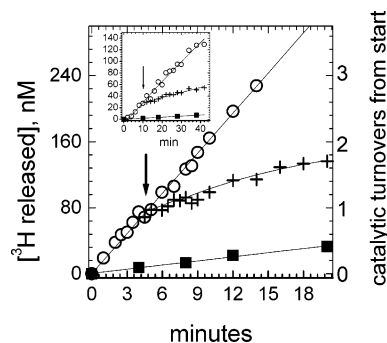


FIGURE 7: ³H-pm-poly(dG-dC) as the substrate and unlabeled pm-poly(dG-dC) as the chase. Inset, ³H-poly(dG-dC) as substrate and unlabeled poly(dG-dC) as the chase. The hot (O) reaction had 10 μM bp ³H-pm-poly(dG-dC) and 12.5 μM of unlabeled AdoMet. Dilute reaction (■) was prepared from a hot reaction aliquot by adding 10-fold excess of unlabeled pm-poly(dG-dC). Both reactions were started simultaneously by adding 85 nM Dnmt1. The chase reaction (+) was started at the start of the second turnover (5 min) by adding 80 μM bp of cold pm-poly(dG-dC) to an aliquot of the hot reaction. The inset shows a chase experiment with ³H-poly(dG-dC) as substrate and cold poly(dG-dC) as the chase. The hot reaction (O) was prepared as 8 μM bp of ³H-GdC (102 cpm/pmol), 15 μM of unlabeled AdoMet, and 200 nM Dnmt1. Dilute reaction (■) was prepared from a hot reaction aliquot by adding 10-fold excess of unlabeled pm-poly(dG-dC). The chase reaction (+) was started 15 min after the start of the hot reaction arrow by adding 80 μM bp of cold poly(dG-dC) to the hot reaction aliquot.

poly(dG-dC) (8 μM bp, 88 cpm/pmol, ratio ^{5m}C:C 1 to 14). The dilute reaction was prepared from a hot reaction aliquot by adding unlabeled pm-poly(dG-dC) (80 μM bp, ratio ^{5m}C:C 1 to 12). Both reactions were started simultaneously by adding Dnmt1 (85 nM) and 15 μM of unlabeled AdoMet. The hot and dilute reaction profiles were analyzed using a linear equation and the best fit rates were $11.3 \pm 0.8 \text{ h}^{-1}$ and $1.0 \pm 0.04 \text{ h}^{-1}$, respectively. The chase reaction was started 5 min later (approximately at the end of the first turnover) by mixing a hot reaction aliquot with 80 μM of unlabeled pm-poly(dG-dC). The slow rates with the two poly(dG-dC) substrates preclude measuring of Dnmt1 processivity in multiple turnovers as with poly(dI-dC) substrates.

The decay in tritium release following the addition of the unlabeled chase was analyzed using the exponential decay equation ($[^3\text{H released}] = A(1 - e^{-kt}) + pt$); The tritium release rate constant (k) immediately following the start of the chase reaction is equal to $5 \pm 0.9 \text{ h}^{-1}$. The ratio between the initial chase and dilute rates is about 46% of the ratio between hot and dilute rates (Table 2B). Thus, addition of the unlabeled chase results in ~46% retention of Dnmt1 on the original labeled DNA (Figure 2, transition **1** → **3**). The lower processivity with pm-poly(dG-dC) relative to pm-poly(dI-dC) can be attributed to lower turnover rates (eq 6), rather than the difference in DNA binding at the allosteric site, because pm-poly(dG-dC) cannot displace Dnmt1 in processive catalysis on pm-poly(dI-dC) (Figure 6).

Dnmt1 catalytic rates with poly(dG-dC) (inset, Figure 7) are even slower than with pm-poly(dG-dC) and consistent with rates measured with other unmethylated substrates (7, 9, 11, 44). It takes about an hour to finish the first turnover and about 3–4 h to finish the second turnover. Thus, we used the chase experiments to analyze the enzyme's commitment for a given DNA substrate during its slow first catalytic turnover (Figure 2). The hot reaction was prepared

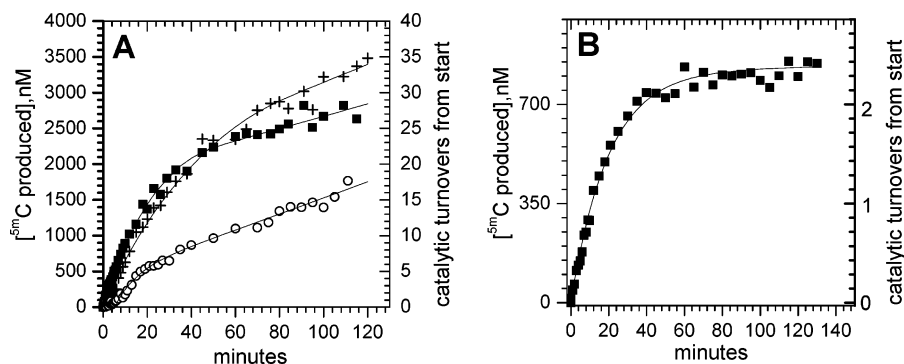


FIGURE 8: (A, B) Dnmt1 methylation reaction with poly(dI-dC) (A, 12 μ M and 260 μ M), pm-poly(dI-dC), and methylation reaction with pm-poly(dG-dC) (B). (A) Dnmt1 methylation reaction with 12 μ M bp (+) poly(dI-dC), 260 μ M bp (O) poly(dI-dC), and 12 μ M pm-poly(dI-dC) (■). All three assays had 125 nM Dnmt1 and 12.5 μ M [3 H methyl] AdoMet (6750 cpm/pmol). All profiles were analyzed using eqs 8, 6, and 7 (Table 2A). Both poly(dI-dC) and pm-poly(dI-dC) were 1960-bp-long, pm-poly(dI-dC) with one in eight cytosines methylated. (B) Analysis of processivity in Dnmt1 (300 nM) methylation reaction with 12 μ M bp (■) pm-poly(dG-dC) and 12.5 μ M [3 H methyl] AdoMet (6750 cpm/pmol). The profile was analyzed using eqs 8, 6, and 7 (Table 2B).

using 8 μ M bp of 3 H-poly(dG-dC) (102 cpm/pmol), 15 μ M of unlabeled AdoMet, and 200 nM Dnmt1 (40 bp per one Dnmt1 molecule). The dilute reaction was prepared from the hot reaction aliquot by adding 144 μ M bp of unlabeled poly(dG-dC). The chase reaction was started 15 min after the start of the hot reaction (at the end of the initial lag; 19) by adding 144 μ M bp of unlabeled poly(dG-dC) to a hot reaction aliquot. The best fit rate constant was 1 ± 0.11 h $^{-1}$ for the hot reaction, 0.06 ± 0.005 h $^{-1}$ for the dilute reaction, and 0.27 ± 0.003 h $^{-1}$ for the chase reaction. The ratio between the chase and dilute reaction rates is 25% of the ratio between the rates measured in the hot and dilute reactions. Thus, at least 75% of the initially bound Dnmt1 can be readily displaced from the poly(dG-dC) (Figure 2, transition 3 \rightarrow 4). This indicates that during the slow turnover the majority of Dnmt1 molecules are not committed to the initially bound substrate (19). This is consistent with our earlier study which showed that slow turnover with unmethylated substrates can be attributed to slow formation of early reaction intermediates leading to target base attack (19). Interestingly, the chase experiments showed that Dnmt1 can be readily displaced from poly(dG-dC) substrates but not from poly(dI-dC) substrates, in contrast to the bacterial enzyme M·HhaI (42).

Dnmt1 Processivity Analysis by Following Methylation (Figure 8 A,B and Figure 9). Dnmt1 reactions often show a gradual decrease in the initial linear profile followed by the late linear phase, as seen in the methylation reaction with poly(dI-dC), pm-poly(dI-dC) (Figure 8A), pm-poly(dG-dC) (Figure 8B), and in the 3 H exchange reaction (Figure 1) with sinefungin and poly(dI-dC) or pm-poly(dG-dC) (Figure 9). Interestingly, the high substrate concentrations that lead to allosteric inhibition also lead to changes in this biphasic profile (Figure 8A). We suggest that this biphasic reaction profile is caused by Dnmt1's processivity. Alternative explanations such as product inhibition, substrate depletion, or enzyme instability with time are unlikely. The observed biphasic profiles (Figures 8 and 9) cannot be attributed to products of the methylation reaction 5 mC or AdoHcy since we observe similar profiles when following the exchange reaction with sinefungin (Figure 9). The exchange reaction has no "chemical" product; the reaction is only replacing 3 H with H at the cytosine carbon 5 (Figure 1). Also, the reaction at high poly(dI-dC) concentration shows an early

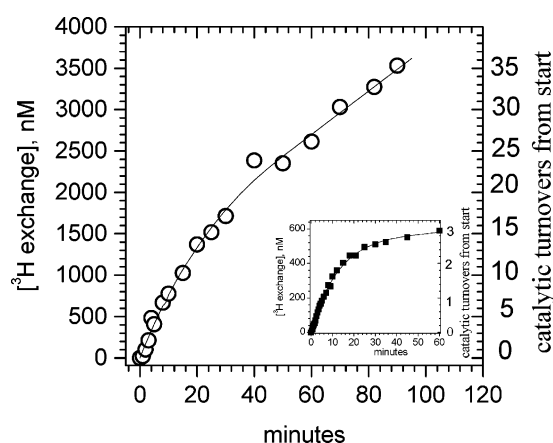


FIGURE 9: 3 H exchange reaction with sinefungin and 3 H-poly(dI-dC) and 3 H-pm-poly(dG-dC) (inset). 3 H exchange reaction (O) with 95 nM Dnmt1 20 μ M sinefungin and 10 μ M bp of 3 H-poly(dI-dC) (18 cpm/pmol). The inset shows processivity profiles with sinefungin and 3 H-pm-poly(dG-dC) (106 cpm/pmol), using 70 nM Dnmt1. The reaction profiles were analyzed using eqs 8, 6, and 7, and the calculated values are given in the Table 2.

transition to the late linear phase even though less product is being generated. The biphasic reaction profiles are also not due to substrate depletion since the late linear profile is observed earlier at the higher concentration of poly(dI-dC). Finally, the biphasic reaction profiles are not due to enzyme instability since all reactions were measured in the same conditions (often in parallel) and the shape of each reaction profile depends on the substrate type and the substrate concentration.

We suggest that Dnmt1's processive catalysis accounts for the biphasic reaction profiles (Figures 8 and 9). Processive catalysis requires that the dissociation rate for the substrate DNA is slower than the turnover rate (see appendix). These conditions are well-known to lead to a pre-steady-state burst with DNA substrates that have only one methylation site (7). However, with substrates that have multiple methylation sites, only a fraction of substrate DNA will dissociate after each turnover during processive catalysis. All enzyme molecules will be initially DNA bound at the start of the first turnover. Since the enzyme is not 100% processive, at the start of the second turnover a fraction of enzyme molecules will go through a slow dissociation step, while the rest will go directly to the next turnover on the same

DNA. With each subsequent turnover, this partitioning results in a gradual rate decrease that is proportional to the fraction of enzyme molecules which enter the slow dissociation step. The partitioning is repeated with each turnover until the catalytic contribution from enzyme molecules retained on the initial DNA is equal to the catalytic contribution from enzyme molecules that are reassociating. At that point a quasi steady state is established, and the reaction profile shows the late linear phase. Consistent with this scenario, pm-poly(dG-dC) shows both poor processivity (Figure 7) and an earlier onset of the late linear phase than poly(dI-dC) and pm-poly(dI-dC) (Figures 3 and 4).

We have analyzed these biphasic reaction profiles numerically to calculate the turnover rate constant k (eq 5, Table 2), the Dnmt1–DNA off rate constant k_{off} (eq 5, Table 2), and the processivity probability (eqs 6 and 7, Table 2). We find that the allosteric inhibition by excess unmethylated poly(dI-dC) (Figure 8A) is caused by a decrease in processivity (Table 2) as a result of an increase in the Dnmt1–DNA off rate constant (Table 2) and a decrease in the catalytic rate constant (Table 2). When Dnmt1 is partially saturated with poly(dI-dC) and substrate inhibition is not present to the full extent, poly(dI-dC) and pm-poly(dI-dC) show similar processivity probabilities (Table 2, eq 6). This similarity is a result of a compensatory difference in the turnover rates (k) and off rates (Table 2). The calculated turnover constants (k , Table 2) from the processivity measurements in the methylation reaction are lower than the turnover constants calculated from the chase processivity experiments (k , Table 1). The difference is due to the earlier described (19) discrepancy between ^3H release and methylation rates with poly(dI-dC) substrates. The calculated processivity in the methylation reaction (Table 2 and Figure 8A) and in the exchange reaction with sinefungin (Table 2, Figure 9) are similar due to similar turnover rates. Also, due to slower turnover rates, pm-poly(dG-dC) substrates show less processivity in methylation (Figure 8B) and the exchange reaction (Figure 9, inset) relative to poly(dI-dC) and pm-poly(dI-dC) substrates.

DISCUSSION

Dnmt1 has at least two DNA binding sites, the active site and the allosteric site (10). Here we use chase experiments (Figure 2) to study the ternary complexes between Dnmt1 and DNA bound at the active and the allosteric sites. In chase experiments an ongoing ^3H release/exchange reaction (Figure 1) on a ^3H -labeled DNA is challenged with an excess of unlabeled DNA (Figure 2), allowing the tracking of which DNA molecule acts as a substrate and which acts as an allosteric regulator (Figure 2, transition $\mathbf{1} \rightarrow \mathbf{3} \rightarrow \mathbf{4}$). The chase experiments (Figures 6 and 7) support proposals (13) that the two sites on Dnmt1 can independently bind two different DNA molecules (trans mechanism) (Figure 10). Alternatively, DNA binding at the active site directly leads to binding of adjacent DNA sites at the allosteric site (cis mechanism). We also show that the allosteric site is open for interaction with different DNA molecules that can regulate the ongoing catalytic activity at the active site (Figures 5 and 6). Our results provide a basis for understanding how DNA sequence, methylation status, and structure regulate Dnmt1's allosteric inhibition and processive catalysis. In the next few paragraphs, we integrate results from

this study with the results from other Dnmt1 studies to provide our current view of allosteric regulation of Dnmt1 (Figure 10B).

The partial inhibition observed with excess unmethylated DNA is often shown in the literature (9, 13, 19, 22, 44). Here we show such inhibition can be due to a decrease in the turnover rate constant and an increase in the substrate DNA off rate (Table 2), both of which can lead to lower processivity (eq 6 and Figure 8A). Interestingly, Dnmt1 undergoes a slow conformational change from an inactive to active form at the start of catalysis on unmethylated DNA (Figure 10B), which can be triggered by cofactor binding and possibly by DNA release from the allosteric site (19).

Studies of a Dnmt1 mutant lacking the functional N terminal domain indicate that some form of allosteric inhibition is present even with premethylated substrates (10). However, there is no evidence that such inhibition results from DNA binding at both the active and the allosteric sites (13, 19, 26, 44). Here we show that unmethylated DNA, but not premethylated DNA, interferes with processive catalysis on premethylated DNA (Figures 4 and 6). This observation may help explain why previous studies showed that Dnmt1 is not self-activated by ^5mC produced during the initial stages of methylation (19). The higher methylation rates with premethylated DNA are only observed in the absence of significant stretches of unmethylated DNA which can cause allosteric inhibition (Figure 10B). Such conditions are seen when at least one methylcytosine lies within one enzyme footprint, independent of the distance between the methylcytosine and the target cytosine (11, 19). Allosteric activation with premethylated substrates is unlikely (19).

We previously described a GC-rich single-stranded oligonucleotide with one ^5mC site as a potent Dnmt1 inhibitor ($K_i \sim 30$ nM), which binds at the allosteric site and reverses DNA methylation in cells (13). We found that the single-stranded oligo inhibitor completely stops the ongoing processive catalysis on unmethylated DNA (Figure 5). This is in contrast to double-stranded unmethylated poly(dI-dC) and poly(dG-dC), which show only a partial inhibition of enzyme activity (13, 26, 44) and processive catalysis in the same conditions (Figure 8A). Interestingly, in contrast to double-stranded DNA, preexisting methylation leads to more potent inhibition with the single-stranded DNA inhibitor (13).

Dnmt1 functions within replication forks (23, 37, 39, 46) and chromatin remodeling complexes (47). Dnmt1 interactions with other proteins may affect its processivity by altering its turnover rate and substrate DNA off rate (eq 6). It seems likely that the two independent DNA binding sites on Dnmt1 and the mechanism present in Figure 10 are also present in vivo. Although which regulatory sequences might bind the allosteric site in vivo are currently unknown, mounting evidence indicates that DNA methylation can be controlled by noncoding RNA molecules (27–31) and poly(ADP-ribose) (45). Twenty years ago, Bolden and co-workers suggested that RNA could regulate Dnmt1 and DNA methylation in vivo (27). The authors found that Dnmt1 is inhibited in HeLa cells extract by RNA; further, the inhibition potency depends on the sequence, including the surprising discovery that Dnmt1 is inhibited by poly(dA)-poly(dT) and poly(dA-dT). Subsequent studies also reported Dnmt1 inhibition by RNA molecules (28) and showed that Dnmt1 interacts with RNA polymerase II in vivo (32) and with several RNA

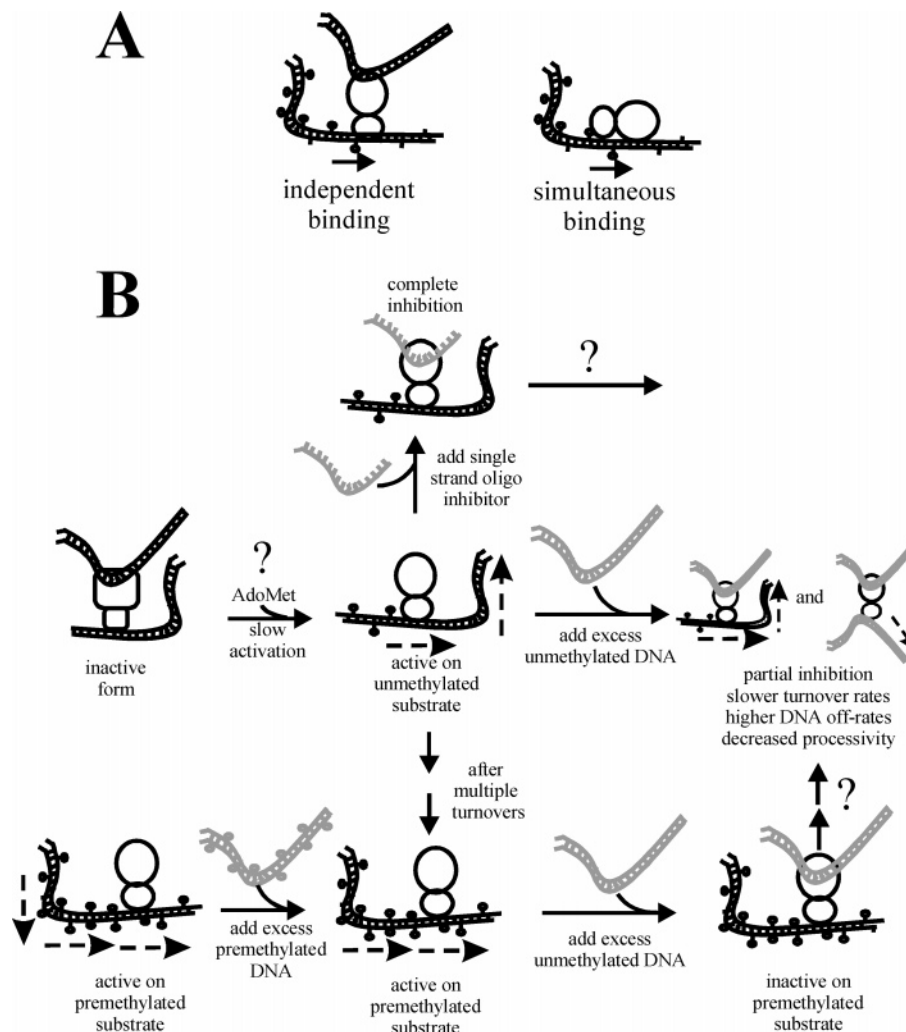


FIGURE 10: (A, B) Allosteric regulation of Dnmt1 (ovals, small catalytic domain and the large regulatory domain) with different DNA molecules. (A) Two modes for allosteric regulation of Dnmt1, DNA binding at the active site leads directly to binding of the adjacent DNA sites at the allosteric site (cis binding), or the active site and the allosteric site can bind DNA independently (trans binding). (B) With unmethylated DNA, DNA binding at the allosteric site can cause slow transition from the inactive to the active form following AdoMet binding and the start of catalysis (19). During the catalytic cycle, the active site can be involved in catalysis, while the allosteric site is accessible to bind “regulatory” DNA. Binding of the single-stranded DNA inhibitor (13) leads to a complete inhibition, and binding of unmethylated DNA results in higher off rates, lower turnover rates, and ultimately lower processivity. With pre-methylated DNA substrates, binding of pre-methylated DNA at the allosteric site does not alter the enzyme’s activity, while binding of unmethylated DNA leads to a stop in catalytic activity. The question marks indicate steps for which the mechanism is not fully understood.

binding proteins (33). These RNA molecules are likely to modulate or completely inhibit the catalytic activity of Dnmt1 by binding at the allosteric site and by forming a ternary complex (Figure 10B). Such inhibition could depend on RNA sequence, methylation, and structure (i.e., double stranded vs single stranded) as suggested in Figure 10B.

In general, Dnmt1’s processivity is determined by its catalytic turnover rate and dissociation rate from the DNA (see appendix, eq 6). Thus, lower turnover rates can account for lower processivity with poly(dG-dC) relative to poly(dI-dC) or lower processivity with unmethylated DNA relative to pre-methylated DNA. Because the rates with poly(dG-dC) are similar to the rates measured with other unmethylated substrates with CG target sites (9, 19, 40, 44), we suggest that previous reports on the lack of processivity with unmethylated DNA substrates can be attributed to the slow turnover rates and a lack of multiple turnovers (40, 48). The catalytic rates measured with pm-poly(dG-dC) are also comparable to the catalytic rates measured with other

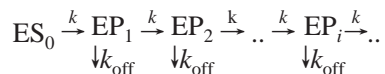
pre-methylated substrates with CG target sites (9, 19, 40, 44). However, despite similar rates, different pre-methylated substrates show different catalytic features (9, 10, 40), which in part could depend on the methylation pattern and the sequence surrounding the target site. Such differences account for the differences in processivity between different pre-methylated substrates (40) including pm-poly(dG-dC) (19).

ACKNOWLEDGMENT

We wish to thank Mr. Jamie Witham for help with these measurements. We are grateful to Dr. D. J. T. Porter from Glaxco Wellcome for his generous advice in deriving the processivity equation. We are grateful to Dr. Jim Flynn for his expert advice and excellent discussions. Thanks to Dr. Peter Vollmayr and Dr. Ana M. Ojeda for their efforts in purification of Dnmt1. We are grateful to R. August Estabrook and Dr. Matthew Purdy for their insightful comments on the text of the manuscript.

APPENDIX: ANALYTICAL DESCRIPTION OF PROGRESSIVE CATALYSIS BY DNA METHYLTRANSFERASES

Analysis of Processivity Data. The mathematical model is an adaptation of similar models used to describe processivity of DNA helicase (49, 50) or the kinetics of polymer growth in polymer chemistry (51). The processivity of a methyltransferase can be schematically described as



Every k is a turnover rate constant for a particular catalytic step (e.g., methylation or ^3H release), and every k_{off} is dissociation rate constant for enzyme–DNA complex. EP_i represents the enzyme that has processed i steps, and ES_0 is the initial enzyme–DNA complex. ES_0 is equal to the total enzyme concentration in the assay if the enzyme and the DNA concentration are well above dissociation constant for the enzyme–DNA complex. The scheme assumes that ^3H release and the methylation reaction are irreversible as previously shown (43). The concentration of EP_i as a function of time can be described with a differential equation:

$$\frac{d[\text{EP}_i]}{dt} = k[\text{EP}_{i-1}] - (k + k_{\text{off}})[\text{EP}_i] \quad (1)$$

Equation 1 can be integrated starting from the initial ES_0 complex to give the expression that describes the concentration of every EP_i species as a function of time:

$$[\text{EP}_i](t) = \frac{k^i t^{i-1}}{i!} [\text{ES}_0] e^{-(k+k_{\text{off}})t} \quad (2)$$

The product formed in the processive step i by EP_{i-1} can be calculated as

$$\frac{d[\text{P}_i]}{dt} = k[\text{EP}_{i-1}] \quad (3)$$

Equation 3 is combined with eq 2 and integrated to give the expression for the product formed in the processive step i :

$$[\text{P}_i] = [\text{ES}_0] \frac{k^i}{(k + k_{\text{off}})^i} \left(1 - e^{-(k+k_{\text{off}})t} - e^{-(k+k_{\text{off}})t} \sum_{l=1}^{i-1} \frac{(k + k_{\text{off}})^l t^l}{l!} \right) \quad (4)$$

The final equation for the product formed in a processive reaction is a sum of all processive steps ($i = 1$ to n) and equal to

$$[\text{P}] = \sum_{i=1}^n [\text{P}_i] \quad (5)$$

Equation 5 is an asymptotic function with the asymptote

parallel to x axis and equal to

$$\lim_{n \rightarrow \infty} \sum_n [\text{ES}_0] p^n$$

where n is the number of the processive steps and p is the processivity probability defined as

$$p = \frac{k}{k + k_{\text{off}}} \quad (6)$$

The probability for the processive step n is equal to

$$p_n = \left(\frac{k}{k + k_{\text{off}}} \right)^n \quad (7)$$

Theoretically n is equal to infinity. In our experience, for all practical purposes the precision of best fit values will not significantly increase once n reaches the values that give a processivity probability of 0.05 or below (eq 7), i.e., 95% of enzyme molecules have dissociated from the original substrate. Equation 5 describes *the first processive cycle*, which includes catalytic turnovers from all Dnmt1 molecules before their first dissociation from the initial DNA substrate.

The main part of our processivity profiles come from the first processive cycle (i.e., Figure 4); however, in some measurements the late linear part and the subsequent processive cycles are substantial (i.e., Figure 3). Accordingly, the experimental processivity profiles show a late linear phase that does not end with an asymptote parallel to the x axis as predicted by the eq 5. Developing a mathematical model that describes multiple processive cycles as a function of k and k_{off} is impractical. Accordingly, we describe the late linear part empirically by adding a second linear factor to the eq 5:

$$[\text{P}] = \left(\sum_{i=1}^n [\text{P}_i] \right) + k_{\text{ss}} [\text{ES}_0] t \quad (8)$$

The first part of the eq 8 comes from eq 5 and represents the analytic description of the first processive cycle. The second part in eq 8 is the late linear phase that represents multiple processive cycles. The k_{ss} is an empirical rate constant that describes the catalytic rate in the late linear phase, while the $[\text{ES}_0]t$ factor indicates that the late linear phase is proportional to the total enzyme concentration and linear with time.

The selection between eqs 5 or 8 is empirical. We analyzed each profile using both equations, and the fit quality for each case was compared. When profiles with no late linear phase are analyzed using eq 8, the fit gives large errors for k_{ss} , and (or) k_{ss} takes nonsense values such as $k_{\text{ss}} < 0$, and (or) k_{ss} becomes highly correlated with k_{off} , all indicating that eq 5 is a better choice for such cases. The experimental profiles can be directly analyzed using eq 5 or 8 with all three parameters (k , k_{off} , k_{ss}) set as the free variables. ES_0 is poorly resolved as the free parameter (i.e., high correlation to k value) using eqs 5 or 8, so in all fits we kept ES_0 constant according to the value calculated from other measurements. All fits converge easily even when the initial values for the

fit parameters are given borderline reasonable estimates (Tables 1 and 2).

REFERENCES

- Jones, P. A., and Takai, D. (2001) The role of DNA methylation in mammalian epigenetics, *Science* 293, 1068–1070.
- Robertson, K. D., and Jones, P. A. (2000) DNA methylation: past, present and future directions, *Carcinogenesis* 21, 461–467.
- Egger, G., Liang, G., Aparicio, A., and Jones, P. A. (2004) Epigenetics in human disease and prospects for epigenetic therapy, *Nature* 429, 457–463.
- Pradhan, S., and Esteve, P. O. (2003) Mammalian DNA (cytosine-5) methyltransferases and their expression, *Clin. Immunol.* 109, 6–16.
- Xie, S., Wang, Z., Okano, M., Nogami, M., Li, Y., He, W. W., Okumura, K., and Li, E. (1999) Cloning, expression and chromosome locations of the human DNMT3 gene family, *Gene* 236, 87–95.
- Okano, M., Xie, S., and Li, E. (1998) Dnmt2 is not required for de novo and maintenance methylation of viral DNA in embryonic stem cells, *Nucleic Acids Res.* 26, 2536–2540.
- Flynn, J., Glickman, J. F., and Reich, N. O. (1996) Murine DNA cytosine-C5 methyltransferase: pre-steady- and steady-state kinetic analysis with regulatory DNA sequences, *Biochemistry* 35, 7308–7315.
- Yokochi, T., and Robertson, K. D. (2002) Preferential methylation of unmethylated DNA by Mammalian de novo DNA methyltransferase Dnmt3a, *J. Biol. Chem.* 277, 11735–11745.
- Bacolla, A., Pradhan, S., Roberts, R. J., and Wells, R. D. (1999) Recombinant human DNA (cytosine-5) methyltransferase. II. Steady-state kinetics reveal allosteric activation by methylated DNA, *J. Biol. Chem.* 274, 33011–33019.
- Bacolla, A., Pradhan, S., Larson, J. E., Roberts, R. J., and Wells, R. D. (2001) Recombinant human DNA (cytosine-5) methyltransferase. III. Allosteric control, reaction order, and influence of plasmid topology and triplet repeat length on methylation of the fragile X CCG·CCG sequence, *J. Biol. Chem.* 276, 18605–18613.
- Aubol, B. E., and Reich, N. O. (2003) Murine DNA cytosine C(5)-methyltransferase: in vitro studies of de novo methylation spreading, *Biochem Biophys. Res. Commun.* 310, 209–214.
- Flynn, J., Azzam, R., and Reich, N. (1998) DNA binding discrimination of the murine DNA cytosine-C5 methyltransferase, *J. Mol. Biol.* 279, 101–116.
- Flynn, J., Fang, J. Y., Mikovits, J. A., and Reich, N. O. (2003) A potent cell-active allosteric inhibitor of murine DNA cytosine C5 methyltransferase, *J. Biol. Chem.* 278, 8238–8243.
- Flynn, J., and Reich, N. (1998) Murine DNA (cytosine-5)-methyltransferase: steady-state and substrate trapping analyses of the kinetic mechanism, *Biochemistry* 37, 15162–15169.
- Pradhan, S., and Esteve, P. O. (2003) Allosteric activator domain of maintenance human DNA (cytosine-5) methyltransferase and its role in methylation spreading, *Biochemistry* 42, 5321–5332.
- Pradhan, S., and Roberts, R. J. (2000) Hybrid mouse-prokaryotic DNA (cytosine-5) methyltransferases retain the specificity of the parental C-terminal domain, *EMBO J.* 19, 2103–2114.
- Lauster, R., Trautner, T. A., and Noyer-Weidner, M. (1989) Cytosine-specific type II DNA methyltransferases. A conserved enzyme core with variable target-recognizing domains, *J. Mol. Biol.* 206, 305–312.
- Yoder, J. A., Soman, N. S., Verdine, G. L., and Bestor, T. H. (1997) DNA (cytosine-5)-methyltransferases in mouse cells and tissues. Studies with a mechanism-based probe, *J. Mol. Biol.* 270, 385–395.
- Svedruzic, Z. M., and Reich, N. O. (2005) DNA Cytosine c(5) methyltransferase Dnmt1: catalysis-dependent release of allosteric inhibition, *Biochemistry* 44, 9472–9485.
- Ivanetich, K. M., and Santi, D. V. (1992) 5,6-dihydropyrimidine adducts in the reactions and interactions of pyrimidines with proteins, *Prog. Nucleic Acid Res. Mol. Biol.* 42, 127–156.
- Araujo, F. D., Croteau, S., Slack, A. D., Milutinovic, S., Bigey, P., Price, G. B., Zannis-Hajopoulos, M., and Szyf, M. (2001) The DNMT1 target recognition domain resides in the N terminus, *J. Biol. Chem.* 276, 6930–6936.
- Bestor, T. H. (1992) Activation of mammalian DNA methyltransferase by cleavage of a Zn binding regulatory domain, *EMBO J.* 11, 2611–2617.
- Chuang, L. S., Ian, H. I., Koh, T. W., Ng, H. H., Xu, G., and Li, B. F. (1997) Human DNA-(cytosine-5) methyltransferase-PCNA complex as a target for p21WAF1, *Science* 277, 1996–2000.
- Glickman, J. F., Pavlovich, J. G., and Reich, N. O. (1997) Peptide mapping of the murine DNA methyltransferase reveals a major phosphorylation site and the start of translation, *J. Biol. Chem.* 272, 17851–17857.
- Leonhardt, H., Page, A. W., Weier, H. U., and Bestor, T. H. (1992) A targeting sequence directs DNA methyltransferase to sites of DNA replication in mammalian nuclei, *Cell* 71, 865–873.
- Pedrali-Noy, G., and Weissbach, A. (1986) Mammalian DNA methyltransferases prefer poly(dI-dC) as substrate, *J. Biol. Chem.* 261, 7600–7602.
- Bolden, A., Ward, C., Siedlecki, J. A., and Weissbach, A. (1984) DNA methylation. Inhibition of de novo and maintenance methylation in vitro by RNA and synthetic polynucleotides, *J. Biol. Chem.* 259, 12437–12443.
- Glickman, J. F., Flynn, J., and Reich, N. O. (1997) Purification and characterization of recombinant baculovirus-expressed mouse DNA methyltransferase, *Biochem. Biophys. Res. Commun.* 230, 280–284.
- Kawasaki, H., and Taira, K. (2004) Induction of DNA methylation and gene silencing by short interfering RNAs in human cells, *Nature* 431, 211–217.
- Morris, K. V., Chan, S. W., Jacobsen, S. E., and Looney, D. J. (2004) Small interfering RNA-induced transcriptional gene silencing in human cells, *Science* 305, 1289–12892.
- Jenuwein, T. (2002) Molecular biology. An RNA-guided pathway for the epigenome, *Science* 297, 2215–2218.
- Carty, S. M., and Greenleaf, A. L. (2002) Hyperphosphorylated C-terminal repeat domain-associating proteins in the nuclear proteome link transcription to DNA/chromatin modification and RNA processing, *Mol. Cell Proteomics* 1, 598–610.
- Jeffery, L., and Nakielny, S. (2004) Components of the DNA methylation system of chromatin control are RNA-binding proteins, *J. Biol. Chem.* 279, 49479–49487.
- Muromoto, R., Sugiyama, K., Takachi, A., Imoto, S., Sato, N., Yamamoto, T., Oritani, K., Shimoda, K., and Matsuda, T. (2004) Physical and functional interactions between Daxx and DNA methyltransferase 1-associated protein, DMAP1, *J. Immunol.* 172, 2985–2993.
- Liu, Z., and Fisher, R. A. (2004) RGS6 interacts with DMAP1 and DNMT1 and inhibits DMAP1 transcriptional repressor activity, *J. Biol. Chem.* 279, 14120–14128.
- Kimura, H., and Shiota, K. (2003) Methyl-CpG-binding protein, MeCP2, is a target molecule for maintenance DNA methyltransferase, Dnmt1, *J. Biol. Chem.* 278, 4806–4812.
- Fuks, F., Hurd, P. J., Deplus, R., and Kouzarides, T. (2003) The DNA methyltransferases associate with HP1 and the SUV39H1 histone methyltransferase, *Nucleic Acids Res.* 31, 2305–2312.
- Fuks, F., Burgers, W. A., Brehm, A., Hughes-Davies, L., and Kouzarides, T. (2000) DNA methyltransferase Dnmt1 associates with histone deacetylase activity, *Nat. Genet.* 24, 88–91.
- Fuks, F., Hurd, P. J., Wolf, D., Nan, X., Bird, A. P., and Kouzarides, T. (2003) The methyl-CpG-binding protein MeCP2 links DNA methylation to histone methylation, *J. Biol. Chem.* 278, 4035–4040.
- Vilkaitis, G., Suetake, I., Klimasauskas, S., and Tajima, S. (2005) Processive Methylation of Hemimethylated CpG Sites by Mouse Dnmt1 DNA Methyltransferase, *J. Biol. Chem.* 280, 64–72.
- Xu, G., Flynn, J., Glickman, J. F., and Reich, N. O. (1995) Purification and stabilization of mouse DNA methyltransferase, *Biochem. Biophys. Res. Commun.* 207, 544–551.
- Svedruzic, Z. M., and Reich, N. O. (2004) The Mechanism of Target Base Attack in DNA Cytosine Carbon 5 Methylation, *Biochemistry* 43, 11460–11473.
- Wu, J. C., and Santi, D. V. (1987) Kinetic and catalytic mechanism of HhaI methyltransferase, *J. Biol. Chem.* 262, 4778–4786.
- Pradhan, S., Bacolla, A., Wells, R. D., and Roberts, R. J. (1999) Recombinant human DNA (cytosine-5) methyltransferase. I. Expression, purification, and comparison of de novo and maintenance methylation, *J. Biol. Chem.* 274, 33002–33010.
- Reale, A., Matteis, G. D., Galleazzi, G., Zampieri, M., and Caiafa, P. (2005) Modulation of DNMT1 activity by ADP-ribose polymers, *Oncogene* 24, 13–19.
- Rountree, M. R., Bachman, K. E., and Baylin, S. B. (2000) DNMT1 binds HDAC2 and a new co-repressor, DMAP1, to form a complex at replication foci, *Nat. Genet.* 25, 269–277.

47. Easwaran, H. P., Schermelleh, L., Leonhardt, H., and Cardoso, M. C. (2004) Replication-independent chromatin loading of Dnmt1 during G2 and M phases, *EMBO Rep.* 5, 1181–1186.
48. Hermann, A., Goyal, R., and Jeltsch, A. (2004) The Dnmt1 DNA-(cytosine-C5)-methyltransferase methylates DNA processively with high preference for hemimethylated target sites, *J. Biol. Chem.* 279, 48350–48359.
49. Porter, D. J., Short, S. A., Hanlon, M. H., Preugschat, F., Wilson, J. E., Willard, D. H., Jr., and Consler, T. G. (1998) Product release is the major contributor to k_{cat} for the hepatitis C virus helicase-catalyzed strand separation of short duplex DNA, *J. Biol. Chem.* 273, 18906–18914.
50. Ali, J. A., and Lohman, T. M. (1997) Kinetic measurement of the step size of DNA unwinding by *Escherichia coli* UvrD helicase, *Science* 275, 377–380.
51. Steinfeld, J. I., Francisco, J. S., and Hase, W. L. (1998) *Chemical Kinetics and Dynamics*, 2nd ed., Prentice Hall, New York.

BI050988F

DNA Cytosine C⁵ Methyltransferase Dnmt1: Catalysis-Dependent Release of Allosteric Inhibition[†]

Željko M. Svedružić[#] and Norbert O. Reich^{*}

Department of Chemistry and Biochemistry, University of California, Santa Barbara, California 93106

Received February 17, 2005; Revised Manuscript Received May 2, 2005

ABSTRACT: We followed the cytosine C⁵ exchange reaction with Dnmt1 to characterize its preference for different DNA substrates, its allosteric regulation, and to provide a basis for comparison with the bacterial enzymes. We determined that the methyl transfer is rate-limiting, and steps up to and including the cysteine–cytosine covalent intermediate are in rapid equilibrium. Changes in these rapid equilibrium steps account for many of the previously described features of Dnmt1 catalysis and specificity including faster reactions with premethylated DNA versus unmethylated DNA, faster reactions with DNA in which guanine is replaced with inosine [poly(dC–dG) vs poly(dI–dC)], and 10–100-fold slower catalytic rates with Dnmt1 relative to the bacterial enzyme M.HhaI. Dnmt1 interactions with the guanine within the CpG recognition site can prevent the premature release of the target base and solvent access to the active site that could lead to mutagenic deamination. Our results suggest that the β -elimination step following methyl transfer is not mediated by free solvent. Dnmt1 shows a kinetic lag in product formation and allosteric inhibition with unmethylated DNA that is not observed with premethylated DNA. Thus, we suggest the enzyme undergoes a slow relief from *allosteric inhibition* upon initiation of catalysis on unmethylated DNA. Notably, this relief from allosteric inhibition is not caused by self-activation through the initial methylation reaction, as the same effect is observed during the cytosine C⁵ exchange reaction in the absence of AdoMet. We describe limitations in the Michaelis–Menten kinetic analysis of Dnmt1 and suggest alternative approaches.

DNA methylation in eukaryotes occurs predominately at CpG dinucleotides and is essential for normal embryogenesis and cellular activity (1). The patterns of DNA methylation are tissue-specific and change dynamically throughout development. Inappropriate DNA methylation of tumor suppressor genes (2) and DNA repair genes (3–5) are nonmutagenic events that occur early in carcinogenesis (6). Dnmt1¹ is one of three predominant isoforms and has both *de novo* and maintenance activity *in vitro* and *in vivo*. Dnmt1 is a large multidomain protein that is structurally and functionally more complex than its smaller, bacterial counterparts (7–15). Mechanism-based inhibition of bacterial and mammalian DNA cytosine methyltransferases by 5-fluorocytosine (14, 16), and the conserved sequence motifs observed in all DNA cytosine methyltransferases (17, 18),

suggest that Dnmt1 and its bacterial counterparts share similar catalytic mechanisms (Figure 1). However, the sequence homology with the bacterial enzymes is found only in the small C terminal domain of Dnmt1 (18), and the large N terminal domain contains numerous regulatory sites, including a site of phosphorylation (Ser 514) (19), an allosteric DNA binding site (8, 20), nuclear localization signal (21), PCNA binding sequence (22), replication foci homing sequence (23), and Zn-finger sequence motifs (20). The N-terminal allosteric site is believed to regulate the enzyme's preference for DNA containing a distribution of 5-methylcytosines (pre-methylated DNA) (11, 20). An N-terminal allosteric site was postulated to cause potent cell-based, sequence-dependent Dnmt1 inhibition (8). The majority of the reported mechanistic studies on mammalian Dnmt1 use the murine (7–10, 24) and human (11, 12, 14) enzymes, which share 78% sequence identity.

Dnmt1's preference for premethylated DNA is frequently invoked as a key regulatory mechanism (7, 10–13, 25). Premethylated DNA includes sequences in which cytosine within the CpG dinucleotide in duplex DNA is methylated (hemimethylated DNA) and in which the 5-methylcytosine lies outside this recognition CpG but within the enzyme's DNA footprint. Hemimethylated DNA occurs predominately following DNA replication and provides a basis for Dnmt1's propagation of methylation patterns, presumably through a multiprotein complex that assembles at the sites of replication (22). 5-Methylcytosines (^{5m}C) positioned outside the target CpG dinucleotide are thought to be important for the allosteric regulation of the enzyme.

[†] This work was supported by NIH GM56289 to N.O.R.

^{*} To whom correspondence should be addressed. E-mail: reich@chem.ucsb.edu; phone 805-893-8368; fax 805-893-4120.

[#] Current address: School of Molecular Biosciences, Department of Biophysics and Biochemistry, Washington State University, Pullman, WA 99164.

¹ Abbreviations: AdoMet, S-adenosyl-L-methionine; AdoHcy, S-adenosyl-L-homocysteine; bp, base pair, as two bases paired in Watson–Crick fashion; C, cytosine; C⁵ or C⁶, etc., carbon 5 or carbon 6 in a pyrimidine ring; ^{5m}C, 5-methylcytosine; dCTP, deoxycytosine triphosphate; dITP, deoxyinosine triphosphate; Dnmt1, DNA methyltransferase type 1; MEL, mouse erythroleukemia; M.HhaI, methyltransferase, *Haemophilus haemolyticus* type I; poly(dG–dC) or dGdC, double-stranded alternating polymer of deoxyguanine and deoxycytosine; poly-(dI–dC), double-stranded polymer of alternating deoxyinosine–deoxycytosine; pm-poly(dG–dC) or pm-dGdC, double-stranded alternating polymer of deoxyguanine and deoxycytosine; pm-poly(dI–dC), pre-methylated poly(dI–dC); sin, sinefungin; SKIE, solvent kinetic isotope effect.

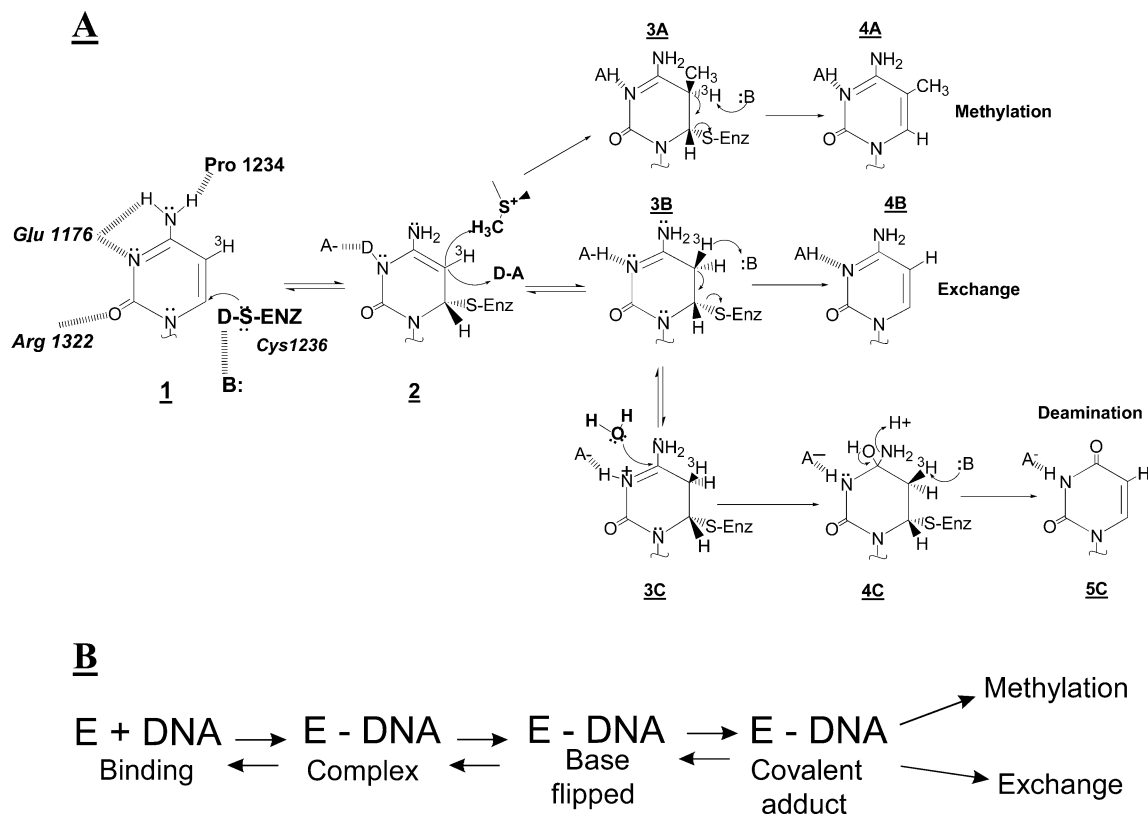


FIGURE 1: (A) Reactions catalyzed by cytosine C⁵ DNA methyltransferases: methylation (A) exchange (B) and deamination (C) (44). The target cytosine interacts with active site residues (1) to facilitate cysteine nucleophilic attack at the C⁶ position. Nucleophilic attack disrupts the pyrimidine's aromaticity, generating the reactive covalent adduct (2). Intermediate 2 can readily undergo electrophilic addition, either through methylation (3A) or protonation (3B). 3B can lead to the exchange reaction (4B) or to mutagenic deamination (3B → 4C → 5C). Acidic groups are labeled as HA and basic groups are labeled as :B. All exchangeable protons that can result in a SKIE are shown as D in intermediates (1 and 2). The pre-steady-state in the methylation reaction are all steps leading to intermediate 3A (or 3B for exchange), while the steady state are subsequent steps (see methods). Conserved active site residues are indicated. (B) Four steps that control the target base attack by pyrimidine methyltransferases in a rapid equilibrium (28).

Dnmt1's catalytic preference for premethylated DNA derives in part from a faster methylation constant (7). Pedrali-Noy et al. postulated that the enzyme's preference for premethylated DNA is due to the inhibitory action of unmethylated DNA (26), which was further suggested to function through an allosteric site on the N-terminal domain (20). A variety of studies have shown that the N-terminal domain is required for Dnmt1 function (11, 27). Removal of the first 501 N-terminal residues results in a mutant Dnmt1 with activities higher than WT with both unmethylated and premethylated DNA (11). Thus, some form of allosteric inhibition is likely to be present with all DNA substrates. Surprisingly, the N-terminal deletion mutant still differentiates between premethylated and unmethylated DNA (11). We previously showed that Dnmt1 forms ternary enzyme/DNA/DNA complexes, that different DNA sequences vary in their binding affinity, and that the binding of a second DNA molecule most likely involves the N-terminal domain (8, 9). In sum, previous studies (8, 11, 12, 26) suggest that the N-terminal domain acts to inhibit the enzyme and that a complex interplay between different DNA binding sites results in the enzyme's regulation. Our interest is to characterize the mechanisms of the enzyme's substrate preference and allosteric regulation.

We recently defined a kinetic approach for M.HhaI providing new insights into which steps limit catalysis and the nature of various reaction intermediates (28). Briefly, intermediate 2 (Figure 1) is readily protonated in the presence

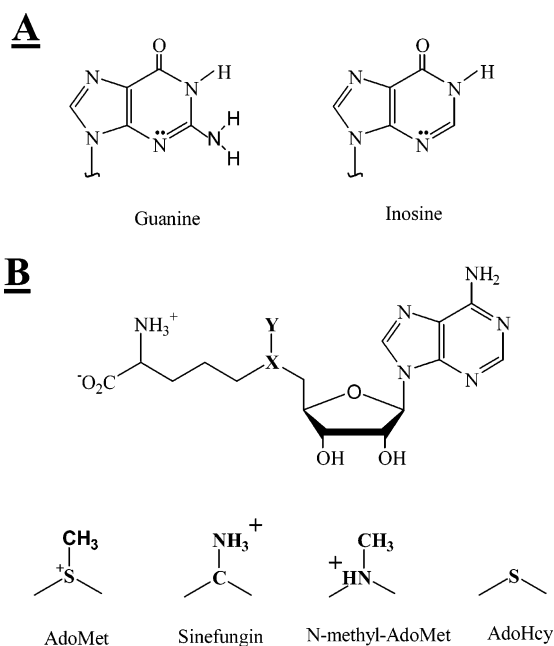


FIGURE 2: Inosine and guanine (A); AdoMet and its analogues (B).

of a proton donor ($pK_a = 11-18$; 29), so the ³H exchange reaction in the presence of AdoMet analogues (i.e., proton donors, Figure 2) represents an opportunity to analyze this crucial stage of catalysis (Figure 1, 1 → 2). Intermediate 2 is most likely important for inhibitors of Dnmt1 like 5-aza-

cytosine, which was recently approved by the FDA to treat blood-related tumors (30), or zebularine which is in phase II clinical trials (30). Here we analyze intermediate **2** with murine Dnmt1, by monitoring the cytosine C⁵ exchange reaction with AdoMet analogues and poly(dG-dC) and poly(dI-dC) substrates. Our primary interest is of the Dnmt1/DNA complex involving the cognate site, as represented either by poly(dG-dC) or poly(dI-dC). These homogeneous substrates cause each enzyme molecule to interact with the same DNA sequence, at both the active and the allosteric sites (Figure 10). Further, all enzyme-DNA complexes are likely to be active since every enzyme molecule bound to the DNA is bound at the recognition site, thereby increasing the sensitivity of the assay for an enzyme as slow as Dnmt1. These studies with poly(dG-dC) and poly(dI-dC) are conveniently compared with prior studies of Dnmt1 (7, 8, 10–12, 26).

MATERIALS

S-Adenosyl-L-[methyl¹⁴C] methionine (59 mCi/mmol or 131 cpm/pmol), S-adenosyl-L-[methyl³H] methionine (66–82 Ci/mmol or 6100–7200 cpm/pmol), deoxy[5-³H] cytidine 5' triphosphate (19.0 Ci/mmol) ammonium salt, and Sequenase 2.0 were purchased from Amersham Corp. Poly(dG-dC) 850 bp, poly(dI-dC) 1960 bp, dITP, and dCTP were purchased from Pharmacia Biotech. DTT, Trizma, BSA fraction V, and activated charcoal were purchased from Sigma Chemical Co. Some BSA batches were inhibitory, and each BSA batch was tested by showing that the reaction rate did not vary with BSA concentration (0.2–1.0 mg/mL). DE81 filters were purchased from Whatman, Inc. Sinefungin was purchased from Sigma Chemical Co. AdoMet 85% pure was purchased from Sigma Chemical Co. and further purified (31). Dnmt1 was prepared from mouse erythroleukemia cells as previously described (32), and its concentration was determined by active site titration (7) and by titration with a potent Dnmt1 inhibitor ($K_d \approx 30$ nM; 8). The enzyme concentration determined by the pre-steady-state burst is 40% lower than the enzyme concentration determined by titration with the inhibitor. Because the pre-steady-state burst is expected to give a lower measure of enzyme concentration (eq 1), we relied on the use of the oligonucleotide inhibitor to determine Dnmt1 concentration. M.HhaI was expressed using *Escherichia coli* strain ER1727 containing plasmid pHSHW-5 (both provided by S. Kumar, New England Biolabs) and purified as previously described (15). The concentration of AdoMet, sinefungin, premethylated and unmethylated poly(dG-dC) and poly(dI-dC) were determined by absorbance at 260 nm. The respective molar absorptivity coefficients are 15.0×10^3 M⁻¹ cm⁻¹ for AdoMet and sinefungin (Merck Index), 6.9×10^3 M⁻¹ cm⁻¹ for poly(dI-dC) bp, 8.4×10^3 M⁻¹ cm⁻¹ for poly(dG-dC) bp (Pharmacia Tech. Info. Sheet).

METHODS

Preparation of Premethylated poly(dG-dC) and poly(dI-dC). The premethylated substrates were prepared with excess AdoMet and M.HhaI. The labeling reaction was run for only one or two turnovers (1.5–2 min) to limit the number of methylated cytosines (^{5m}C) to the number of initially bound M.HhaI molecules. For example, 30–40 μM M.HhaI and

100 μM of [methyl ¹⁴C] AdoMet were incubated with 300 μM bp DNA (approximately 30 μM of binding sites for M.HhaI on the DNA substrate, based on a 10 bp footprint; Figure 10 and ref 33). This reaction was quenched (90 °C water bath for 3–5 min), followed by slow cooling (2–3 h) to room temperature to ensure gradual annealing of self-complementary DNA. M.HhaI was removed by centrifugation, and the remaining labeling mixture was dialyzed against 10 mM Tris/HCl pH (8.0) and 10 mM EDTA. The extent of dialysis was determined with DE81 filter papers and washing the filters with 500 mM KPi buffer pH = 6.8. Dialysis was continued until the washed and unwashed samples had the same counts. The final DNA concentration and extent of methylation were determined by measuring the absorbance at 260 nm and ¹⁴C radioactivity, respectively. The substrates prepared by this procedure contain an average of one ^{5m}C every 7 to 20 bp, depending on the length of the labeling reaction and the ratio between total M.HhaI and DNA. All substrates prepared in this fashion showed a characteristic pre-steady-state burst (7).

Preparation of [5-³H] Cytosine-poly(dG-dC) and poly(dI-dC). Poly(dI-dC) was labeled by incubating 500 μM (bp) of poly(dI-dC) with 100 μM [5-³H] dCTP, 1 mM CTP, 10 mM dITP with 0.62 U/μL of Sequenase 2.0 in 40 mM Tris/HCl (pH 7.5), 10 mM MgCl₂, 50 mM NaCl, 10 mM DTT and 1.0 mg/mL BSA. The same approach was used in the labeling reactions with poly(dG-dC) except that poly(dI-dC) and 10 mM dITP were replaced by poly(dG-dC) and 1 mM dGTP. The labeling reactions were run for 5 h at room temperature. Incorporation of [5-³H] cytosine was determined by placing the reaction aliquots onto DE81 filter papers. Filters were washed twice for 5 min in 500 mM KPi buffer (pH 6.8) and dried under a heat lamp. The high ionic strength (500 mM KPi) removes free nucleotides from the DE81 filters without impacting the bound DNA. The extent of label incorporation was calculated by comparing the counts from unwashed and washed papers. The procedure routinely results in approximately 30–60% label incorporation. The quenching, annealing, and dialysis procedures were as described for the premethylated substrates. The removal of reaction components was determined by comparing the radioactivity from unwashed and washed DE81 papers as indicated above. The labeling gives 13–40 cpm/pmol of base pairs for poly(dI-dC) and 60–105 cpm/pmol of base pairs for poly(dG-dC).

Methylation Reactions. The methylation reactions were prepared by incubating Dnmt1, DNA substrate, and radioactive AdoMet in 100 mM Tris/HCl (pH, 8.0), 10 mM EDTA, 10 mM DTT, and 0.5 mg/mL of BSA at 37 °C. The enzyme and DNA concentrations are specific for each assay and described in the figure legends. Incorporation of tritiated methyl groups into DNA was determined as previously described (31). Briefly, a typical reaction was followed by placing reaction aliquots onto DE81 paper, in which case DNA methylation is detected as soon as the methyl group is transferred to DNA (Figure 1, **3A**). Thus, the pre-steady-state and steady-state rates are determined by the steps that lead to and follow formation of intermediate **3A** (Figure 1), respectively.

Tritium Exchange Reactions. The tritium exchange reaction was followed essentially as previously described (34). Briefly, tritium exchange is measured by quenching reaction aliquots in an acid suspension (HCl, pH = 2.0–2.5) of

activated charcoal. Because **3A** and **3B** (Figure 2) rapidly degrade in acid, their formation can be detected prior to release from the enzyme, thereby allowing the determination of kinetic constants up to and including the formation of **3A** and **3B**. The enzyme concentration, DNA concentration, and cofactor concentration are specific for each assay and described in the figure legends. All reactions were saturated with the cofactor. The reaction buffer was 100 mM Tris/HCl (pH, 8.0), 10 mM EDTA, 10 mM DTT, and 0.5 mg/mL of BSA.

Preparation of [5-³H] Cytosine pm-poly(dG-dC) and pm-poly(dI-dC). ³H-labeled premethylated DNA was prepared from [5-³H] cytosine-poly(dG-dC) or [5-³H] cytosine-poly(dI-dC) using the procedure described for the preparation of premethylated DNA.

Data Analysis. All reaction profiles were analyzed using the Microcal Origin 5.0 program. All rates were reported as the best fit values \pm standard deviation. The burst profiles were fit to a two-step irreversible mechanism (35):

$$[P](t) = \alpha E_t(1 - e^{-k_{\text{psst}}t}) + E_t k_{\text{ss}} t \quad (1)$$

where $[P](t)$ is product at time t , E_t is total enzyme in the assay, α is a constant that relates the burst magnitude and the actual enzyme concentration, k_{psst} is the pre-steady-state rate constant, and k_{ss} is the lag transition rate constant. All initial velocity lags were analyzed using a model equation that represents two enzymes forms with different catalytic activities (36):

$$[P](t) = E_t k t - \frac{E_t k}{k_1} (1 - e^{-k_1 t}) \quad (2)$$

where $[P](t)$ is product at time t , E_t is total enzyme in the assay, k is the catalytic rate constant, and k_1 is the lag transition rate constant and corresponds to the transition rate between the inhibited and uninhibited forms. Unless otherwise indicated all other profiles were analyzed using a linear equation ($[P](t) = E_t k$; $[P](t)$ product at time t , E_t total enzyme, k turnover rate constant). Each experiment was repeated with different enzyme and substrate concentrations to test for the consistency in the observed phenomena; shown are representative examples.

SKIE Measurements. All experiments in D₂O buffers were measured in parallel with the corresponding H₂O experiments and were identical in all other parameters. The D₂O buffer was prepared as a 10-fold concentrate, and its pH was adjusted taking into account the pD vs pH correction (37) to be the same as in the corresponding H₂O buffer. H inventory profiles were analyzed using different forms of the Gross-Butler equation (37):

$$k_v^{\text{D}_2\text{O}} = k^{\text{H}_2\text{O}} \frac{(1 + v - v\phi^{\text{T}})^n}{(1 + v - v\phi^{\text{G}})^m} \quad (3)$$

where $k_v^{\text{D}_2\text{O}}$ is the measured rate constant when the fraction of D₂O is equal v , $k^{\text{H}_2\text{O}}$ is the rate constant measured in pure H₂O, v is the fraction D₂O at which the rate constant was measured (i.e., 0.1, 0.2, 0.3, etc), and ϕ^{T} or ϕ^{G} are deuterium fractionation factors at the transition and the ground state, respectively (37). Different forms of eq 4 can be produced

by changing the values for parameters n , m , as we described earlier (28).

Fluorescence Measurements. The equilibrium dissociation constant for the Dnmt1 CRE a^{Fb}m complex was measured in the presence and absence of AdoMet by following changes in the intrinsic protein fluorescence as a function of increasing DNA concentration. The fluorescence was measured using a Perkin-Elmer LS50B instrument, with excitation at 290 nm (5 nm band-pass), and the emission at 340 nm (10 nm band-pass). To a first approximation an apparent dissociation constant (K_d) was calculated using the following equation:

$$\frac{F_o - F_i}{F_o - F_F} = \frac{(E_t - S_i + K_d) - \sqrt{(E_t - S_i + K_d)^2 - 4E_t S_i}}{2 \cdot [E_t]} \quad (4)$$

where F_i is fluorescence at DNA concentration S_i , E_t is total Dnmt1 concentration, and F_o and F_F are the initial and the final fluorescence, respectively. The experimental data were analyzed by nonlinear least-squares fits using eq 4 and the Microcal Origin 5.0 program, with K_d , F_o , and F_F set as the free fit parameters. Prior to fitting using eq 4, the measured Dnmt1 fluorescence profiles were corrected for the inner filter effect that is caused by added DNA. The inner filter effect was measured by replacing Dnmt1 with free Trp at a concentration to get the same fluorescence as the initial Dnmt1 solution, using the following equation:

$$F_i = F_m + (F_o - F_w) \quad (5)$$

where F_i is the corrected fluorescence value that was used in the eq 4, F_m and F_w are measured Dnmt1 and free Trp fluorescence before the correction at a specific DNA concentration, and F_o is the initial fluorescence of the Dnmt1 (and free Trp) solution before addition of DNA or AdoMet. The correction curve showed that at the highest DNA concentration the inner filter effect was between 5 and 15% of the actual signal.

RESULTS

Pre-Steady-State and Initial Steady-State Methylation Reactions with poly(dI-dC) and pm-poly(dI-dC) (Figures 3A and 4A,C), poly(dG-dC) and pm-poly(dG-dC) (Figures 3B and 4B,C). Our initial interest was to characterize the methylation reaction (Figures 3A,B and 4A–C) with pre-methylated and unmethylated poly(dI-dC) and poly(dG-dC) substrates to provide a basis for a direct comparison with our recent study of M.HhaI (28) and prior studies of Dnmt1 with different DNA substrates (Table 1). The relatively fast reactions with poly(dI-dC) and pm-poly(dI-dC) allow the measurement of multiple turnovers (Figure 3A, Table 1). In contrast, the slow nonlinear reactions with poly(dG-dC) and pm-poly(dG-dC) limited our measurements to one or two turnovers, respectively (Figure 3B, Table 1). Both pre-methylated poly(dI-dC) and poly(dG-dC) show a mild pre-steady-state burst (Figure 3A,B) and no substrate inhibition (Figure 4C). Both unmethylated poly(dI-dC) and poly(dG-dC) show initial lags (Figure 3A,B), and increasing DNA concentrations leads to longer lags (Figure 3A,B) and greater substrate inhibition (Figure 4A,B). In summary, the pre-methylated and unmethylated substrates show distinct sub-

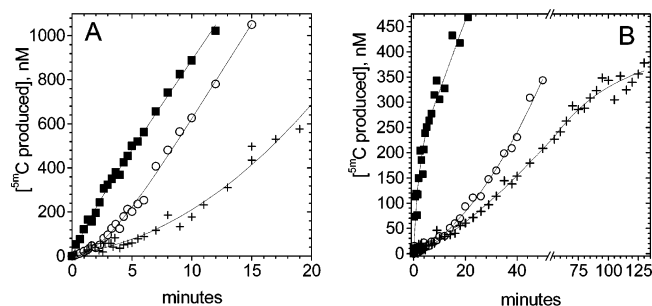


FIGURE 3: Dnmt 1 methylation reaction with different DNA substrates. (A) Methylation profiles (■) with pm-poly(dI-dC) (12 μM bp) and with poly(dI-dC) [12 μM bp (○) and 260 μM (+) bp] in the presence of 145 nM Dnmt1. pm-poly(dI-dC) has an average of one out of eight cytosines methylated. (B) Methylation profiles (■) with pm-poly(dG-dC) (10 μM bp) and with poly(dG-dC) [4 μM bp (○) and 20 μM (+) bp] in the presence of 270 and 350 nM Dnmt1, respectively. pm-poly(dG-dC) has an average of one out of seven cytosines methylated. All reactions were measured in the presence of 12.5 μM of AdoMet (6100 cpm/pmol).

strate inhibition characteristics and initial rates (Table 1). The catalytic rates measured with poly(dI-dC) are comparable to rates measured in previous studies (Table 1), demonstrating that this substrate provides a reliable basis to study Dnmt1. The catalytic rates with unmethylated and pre-methylated poly(dG-dC) are comparable to rates measured with other substrates with GC target sites (Table 1), suggesting that poly(dG-dC) is representative of such substrates.

The initial lag correlates with the extent of substrate inhibition (Figures 3 and Figure 4, and ref 26). In general, features of both the assay design and inherent reaction mechanism can cause an initial lag during a normal reaction cycle (36, 38). The lag is not due to our assay design since the lag is substrate-dependent and the lag is observed during methylation and exchange assays (Figures 3A,B and 5A,B). Preincubation of Dnmt1 with DNA for 10 min does not change the lag, changing Dnmt1 concentrations does not affect the lag, and changing the order of substrate addition (DNA and AdoMet) does not alter the lag. Thus, a slow ligand binding step does not cause the lag. A slow relief from enzyme inhibition is a well-known mechanism leading to a kinetic lag (36, 38). In summary, we propose that for Dnmt1, the start of the catalytic action with the unmethylated substrate results in a slow relief from the allosteric inhibition causing an initial lag in the catalytic activity.

The lag transition rate constant and the subsequent catalytic rate constant (Table 1) can be calculated using the equation modeled on two enzyme forms whose interconversion is

initiated at the start of catalysis (eq 2; 36, 38). The initial lag is only observed when the transition between the inhibited and uninhibited enzyme forms is slower than the catalytic rate (36, 38). Thus, the lag is observed only in methylation (Figure 3) and during the exchange reaction with sinefungin (Figure 5), but not during the slow exchange reaction with *N*-methyl-AdoMet (data not shown). Finally, we also point out that saturation with poly(dG-dC) and poly(dI-dC) leads to partial inhibition (Figure 4A,B), indicating that occupancy of the allosteric site leads only to modulation, rather than complete loss of catalytic activity.

The premethylated substrate is similar to the substrate used in the original study which revealed differences in the initial lag and substrate inhibition (26). Interestingly, modifications in the ratio of ^{5mC} to C (^{5mC}/C) greater than 1:20 do not cause changes in the kinetic parameters (data not shown). This density of ^{5mC} corresponds to approximately one ^{5mC} per enzyme/DNA footprint (Figure 10A). This is consistent with our previous study showing that Dnmt1 has similar activities with premethylated substrates in which the distance between the target cytosine and ^{5mC} varies from 5 to 18 bp (24). The highest density between ^{5mC} and C sites was 1 to 7, to avoid problems associated with the potential depletion of the target cytosines. The pm-poly(dG-dC) and pm-poly(dI-dC) substrates show a mild pre-steady-state burst (Figure 3A,B), like the hemimethylated oligo substrates ((7) and Table 1).

The Exchange Reaction with AdoMet Analogues and Premethylated and Unmethylated poly(dG-dC) and poly(dI-dC) Substrates (Table 2 and Figure 5A,B). To analyze the enzyme's preference for premethylated DNA and its allosteric regulation, we used the cytosine C⁵ exchange assay (Figure 1, 2 → 3B → 4B) and AdoMet analogues (28). The exchange rates are high with sinefungin, intermediate with *N*-methyl-AdoMet, and low with AdoHcy, and in the absence of the cofactor (Table 2). The AdoMet analogues used in this study differ only in the position that corresponds to the active methyl group on AdoMet (Figure 2), and the exchange rates correlate with the availability of proximal proton(s) in the position of the active methyl group. In summary, just as with M.HhaI (Table 2), the AdoMet analogues alter the exchange reaction by Dnmt1 by changing the rate-limiting proton transfer at the activated target base (Figure 2 → 3B). Interestingly, the enzyme's DNA preferences are retained with AdoMet analogues that modulate the exchange reaction rate by over 3 orders of magnitude: the fastest exchange rates are observed with pm-poly(dI-dC), followed by poly(dI-dC), pm-poly(dG-dC), and poly(dG-dC) (Table 2). Thus,

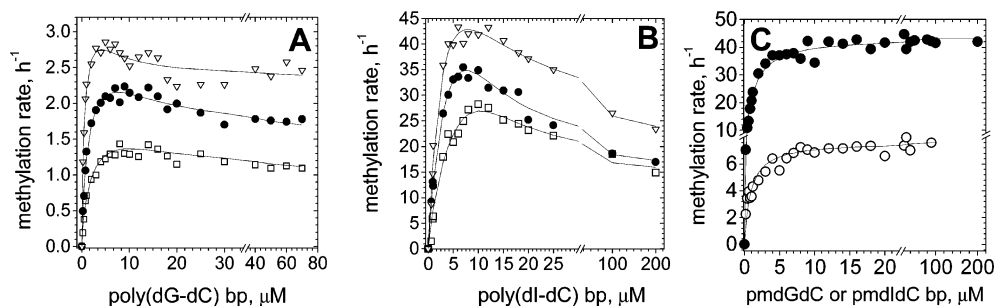


FIGURE 4: Methylation rate as a function of increasing concentration of substrate DNA. (A) poly(dG-dC) as the substrate and 80 nM (▽), 160 nM (●), and 250 nM (□) Dnmt1. (B) poly(dI-dC) as the substrate and 100 nM (▽), 200 nM (●), and 300 nM (□) Dnmt1. (C) pmpoly(dI-dC) (●) and pmpoly(dG-dC) (○) as substrates and 100 nM Dnmt1.

Table 1: Dnmt1 Pre-Steady State and Steady-State Methylation Rates with Different DNA Substrates^a

substrate	first turnover, h ⁻¹	multiple turnovers, h ⁻¹	conditions	references and enzyme source	comments
poly(dG-dC)	1.6 ± 0.6	<i>b</i>	4 μM bp, 15 μM AdoMet	Fig 3B, this study, mouse	Lag ^d : 1.2 ± 0.4 h ⁻¹
	1 ± 0.3	0.2 ± 0.02	20 μM bp, 15 μM AdoMet	Fig 3B, this study, mouse	Lag ^d : 0.7 ± 0.3 h ⁻¹
pm-poly(dG-dC)	8.8 ± 0.6	5.1 ± 0.7	10 μM bp, 15 μM AdoMet	Fig 3B, this study, mouse	pre-steady state burst
poly(dI-dC)	<i>c</i>	37 ± 0.4	10 μM bp, 15 μM AdoMet	Fig 3A, this study, mouse	Lag ^d : 19.2 ± 1.2 h ⁻¹
	<i>c</i>	20.6 ± 0.3	260 μM bp, 15 μM AdoMet	Fig 3A, this study, mouse	Lag ^d : 9.6 ± 0.6 h ⁻¹
pm-poly(dI-dC)	56 ± 11	36 ± 0.5	12 μM bp, 15 μM AdoMet	Fig 3A this study, mouse	pre-steady state burst
poly(dI-dC)	<i>b</i>	20 ^e	6.25 μM IC, 15 μM AdoMet	Fig 1 in (7), mouse	
poly(dI-dC)	<i>b</i>	26 ^e	0.5 μM IC, 15 μM AdoMet	Fig 2A in (8), mouse	
poly(dI-dC)	<i>b</i>	70 ^e	1 μM IC, 10 μM AdoMet,	Fig 4A in (14), human	
poly(dI-dC)	<i>b</i>	36 ^e	1 μM IC, 10 μM AdoMet,	Fig 3A in (14), human	
-CGG CGG CGG- -GCC GCC GCC-		0.85 ^{e,g}	50 μM AdoMet, 1 μM CG, or 41 nM oligo	Fig 4A in (12), human	unmethylated GC rich oligo 36 bp
-MGG MGG MGG- -GCC GCC GCC-		3.0 ^{e,g}	10 μM AdoMet, 1 μM CG, or 83 nM oligo	Fig 4C in (12), human	hemimethylated GC rich oligo 36 bp
-CGG CGG CGG- -GCM GCM GCM-		13.5 ^{e,g}	10 μM AdoMet, 1 μM CG, or 41 nM oligo	Fig 6A in (12), human	pre-methylated GC rich oligo 36 bp
PRW3602 plasmid	1.5 ^e	1.5 ^e	10 μM AdoMet, 25 μM GC	Fig 1A in (12), human	unmethylated plasmid 2705 bp
-ATTGACGTCAA- -TAACTGCAGTT-	0.59 ± 0.02	<i>b</i>	15 μM oligo, 15 μM AdoMet	Table 3 in (7), mouse	unmethylated 30 bp oligo CG site in AT rich sequence
-ATTGAMGTCAA- -TAACTGCAGTT-	3.0 ± 0.2	0.6 ± 0.05	15 μM oligo, 15 μM AdoMet	Fig 4 in (7), mouse	hemimethylated 30 bp oligo CG site in AT rich sequence; pre-steady state burst
-AGGGGCGGGGC- -TCCCCGCCCGG-	0.15 ± 0.02	<i>b</i>	15 μM oligo, 15 μM AdoMet	Table 3 in (7), mouse	unmethylated 30 bp oligo CG site in GC rich sequence
-AGGGGCGGGGC- -TCCCCGMCCCG-	1.2 ± 0.1	<i>b</i>	15 μM oligo, 15 μM AdoMet	Table 3 in (7), mouse	hemimethylated 30 bp oligo CG site in GC rich sequence; pre-steady state burst

^a The present rates are measured at DNA and AdoMet concentrations that give the highest rates. In compiling the table, we did not use reported k_{cat} values, since different publications used different procedures to calculate those values, which can lead to large variations in otherwise comparable reactions (see appendix). ^b Not measured. ^c Cannot be calculated due to initial lag. ^d Lag transition rate as defined in eq 2 k_t . ^e The values were estimated from the actual data figures, and thus we cannot show error. ^f M stands for ^{5m}C, and methylation target sites are shown in bold. ^g Not enough information available to differentiate between turnovers. The table shows results only from Dnmt1 studies that gave enough experimental description (enzyme and substrate concentration, product concentration) to allow independent evaluation.

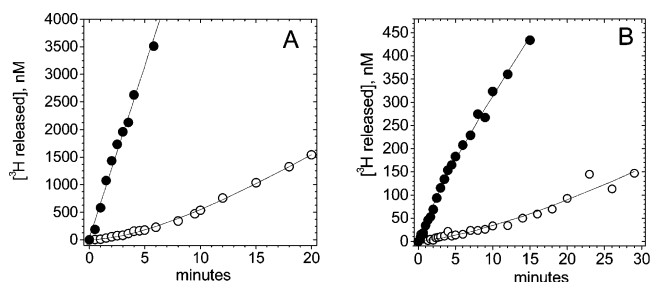


FIGURE 5: Tritium exchange reaction in the presence of sinefungin with different DNA substrates. (A) The exchange reaction with 105 nM Dnmt1, 20 μM of sinefungin, and 10 μM bp of ³H-pmpoly(dI-dC) (●) 19 cpm/pmol, ^{5m}C:C = 1:14, or ³H-poly(dI-dC) (○), 33 cpm/pmol. (B) The exchange reaction with 160 nM Dnmt1, 20 μM of sinefungin, and 8 μM bp of ³H-pmpoly(dG-dC) (●) 56 cpm/pmol, ^{5m}C:C = 1:15, or 8 μM bp of ³H-poly(dG-dC) (○) (88 cpm/pmol).

differences between premethylated and unmethylated DNA, or between poly(dI-dC) and poly(dG-dC), do not derive from differences in the methyltransfer (Figure 1, 2 → 3A) or proton-transfer rates (Figure 1, 2 → 3B).

The exchange reaction with sinefungin is particularly revealing. First, an initial lag is observed in the absence of any production of ^{5m}C (Figure 5). Importantly, this shows that the increased rate following the initial lag in the methylation reaction (Figure 3A,B) cannot be due to self-activation through the AdoMet-dependent production of ^{5m}C at the start of catalysis. Also, the *steady-state* exchange rate constants for poly(dI-dC) and pm-poly(dI-dC) (Figure 5, Table 2) differ by 9-fold, in contrast to the nearly identical AdoMet-dependent methylation rates (Figure 3A, Table 1). Furthermore, the apparent $K_m^{sinefungin}$ measured with poly(dI-dC) is 9 times higher than with pm-poly(dI-dC) (5.1 ± 1.4 vs 0.6 ± 0.1 μM). For comparison, K_m^{AdoMet} in the methylation reaction with poly(dI-dC) is two times higher than with pm-poly(dI-dC) (1.3 ± 0.21 vs 2.7 ± 0.4 μM). Thus, these results indicate that studies of steps prior to methyltransfer (Figure 1, 2 → 3A) can reveal unique insights into the enzyme's preference for different DNA substrates.

Tritium Release Rates during the AdoMet-Dependent Methylation Reaction with Premethylated and Unmethylated poly(dG-dC) and poly(dI-dC) Substrates (Figure 6A–C). We sought to determine the basis of Dnmt1's sinefungin-

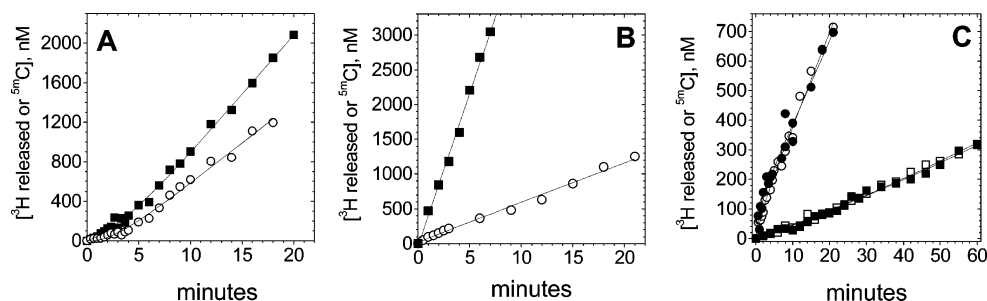


FIGURE 6: Methylation and tritium release profiles in the reaction with different DNA substrates. (A) Methylation (○) and tritium release (■) profiles with 12 μM bp ^3H -poly(dI-dC) (33 ± 2 cpm/pmol of bp) and 125 nM Dnmt1. (B) Methylation (○) and tritium release (■) with 12 μM bp ^3H -pmpoly(dI-dC) (19 ± 1.3 cpm/pmol of bp, $^{5\text{mC}}\text{C} = 1:14$) and 125 nM Dnmt1. (C) Methylation (●) and tritium release (○) profiles with 8 μM bp ^3H -pmpoly(dG-dC) (76 ± 5 cpm/pmol of bp, $^{5\text{mC}}\text{C} = 1:17$); methylation (■) and tritium release (□) profiles with 8 μM bp ^3H -poly(dG-dC) (102 ± 8 cpm/pmol of bp). The reactions with poly(dG-dC) and pmpoly(dG-dC) had 250 nM Dnmt1. All of reactions had 12.5 μM [^{14}C -methyl] AdoMet (131 cpm/pmol).

Table 2: (A) Exchange Rates with Unmethylated and Premethylated poly(dG-dC) and poly(dI-dC) with AdoMet Analogues and in the Absence of the Cofactor, for Dnmt1 and Small Bacterial Enzyme M.HhaI (28) and (B) Methylation and accompanying tritium release rates for Dnmt1 and bacterial enzyme M.HhaI (28)

(A)				
	sinefungin rates, h^{-1}	<i>N</i> -methyl-AdoMet rates h^{-1}	AdoHcy rates, h^{-1}	no cofactor rates, h^{-1}
Dnmt1 Exchange Rates, This Study				
poly(dG-dC)	3.5 ± 0.8	0.1 ± 0.02	<0.01	0.02 ± 0.001
poly(dI-dC)	42 ± 6	0.9 ± 0.1	0.1 ± 0.02	0.18 ± 0.02
pm-poly(dG-dC)	21 ± 4	0.5 ± 0.2	0.2 ± 0.05	0.08 ± 0.01
pm-poly(dI-dC)	438 ± 18	9 ± 0.8	2 ± 0.4	4.4 ± 0.5
M.HhaI exchange rates ^a				
poly(dG-dC)	500 ± 200	33 ± 5	0.1 ± 0.02	650 ± 200
	44 ± 3^b			105 ± 10^b
poly(dI-dC)	165 ± 20	145 ± 15	0.5 ± 0.005	10 ± 1
(B)				
	Dnmt1		M.HhaI	
	methylation rates, h^{-1}	exchange rates, h^{-1}	methylation rates, h^{-1}	exchange rates, h^{-1}
poly(dG-dC)	1.7 ± 0.4	1.5 ± 0.3	140 ± 20	146 ± 15
			40 ± 4^b	43 ± 4^b
poly(dI-dC)	37 ± 0.4	60 ± 2		
pm-poly(dG-dC)	8 ± 0.6	8.4 ± 0.6	65 ± 8	230 ± 25
pm-poly(dI-dC)	36 ± 0.5	257 ± 8		

^a M.HhaI shows no difference between premethylated and unmethylated substrates prepared for this study. ^b Pre-steady-state and steady-state values, respectively.

dependent preference for pm-poly(dI-dC), which is not revealed during methylation (Figure 3 vs Figure 5). Accordingly, we measured the methylation and accompanying tritium release reactions simultaneously (Figure 6A–C) using ^{14}C -AdoMet and DNA substrates labeled with tritium at the C⁵ position. On the basis of the reaction mechanism, every methyltransfer (Figure 1, **2** → **3A**) is expected to result in one tritium release (Figure 1, **3A** → **4A**) and the methylation and the accompanying tritium release rates are expected to be identical (28, 34). We observe this 1:1 stoichiometry in both the pre-steady-state and steady-state methylation reactions with poly(dG-dC) and pm-poly(dG-dC) (Figure 6C and Table 2). Thus, intermediate **2** (Figure 1) leads only to methyltransfer (Figure 1, **2** → **3A**) with poly(dG-dC) and pm-poly(dG-dC) substrates. In contrast, Dnmt1 like M.HhaI (Table 2) shows an excess release of tritium during the AdoMet-dependent methylation of poly(dI-dC) and pm-poly(dI-dC) (Figure 6A,B and Table 2). The faster tritium release in the methylation reaction during the first turnover indicates that proton transfer at C⁵ (Figure 1, **2** → **3B**) can take place before the methyltransfer step (Figure 1, **2** → **3A**)

(28). Furthermore, since a single target base attack can result in only one tritium release (Figure 1, **2** → **3B** → **4B**), the severalfold difference between the tritium release and the methylation rates indicates that the enzyme can attack and release several bases prior to catalyzing one methyl transfer (28). Thus, the target base activation (Figure 1, **1** → **2**) is fast, and there is a direct competition between the target base release (i.e., breakdown of intermediate **1**) and the rate-limiting methyltransfer step (**2** → **3A**, Figure 1). The difference between poly(dI-dC) and pm-poly(dI-dC) (Figure 6A vs 6B) indicates that intermediate **2** (Figure 1, **1** → **2**) is formed faster with pm-poly(dI-dC) as already indicated by the data in Figure 5.

H Inventory Studies (Figure 7A,B). The rate-limiting step during the Dnmt1 exchange reaction with different DNA substrates and AdoMet analogues (Table 2) is proton transfer at the C⁵ position, despite catalytic rates differing by 10–100-fold. We used H inventory studies to test whether the exchange reaction with sinefungin and different DNA substrates share the same rate-limiting step and catalytic intermediates despite large differences in the catalytic rates

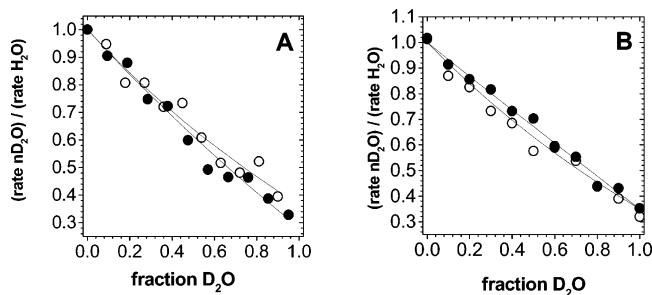


FIGURE 7: H inventory profiles during the exchange reaction with sinefungin and different DNA substrates. (A) The H inventory profiles for the exchange reaction with 10 μM bp poly(dG-dC) (○) and 10 μM bp premethylated poly(dG-dC) (●) in the presence of 20 μM sinefungin and 250 nM Dnmt1. The rates in H_2O and D_2O mixtures were measured during the first catalytic turnover (Figure 3B). (B) The H inventory profiles for the exchange reaction with 10 μM bp poly(dI-dC) (○) and 10 μM bp premethylated poly(dI-dC) (●) in the presence of 20 μM sinefungin and 250 nM Dnmt1. The rates in H_2O and D_2O mixtures were measured in the linear part of the reaction during multiple turnovers (Figure 3A). The data in both panels were analyzed using eq 3 as indicated in the text.

(Figure 7A,B). Proton inventory profiles are rate studies performed at varying D_2O and H_2O ratios (37) and are very sensitive to the reaction mechanism (28).

Using the Gross-Butler equation (eq 5; 37), we found that for all four DNA substrates the transition state fractionation factor (ϕ^T) is between 0.32 and 0.35 (0.35 \pm 0.03 poly(dI-dC); 0.30 \pm 0.05 pm-poly(dI-dC); 0.34 \pm 0.04 poly(dG-dC); 0.30 \pm 0.05 pm-poly(dG-dC)). The ground-state fractionation factor (ϕ^G) is between 2.1 and 2.4 [2.5 \pm 0.2 poly(dI-dC); 2.5 \pm 0.3 pm-poly(dI-dC); 2.3 \pm 0.3 poly(dG-dC); 2.5 \pm 0.3 pm-poly(dG-dC)]. The similar ϕ^T values suggest that reactions with the four different DNA substrates share the same rate-limiting step, while the similar ϕ^G values suggest that the reactions also share similar intermediates (37). The measured ϕ^T values are expected for reactions involving N–H–C proton bridges in the transition state (p 86 in ref 37). A N–H–C proton bridge could form between the amino group on sinefungin (Figure 2) and intermediate 2 (Figure 1) if the rate-limiting step is proton transfer from the cofactor to the carbon 5 (Figure 1, 2 \rightarrow 3B) as we suggested earlier (Table 2 and ref 28). Finally, the calculated ϕ^T and ϕ^G values are very similar to the values observed with M.HhaI (28), indicating that Dnmt1 and M.HhaI share similar proton inventory profiles in the exchange reaction with sinefungin. In summary, the proton inventory analysis indicates that Dnmt1's exchange reaction with different DNA substrates, as well as the exchange reaction by Dnmt1 and M.HhaI, can share the same intermediates and the rate-limiting step (Figure 1) even though the catalytic rates can vary by orders of magnitude (Table 2).

Fluorescence Titration of Dnmt1 with CRE a^Fb^m oligo (Figure 8). AdoMet binding by M.HhaI leads to a large conformational change, an increase in DNA binding affinity by 3 orders of magnitude (15), and a change in the mechanism of the target attack (28). We sought to determine if similar cofactor-mediated changes occur with Dnmt1. Dnmt1 interacts with hemimethylated DNA to form a 1:1 complex (7, 9), and replacing the target cytosine with 5-fluorocytosine (5FC) causes the methyl transfer (2 \rightarrow 3A, Figure 1) to be slowed considerably. Thus, 5FC provides an opportunity to investigate how AdoMet alters Dnmt1–DNA

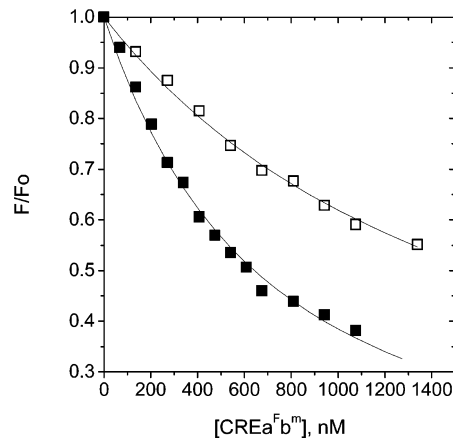


FIGURE 8: Fluorescence titration of Dnmt 1 with CRE a^Fb^m substrate. Equilibrium dissociation constant between 150 nM of Dnmt1 and increasing concentration of CRE a^Fb^m was measured in the presence of 12.5 μM of AdoMet (■), and in the absence of the cofactor (□) (100 mM Tris/HCl pH = 8.0, 10 mM EDTA, 10 mM DTT). Dnmt1 intrinsic fluorescence was measured in a microcuvette (sample slot 2 mm wide, 10 mm long) using a Perkin-Elmer LS50B fluorimeter at 25 $^\circ\text{C}$. The total sample volume was 220 μL . The excitation was set at 290 nm (5 nm slit band-pass), and the emission was monitored at 335 nm (10 nm band-pass). The profiles were analyzed using the eqs 4 and 5.

interactions when the enzyme is trapped in the form of transient catalytic intermediates 1 and 2 (Figure 1; 39). The DNA substrate was a 30-bp-long hemimethylated CRE ab^m substrate (7), and the binding was measured by following changes in intrinsic protein fluorescence as a function of increasing DNA concentration (see methods). The change in protein fluorescence caused by the Dnmt1–CRE a^Fb^m interaction can be described as an apparent dissociation constant of 1.56 \pm 0.2 μM and 0.6 \pm 0.08 μM (eq 4) for binding in the presence and in the absence of AdoMet, respectively. These values are very similar to the previous dissociation constants measured with Dnmt1 and CRE ab^m substrate (7, 9). In summary, unlike M.HhaI, AdoMet binding by Dnmt1 has minimal effects on its DNA binding affinity.

DISCUSSION

Substrate Inhibition by Dnmt1 Derives from the Turnover-Dependent Relief from Allosteric Inhibition. Our initial interest was to characterize why premethylated and unmethylated DNA show differential substrate inhibition (Figure 4A–C), differences in initial lags (Figure 3A,B) and catalytic rates (Table 1). The increased inhibition observed with increasing concentrations of unmethylated substrate (Figure 4A,B) is consistent with DNA binding at the active site and inhibition site (Figure 10C) as suggested in earlier studies (8). The kinetic lag correlates with the extent of substrate inhibition (Figures 3A,B and 4A–C) and is not due to our assay design. Slow relief from enzyme inhibition induced by the start of catalysis is known to lead to an initial lag (36, 38). Thus, we propose that the start of catalysis on unmethylated DNA initiates a slow relief from allosteric inhibition. The initial lag was not routinely described in prior kinetic studies of Dnmt1, in contrast to various forms of substrate inhibition; however, a lag is apparent in some cases (7, 26). The precise nature of this slow relief from allosteric inhibition remains obscure. Plausible driving forces include

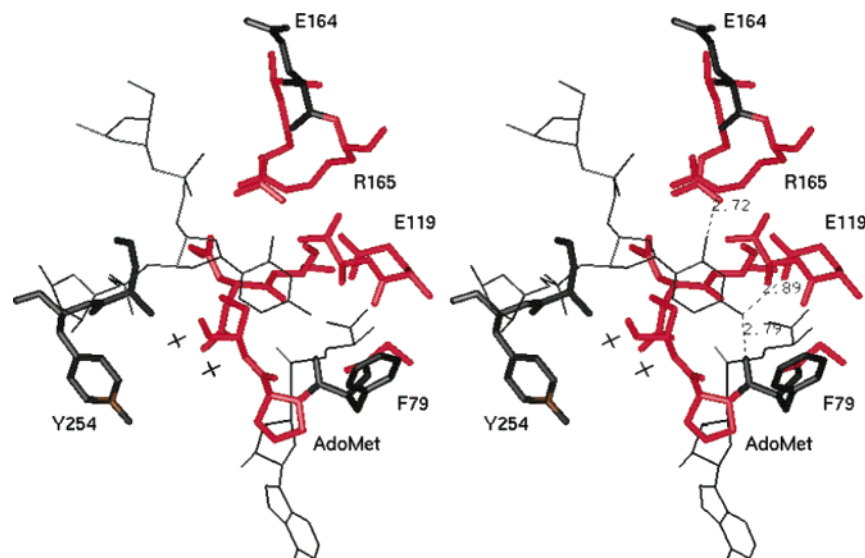


FIGURE 9: Sequence similarity between M.HhaI and Dnmt1 in the active site. Stereo figure (Biosym, InsightII) of M.HhaI active site (pdb code 3MHT, (53)). The target base and AdoMet are shown as thin lines, the amino acids forming the catalytic pocket are in bold. The AdoMet structure is taken from pdb file 6MHT (59) and superimposed onto the backbone of AdoHcy present in the original structure. Water molecules are indicated as crosses (+). The image was generated in an attempt to construct the Dnmt1 active site by mapping the M.HhaI and Dnmt1 sequences to the M.HhaI structure. The amino acids colored red are identical between M.HhaI and Dnmt1 and belong to the highly conserved domains of the methyltransferase family [motifs IV, VI, and X (60)]. Four residues, R¹⁶⁵, E¹¹⁹, F⁷⁹, and C⁸¹ make direct contact with the target base and mediate the methylation chemistry. Three of these four residues (R, E, and C) are found in M.HhaI and all known metazoan methyltransferases. F⁷⁹ forms a hydrogen bond between the backbone carbonyl oxygen and the C⁴ amine of the target base. F⁷⁹ in M.HhaI is replaced by P¹²³⁴ in Dnmt1.

AdoMet binding, DNA release from the site of inhibition, a combination of these two processes, or some other slow conformational change. AdoMet binding is the most likely factor since DNA inhibition is more pronounced at subsaturating AdoMet concentrations (11) and since the mutant lacking the functional regulatory domain shows different responses to changes in AdoMet concentration (11, 12) relative to the wild type. In summary, we propose that AdoMet binding to Dnmt1 initiates a slow relief from the allosteric inhibition; a slow relief from allosteric inhibition induced by ligand binding is well documented in the literature (40 and Figure 10D).

The lack of an initial lag with premethylated substrates (Figures 3A,B and 5A,B) indicates that there is no slow relief from allosteric inhibition at the start of catalysis. The reactions with the premethylated substrate show a pre-steady-state burst (Figure 3) as reported earlier for hemimethylated substrates (7). In general, the initial burst indicates that the steps leading to the detection step are faster than the steps following the detection step (p 274 in ref 43). Thus, the mild pre-steady-state burst indicates that for premethylated substrates the steps leading to intermediate **3A** (Figure 1) are rate-limiting during the initial target base attack, while the subsequent turnovers are partially controlled by formation of intermediate **3A** and by the steps that come after intermediate **3A**. This is consistent with the exchange results (Figures 5 and 6A,B) which showed that with the premethylated substrate the initial target base attack is fast and the rate-limiting step is primarily controlled by the methyltransfer step (Figure 1, **2** → **3A**).

Dnmt1 and M.HhaI Share Similar Reaction Intermediates and Rate-Limiting Steps. We previously used AdoMet analogues and poly(dG-dC) and poly(dI-dC) to study the reaction intermediates and rate-limiting steps of the M.HhaI-catalyzed reaction (28). We sought to apply this approach

to Dnmt1 to further characterize the enzyme's preference for premethylated DNA and allosteric regulation. The ability of Dnmt1 to catalyze the exchange reaction supports results from studies of 5FC inhibition (16) and shows that Dnmt1 has a similar catalytic mechanism as other pyrimidine methyltransferases (Figure 1; 44). Dnmt1 and M.HhaI share similarities in key aspects of the cytosine C⁵ exchange reaction, even though the catalytic rates can differ by 10–100 fold (Table 2). AdoMet analogues modulate the exchange rates by orders of magnitude for both Dnmt1 and M.HhaI (Table 2), indicating that the availability of proximal proton(s) (Figure 2B) in the position of the active methyl moiety is critical (Figure 1). Both Dnmt1 and M.HhaI (Table 2) cause an excess tritium release during the methylation reaction with poly(dI-dC) [and pm-poly(dI-dC), Figure 6A,B], while no excess tritium release is observed with poly(dG-dC) [and pm-poly(dG-dC), Figure 6C]. Finally, we also found that Dnmt1 and M.HhaI show similar proton inventory profiles in the exchange reaction with sinefungin (Figure 7A,B). On the basis of these similarities, we propose that, for both Dnmt1 and M.HhaI, the AdoMet analogues modulate the exchange rates by controlling the proton access at the C⁵ on intermediate **2** (Figure 2 and solvent in Figure 9). For both Dnmt1 and M.HhaI, intermediates leading to **1** and **2** accumulate as a dynamic equilibrium (Figure 1B), prior to the slow methyltransfer (Figure 1, **2** → **3A**), or proton-transfer step (Figure 1, **2** → **3B**). If Dnmt1 flips the target base like M.HhaI and other methyltransferases (45), the rapid equilibrium would include base flipping and base restacking steps, and the equilibrium between intermediates **1** and **2** (Figure 1B).

In the case of a rapid equilibrium between the steps leading to intermediates **1** and **2**, the observed catalytic rates are not solely dependent on a single rate-limiting event (28). Rather, the catalytic rates are simultaneously and independently

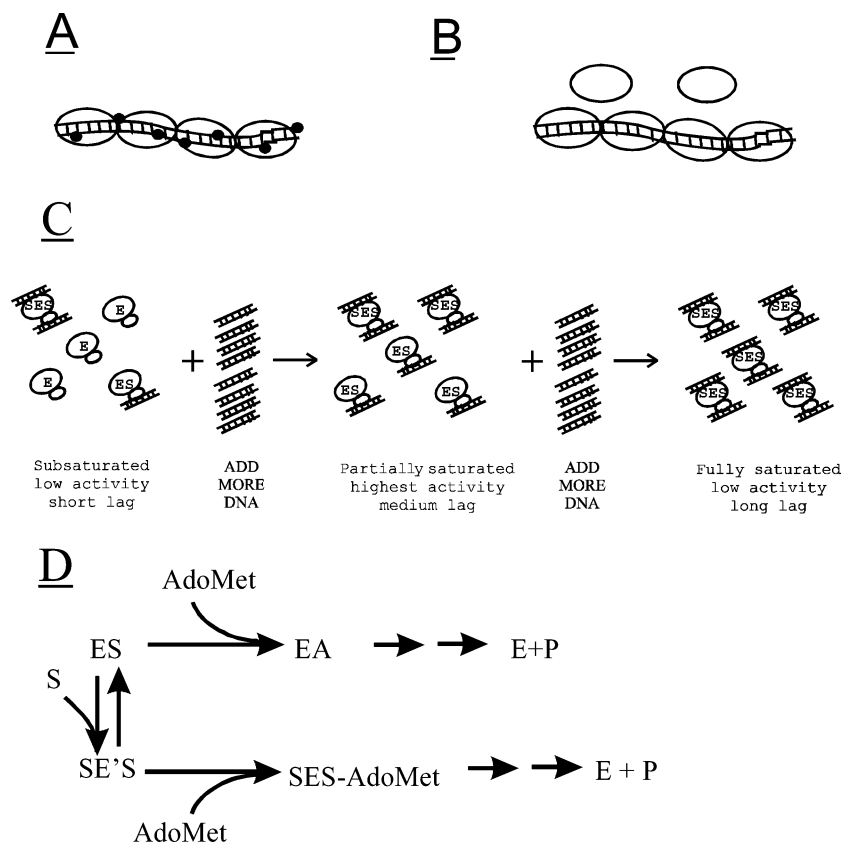


FIGURE 10: (A) Schematic for the interaction between Dnmt1 (oval) and its DNA substrate (rail). Dnmt1 bound on poly(dG-dC) or poly(dI-dC) with ^{5m}C groups (small filled circles) evenly distributed once or twice per enzyme footprint. (B) Given a DNA footprint of approximately 30 bp for Dnmt1 (7), a poly(dG-dC) substrate of 120 bp provides 120 CpG methylation sites but only enough flanking DNA to afford binding of approximately four Dnmt1 molecules. Thus, Dnmt1 and DNA are present in close stoichiometric concentrations (see appendix). Substrate concentrations are commonly represented in terms of CpG or CpI sites (12–14), or in terms of total concentration of long DNA molecules (7, 8, 10). In both cases, the Dnmt1 to DNA ratios need to be considered (see appendix). (C) The active site (small oval) and the allosteric site (large oval) on Dnmt1 can bind DNA independently (8, 11, 27). Dnmt1 (E) with DNA bound at the active site (ES), and the active site and the allosteric site (SES) at subsaturating and saturating DNA substrate as in Figures 4A–C. (D) AdoMet binding can initiate a relief from allosteric inhibition and slow transition between the inactive (SE'S) and active form (SES).

regulated by factors that control the concentrations of intermediates **1** and **2** (Figure 1), and by factors that control the methyl transfer (Figure 1, **2** → **3A**) or proton-transfer steps (**2** → **3B**). The methyl transfer rate (Figure 1, **2** → **3A**) is directly proportional to the lifetime of intermediate **2**, which in turn depends on the factors that control the equilibrium between intermediates **1** and **2**, like the pK_a of the active site cysteine (28). The lifetime of intermediate **1** is dependent on the ratio between base flipping and the base restacking rates, and the ratio between the conversion rates **1** → **2** and **2** → **1**. For illustration, the base flipping rate can be close to 200 s^{-1} (46), while the methyltransfer rate constants are less than 100 h^{-1} (Table 2). If the interchange between the intermediates is predominantly sequential (i.e., **A** → **B** → **C** → **D**) the base flipping rate can vary by 2 orders of magnitude without significantly affecting the methylation rates ($1/k_{\text{tot}} = 1/k_1 + 1/k_2 + 1/k_3 \dots$ etc.). However, if there is a rapid equilibrium between intermediates (i.e., **A** ↔ **B** → **C**) even a small change in the base flipping vs base restacking rate will affect the equilibrium concentration of intermediate **B** and consequently the rate of formation for the subsequent intermediates (i.e., $d[C]/dt = k[B]_{\text{eq}}$).

In the next few paragraphs, we use the concept of a dynamic equilibrium preceding the slow methyl transfer step to describe the factors that control Dnmt1's catalytic rates.

We describe the rate differences between premethylated and unmethylated substrates, the difference between poly(dI-dC) and poly(dG-dC) substrates (Table 2), and the difference between Dnmt1 and M.HhaI (Table 2).

The Dnmt1 Reaction with Premethylated and Unmethylated Substrates Differ in the Rate of Formation of the Covalent Intermediate. The unmethylated and premethylated substrates have different rates of target base attack (Figure 6A,B), yet the methyltransfer step is rate-limiting with both substrates (Figure 6A,B). The tritium exchange rates with sinefungin and premethylated and unmethylated substrates differ by 9-fold (Table 2), yet the proton inventory data show that both reactions are limited by proton transfer at cytosine C^5 (Figure 7A,B). The exchange rates with both premethylated and unmethylated substrates are modulated by orders of magnitude with various AdoMet analogues, yet the rates with the premethylated substrates are uniformly faster (Table 2). In summary, the difference between the unmethylated and premethylated substrates does not derive from the rate-limiting events on intermediate **2** (Figure 1, **2** → **3A** or **2** → **3B**). Rather, the difference derives from changes that favor the accumulation of intermediates **1** and **2** (Figure 6A,B).

Since each target base attack can lead to only one tritium release (Figure 1, **2** → **3B** → **4B**), severalfold higher exchange rates with the premethylated substrates (Figures 5 and 6A,B) indicate that intermediates **1** and **2** are formed

faster with premethylated DNA. In another words, the preference for the premethylated substrate must involve all steps leading to intermediates **1** and **2** (Figure 1B, 45). Interestingly, the exchange rates with unmethylated DNA are never as fast as with premethylated DNA (Figures 5 and 6A,B), despite the relief from inhibition observed after the lag. Thus, the enzyme's preference for premethylated DNA is determined by the interactions beyond the allosteric site, as earlier studies suggested (11).

Variations in the Rates of Covalent Intermediate Formation Account for the Differences between Dnmt1 and M.HhaI and between poly(dI-dC) and poly(dG-dC). Dnmt1's preference for poly(dI-dC) is unusual, resulting in rates comparable to those observed for M.HhaI (Table 2), in contrast to the 2 orders of magnitude difference in pre-steady-state methylation rates with poly(dG-dC) (Table 2 and (7)) or other DNA substrates (15). The preference for poly(dI-dC) cannot be caused by differences in the allosteric regulation since poly(dI-dC) shows faster rates than pm-poly(dG-dC), even though pm-poly(dG-dC) does not show substrate inhibition. Also, the Dnmt1 mutant lacking the functional allosteric site shows 3–18-fold slower rates with G:C-rich substrates relative to the poly(dI-dC) substrate (11, 12). The preference for poly(dI-dC) substrates is unlikely to result directly from faster catalytic processes at cytosine C⁵ (Figure 1, **2** → **3A** or **2** → **3B**) since the reactions with poly(dI-dC) are uniformly faster than poly(dG-dC), even though AdoMet analogues can modulate the exchange rates by 3 orders of magnitude (Table 2). Finally, the proton inventory studies (Figure 7A,B) suggest that all four DNA substrates share the same rate-limiting steps. In summary, our results indicate that the higher catalytic rates with poly(dI-dC) vs poly(dG-dC) (Tables 1 and 2) are not due to the differences in allosteric regulation or in the conversion of intermediates **2** → **3A** or **2** → **3B**. We therefore propose that variations in the accumulation of intermediates **1** and **2** (Figure 1) are most likely responsible. The crystal structures of I:C and G:C base pairs can be superimposed (47); however, unlike the G:C base pair, the I:C base pair has only two hydrogen bonds (Figure 2). Thus, a disruption of the I:C base pair during the base flipping process requires less energy, so it is tempting to attribute the faster rates with poly(dI-dC) substrate to a more favorable accumulation of "base-flipped" intermediate (Figure 1B).

Similar to the differences between Dnmt1 reactions with poly(dG-dC) and poly(dI-dC), the difference between Dnmt1 and M.HhaI can be traced to the accumulation of intermediates **1** and **2**. Dnmt1 and M.HhaI show similar rates with poly(dI-dC) substrates (Table 2); however, unlike Dnmt1, M.HhaI shows similar catalytic rates with poly(dI-dC) and poly(dG-dC) substrates (28). Thus, the relative slowness of Dnmt1 with poly(dG-dC) substrates accounts for the difference with M.HhaI (Table 2; 15). On the basis of our exchange reaction results (Figure 2, Table 2) and proton inventory studies (Figure 7), Dnmt1 and M.HhaI share the same mechanism with poly(dI-dC) and poly(dG-dC) once intermediates **1** and **2** are formed. Thus, the uniformly faster rates with M.HhaI (Table 2) must come from early steps leading to intermediates **1** and **2** (Figure 1B) rather than from methyltransfer (Figure 1, **2** → **3A**) or proton-transfer steps (Figure 1, **2** → **3B**).

³H Exchange Reaction and Mutagenic Deamination Share Reaction Intermediates. Mammalian DNA methylation sites are mutation hot spots, which frequently occur in critical cancer-related genes (48), as a result of deamination of cytosine to uracil, and 5-methylcytosine to thymine (Figure 1). Bacterial DNA cytosine methyltransferases are known to catalyze the mutagenic deamination of cytosine (49), and deamination rates are affected by AdoMet analogues (50, 51). The M.HhaI-catalyzed exchange and deamination reactions are affected by AdoMet analogues in the same fashion (28), supporting the idea that the two reactions share similar intermediates (Figure 1, **1** → **2** → **3B** → **3C** → **4C** and refs 44, 49–52). The deamination reaction is extremely slow and thus difficult to study mechanistically. We studied the Dnmt1-catalyzed exchange reaction to obtain insights into the enzyme's ability to catalyze this, and the related deamination reactions.

Cytosine C⁵ methyltransferases need to balance the solvent access at the active site (Figure 9) because the solvent forms part of the obligatory β -elimination step (Figure 1, **3B** → **3C**), and the solvent could lead to mutagenic deamination (Figure 1, **1** → **2** → **3B** → **3C** → **4C**). Intermediates **1** and **2** accumulate prior to the slow methyltransfer step (Figure 6A,B, and ref 28), thus enhancing the opportunity for solvent access to these intermediates. Intermediate **2** is readily protonated (Figure 1, **2** → **3B**, $pK_a = 11$ –18; 29), thereby increasing the mutagenic deamination process by at least 4 orders of magnitude (44). In the case of M.HhaI (28), the rate of excess tritium release in the methylation reaction with poly(dI-dC) is enhanced by the positioning of the active site loop (residues 80–99) and enzyme–DNA interactions with the guanine 5' to the target cytosine. Like M.HhaI, Dnmt1 shows excess tritium release in the methylation reaction with poly(dI-dC), but not with poly(dG-dC) (Figure 6A–C). Thus, for both Dnmt1 and M.HhaI, enzyme interactions with the guanine within the recognition site limit the solvent access to the active site, the exchange reaction, and presumably the mutagenic deamination (Figure 1, **1** → **2** → **3B** → **3C** → **4C**). Aside from the active site loop, the cofactor may also protect intermediates **1** and **2** from solvent (Table 2 and Figure 9). The slow ³H exchange reaction with AdoHcy (Table 2) indicates that for both M.HhaI and Dnmt1, the β -elimination step (Figure 1, **3A** → **4A**) is unlikely to take place through a direct solvent access to intermediate **2** ((53, 54) and Figure 9).

Factors that decrease the lifetime of the extrahelical base are likely to slow down both the exchange and mutagenic deamination reaction. For example, our proposal that Dnmt1 is slower than M.HhaI because intermediates **1** and **2** accumulate to a lesser extent would predict that Dnmt1 is less mutagenic than M.HhaI. In contrast to M.HhaI, the exchange reaction for Dnmt1 is very slow in the absence of cofactor (Table 2). Thus, Dnmt1 is unlikely to form intermediates **1** and **2** (Figure 1) in the absence of the cofactor. Accordingly, Dnmt1 is unlikely to efficiently deaminate cytosine in the absence of the cofactor, which is precisely the condition that shows the most extensive deamination for the majority of bacterial enzymes (49–52). Unlike M.HhaI (15), AdoMet binding by Dnmt1 does not lead to a large change in DNA binding affinity (Figure 8). Thus, cofactor binding by Dnmt1 may not induce the same active site closure as shown for M.HhaI (33).

Dnmt1 Is Not Self-Activated by the ^{5m}C Groups Deposited at the Start of the Methylation Reaction on Unmethylated Substrate. It is unclear from the current literature whether Dnmt1's preference for premethylated substrates derives from activation by the premethylated substrates, inhibition by unmethylated substrates, or some combination of these. Here we find that Dnmt1's preference for premethylated substrates derives from allosteric inhibition by unmethylated substrates, rather than allosteric activation by premethylated substrates. First, premethylated DNA (Figure 4C) does not show a sigmoidal curve which is characteristic of substrates that act as allosteric activators (pp 21–29 in ref 38 or pp 203–234 in ref 43). Second, our observation of a kinetic lag and the resultant "activation" during the sinefungin-mediated exchange reaction (Figure 5) indicates that the faster catalysis following the initial lag is not due to activation caused by the deposition of methyl groups at the start of catalysis (Figure 1). Finally, after 10 min of methylation (Figure 6A), the fraction of ^{5m}C becomes comparable to the fraction of ^{5m}C that is present in premethylated poly(dI-dC) ($^{5m}C:C = 1:12$); yet, we do not see a gradual increase in the tritium release rates to that observed with premethylated poly(dI-dC) (Figure 5, panel B vs A). In summary, at the start of catalysis when there is an excess of unmethylated DNA, the mere presence of ^{5m}C is not enough to induce higher catalytic rates with Dnmt1.

ACKNOWLEDGMENT

We wish to thank UCSB undergraduate students Jamie Witham, Ben Hopkins, and Stephen Fiocco for their excellent help in these experiments. We are grateful to Prof. H. Olin Spivey from Oklahoma State University, Dr. Sriharsa Pradhan at New England Biolabs, and Dr. Albino Bacolla at Texas A&M University for their correspondence during these studies. We are grateful to Prof. Nancy C. Horton at University of Arizona for help in the molecular modeling studies. We gratefully acknowledge Ana M. Ojeda and Dr. Peter Vollmyer for help in purifying Dnmt1.

APPENDIX

Limitation of Michaelis–Menten Kinetics in Dnmt1 Studies and Alternative Approaches in Assay Design. Michaelis–Menten kinetics requires an excess of substrate over enzyme, an initial linear reaction profile, and multiple catalytic turnovers (43), all of which are often impossible, or very difficult to achieve with exceptionally slow enzymes such as Dnmt1 (Table 1). The slow catalytic rates require that Dnmt1 concentrations are often comparable to the varied substrate concentration (Figure 10B) (7–9, 11, 12, 24, 27, 55). Thus, competitive and noncompetitive patterns in double reciprocal plots, and the calculated K_m , k_{cat} , and K_i constants reflect the enzyme/DNA ratios and assay design, rather than the kinetic properties of Dnmt1. Accordingly, some of the earlier conclusions regarding the catalytic properties of Dnmt1 should be reevaluated. Similar concerns apply to Dnmt3 studies (56). We did not use Michaelis–Menten kinetics to analyze our data or the previously published results (Table 1 and refs 7, 8, 10–12, 14, 24, 55). We find a satisfying consensus between different Dnmt1 studies when Michaelis–Menten kinetics is not used for data interpretation (Table 1).

In the earlier studies (7, 8, 10–12, 14, 24, 55), as in Figure 4, at low DNA concentrations (i.e., less than one 30 bp segment per each Dnmt1 molecule, Figure 10 B), there is an excess Dnmt1 (Figure 10C) and catalytic rates are low since only a small fraction of Dnmt1 can bind DNA (ES and SES forms in Figure 10C). Further increases in DNA concentration increase the ES and SES forms and result in higher catalytic rates (Figure 10C). The highest catalytic rates are achieved when the ES form predominates relative to the E, ES, and SES forms (Figure 10C). Once the maximal rates are achieved, a further increase in DNA concentration results primarily in the conversion of the ES to SES form and the visible substrate inhibition (Figure 10C). The fastest rates in Figure 4 and in prior work with similar substrates are attained when 30–60 base pairs of DNA are present per Dnmt1 molecule.

The inability to use Michaelis–Menten kinetics in Dnmt1 studies requires the development of alternative approaches. Briefly, we suggest that Dnmt1 catalytic rates with different DNA substrates should be measured as a function of increasing substrate concentration (as in Figure 4A–C) until full saturation is achieved (as in Figure 10B). This reveals the highest catalytic rates attainable with the tested DNA substrate, and any allosteric inhibition (Figure 4A,B), the lack of allosteric inhibition (Figure 4C), or allosteric activation. If allosteric activation occurs, a change in substrate concentration will give a characteristic sigmoidal change in catalytic rates (38, 43). Studies reporting the allosteric activation of Dnmt1 were not designed to differentiate between the lack of allosteric inhibition (Figure 4C vs Figure 4A,B) from true allosteric activation. Allosteric inhibition was the first and to this day the most consistent and credible evidence of allosteric regulation of Dnmt1 (7, 8, 10, 11, 14, 20, 26, 57). A clear inhibition pattern as observed in Figure 4A,B can be seen only when DNA binding affinity at the allosteric site is higher than the binding affinity at the active site. Thus, in some cases detecting allosteric inhibition can require additional experiments (8). When comparing catalytic rates with different DNA substrates it is necessary to separate initial lag effects or other nonlinear effects such as processivity (41, 42) so that different DNA substrates can be compared at equivalent first turnover or multiple turnover stages.

Since it is not possible to measure K_m values for DNA substrates, Dnmt1's preference for DNA substrates has to be determined by measuring binding constants in addition to the catalytic rates. With poly(dG-dC) and poly(dI-dC), formation of ES and SES species is relatively easy to track (Figure 10C). Both substrates show the initial lag even at subsaturating substrate concentration (Figure 3 and Figure 4), indicating that the active site and the allosteric site have similar binding affinities for poly(dG-dC) and poly(dI-dC) (Figure 10C). The change in the lag transition rates (eq 2, k_l) and the catalytic rates as a function of the substrate concentration (Figure 4A,B) can be used with the Adair's equation (58) for quantitative determination of the fraction of enzyme molecules present in E, ES, and SES form (Figure 10C), and DNA binding constant for the active site and the allosteric site. Furthermore, experiments such as those shown in Figure 4A–C can be used to test for competitive or uncompetitive inhibitors with regard to DNA substrate. However, such data cannot be analyzed with double recipro-

cal plots, and in such experiments it is necessary to make sure that the chosen substrate and competitor concentration can allow the full range of competition (Figure 10B).

REFERENCES

- Li, E., Bestor, T. H., and Jaenisch, R. (1992) Targeted mutation of the DNA methyltransferase gene results in embryonic lethality, *Cell* 69, 915–926.
- Ahuja, N., Li, Q., Mohan, A. L., Baylin, S. B., and Issa, J. P. (1998) Aging and DNA methylation in colorectal mucosa and cancer, *Cancer Res.* 58, 5489–5494.
- Cunningham, J. M., Christensen, E. R., Tester, D. J., Kim, C. Y., Roche, P. C., Burgart, L. J., and Thibodeau, S. N. (1998) Hypermethylation of the hMLH1 promoter in colon cancer with microsatellite instability, *Cancer Res.* 58, 3455–3460.
- Kane, M. F., Loda, M., Gaida, G. M., Lipman, J., Mishra, R., Goldman, H., Jessup, J. M., and Kolodner, R. (1997) Methylation of the hMLH1 promoter correlates with lack of expression of hMLH1 in sporadic colon tumors and mismatch repair-defective human tumor cell lines, *Cancer Res.* 57, 808–811.
- Veigl, M. L., Kasturi, L., Olechnowicz, J., Ma, A. H., Lutterbaugh, J. D., Periyasamy, S., Li, G. M., Drummond, J., Modrich, P. L., Sedwick, W. D., and Markowitz, S. D. (1998) Biallelic inactivation of hMLH1 by epigenetic gene silencing, a novel mechanism causing human MSI cancers, *Proc. Natl. Acad. Sci., U.S.A.* 95, 8698–8702.
- Egger, G., Liang, G., Aparicio, A., and Jones, P. A. (2004) Epigenetics in human disease and prospects for epigenetic therapy, *Nature* 429, 457–463.
- Flynn, J., Glickman, J. F., and Reich, N. O. (1996) Murine DNA cytosine-C5 methyltransferase: pre-steady- and steady-state kinetic analysis with regulatory DNA sequences, *Biochemistry* 35, 7308–7315.
- Flynn, J., Fang, J. Y., Mikovits, J. A., and Reich, N. O. (2003) A potent cell-active allosteric inhibitor of murine DNA cytosine C5 methyltransferase, *J. Biol. Chem.* 278, 8238–8243.
- Flynn, J., Azzam, R., and Reich, N. (1998) DNA binding discrimination of the murine DNA cytosine-C5 methyltransferase, *J. Mol. Biol.* 279, 101–116.
- Flynn, J., and Reich, N. (1998) Murine DNA (cytosine-5)-methyltransferase: steady-state and substrate trapping analyses of the kinetic mechanism, *Biochemistry* 37, 15162–15169.
- Bacolla, A., Pradhan, S., Larson, J. E., Roberts, R. J., and Wells, R. D. (2001) Recombinant human DNA (cytosine-5) methyltransferase. III. Allosteric control, reaction order, and influence of plasmid topology and triplet repeat length on methylation of the fragile X CCG.CCG sequence, *J. Biol. Chem.* 276, 18605–18613.
- Bacolla, A., Pradhan, S., Roberts, R. J., and Wells, R. D. (1999) Recombinant human DNA (cytosine-5) methyltransferase. II. Steady-state kinetics reveal allosteric activation by methylated DNA, *J. Biol. Chem.* 274, 33011–33019.
- Pradhan, S., and Roberts, R. J. (2000) Hybrid mouse-prokaryotic DNA (cytosine-5) methyltransferases retain the specificity of the parental C-terminal domain, *EMBO J.* 19, 2103–2114.
- Pradhan, S., Bacolla, A., Wells, R. D., and Roberts, R. J. (1999) Recombinant human DNA (cytosine-5) methyltransferase. I. Expression, purification, and comparison of de novo and maintenance methylation, *J. Biol. Chem.* 274, 33002–33010.
- Lindstrom, W. M., Jr., Flynn, J., and Reich, N. O. (2000) Reconciling structure and function in HhaI DNA cytosine-C-5 methyltransferase, *J. Biol. Chem.* 275, 4912–4919.
- Yoder, J. A., Soman, N. S., Verdine, G. L., and Bestor, T. H. (1997) DNA (cytosine-5)-methyltransferases in mouse cells and tissues. Studies with a mechanism-based probe, *J. Mol. Biol.* 270, 385–395.
- Pradhan, S., and Esteve, P. O. (2003) Mammalian DNA (cytosine-5) methyltransferases and their expression, *Clin. Immunol.* 109, 6–16.
- Lauster, R., Trautner, T. A., and Noyer-Weidner, M. (1989) Cytosine-specific type II DNA methyltransferases. A conserved enzyme core with variable target-recognizing domains, *J. Mol. Biol.* 206, 305–312.
- Glickman, J. F., Pavlovich, J. G., and Reich, N. O. (1997) Peptide mapping of the murine DNA methyltransferase reveals a major phosphorylation site and the start of translation, *J. Biol. Chem.* 272, 17851–17857.
- Bestor, T. H. (1992) Activation of mammalian DNA methyltransferase by cleavage of a Zn binding regulatory domain, *EMBO J.* 11, 2611–2617.
- Bestor, T. H., and Verdine, G. L. (1994) DNA methyltransferases, *Curr. Opin. Cell Biol.* 6, 380–389.
- Chuang, L. S., Ian, H. I., Koh, T. W., Ng, H. H., Xu, G., and Li, B. F. (1997) Human DNA-(cytosine-5) methyltransferase-PCNA complex as a target for p21WAF1, *Science* 277, 1996–2000.
- Leonhardt, H., Page, A. W., Weier, H. U., and Bestor, T. H. (1992) A targeting sequence directs DNA methyltransferase to sites of DNA replication in mammalian nuclei, *Cell* 71, 865–873.
- Aubol, B. E., and Reich, N. O. (2003) Murine DNA cytosine C(5)-methyltransferase: in vitro studies of de novo methylation spreading, *Biochem. Biophys. Res. Commun.* 310, 209–214.
- Jones, P. A., and Takai, D. (2001) The role of DNA methylation in mammalian epigenetics, *Science* 293, 1068–1070.
- Pedrali-Noy, G., and Weissbach, A. (1986) Mammalian DNA methyltransferases prefer poly(dI-dC) as substrate, *J. Biol. Chem.* 261, 7600–7602.
- Pradhan, S., and Esteve, P. O. (2003) Allosteric activator domain of maintenance human DNA (cytosine-5) methyltransferase and its role in methylation spreading, *Biochemistry* 42, 5321–5332.
- Svedruzic, Z. M., and Reich, N. O. (2004) The Mechanism of Target Base Attack in DNA Cytosine Carbon 5 Methylation, *Biochemistry* 43, 11460–11473.
- Perakyla, M. (1998) A Model Study of the Enzyme-Catalyzed Cytosine Methylation Using ab Initio Quantum Mechanical and Density Functional Theory Calculations: pK_a of the Cytosine N3 in the Intermediates and Transition States of the Reaction, *J. Am. Chem. Soc.* 120, 12895–12902.
- Brueckner, B., and Lyko, F. (2004) DNA methyltransferase inhibitors: old and new drugs for an epigenetic cancer therapy, *Trends Pharmacol. Sci.* 25, 551–554.
- Reich, N. O., and Everett, E. A. (1990) Identification of peptides involved in S-adenosylmethionine binding in the EcoRI DNA methylase. Photoaffinity labeling with 8-azido-S-adenosylmethionine, *J. Biol. Chem.* 265, 8929–8934.
- Xu, G., Flynn, J., Glickman, J. F., and Reich, N. O. (1995) Purification and stabilization of mouse DNA methyltransferase, *Biochem. Biophys. Res. Commun.* 207, 544–551.
- Klimasauskas, S., Kumar, S., Roberts, R. J., and Cheng, X. (1994) HhaI methyltransferase flips its target base out of the DNA helix, *Cell* 76, 357–369.
- Wu, J. C., and Santi, D. V. (1987) Kinetic and catalytic mechanism of HhaI methyltransferase, *J. Biol. Chem.* 262, 4778–4786.
- Johnson, K. A. (1992) in *The Enzymes* (Boyer, P. A., Ed.), Academic Press, Inc., New York.
- Frieden, C. (1970) Kinetic aspects of regulation of metabolic processes. The hysteretic enzyme concept, *J. Biol. Chem.* 245, 5788–5799.
- Quinn, D. M., and Sutton, L. D. (1991) in *Enzyme Mechanism from Isotope Effects* (Cook, P. F., Ed.) pp 73–126, CRC Press, Boca Raton, FL.
- Tipton, K. F. (2002) in *Practical Approach* (Eisenthal, R., and Danson, M. J., Eds.) p 282, Oxford University Press.
- Klimasauskas, S., Szyperki, T., Serva, S., and Wutrich, K. (1998) Dynamic modes of the flipped-out cytosine during HhaI methyltransferase-DNA interactions in solution, *EMBO J.* 17, 317–324.
- Neet, K. E. (1995) Cooperativity in enzyme function: equilibrium and kinetic aspects, *Methods Enzymol.* 249, 519–567.
- Vilkaitis, G., Suetake, I., Klimasauskas, S., and Tajima, S. (2005) Processive Methylation of Hemimethylated CpG Sites by Mouse Dnmt1 DNA Methyltransferase, *J. Biol. Chem.* 280, 64–72.
- Hermann, A., Goyal, R., and Jeltsch, A. (2004) The Dnmt1 DNA-(cytosine-C5)-methyltransferase methylates DNA processively with high preference for hemimethylated target sites, *J. Biol. Chem.* 279, 48350–48359.
- Cornish-Bowden, A. (1999) *Fundamentals of Enzyme Kinetics*, Portland Press.
- Ivanetich, K. M., and Santi, D. V. (1992) 5,6-dihydropyrimidine adducts in the reactions and interactions of pyrimidines with proteins, *Prog. Nucleic Acid Res. Mol. Biol.* 42, 127–156.
- Roberts, R. J., and Cheng, X. (1998) Base flipping, *Annu. Rev. Biochem.* 67, 181–198.
- Allan, B. W., Reich, N. O., and Beechem, J. M. (1999) Measurement of the absolute temporal coupling between DNA binding and base flipping, *Biochemistry* 38, 5308–5314.

47. Kumar, V. D., Harrison, R. W., Andrews, L. C., and Weber, I. T. (1992) Crystal structure at 1.5-Å resolution of d(CGICICIG), an octanucleotide containing inosine, and its comparison with d(CGCG) and d(CGCGCG) structures, *Biochemistry* *31*, 1541–1550.
48. Pfeifer, G. P., Tang, M., and Denissenko, M. F. (2000) in *DNA Methylation and Cancer* (Johns, P. A., and Vogt, P. K., Eds.) pp 1–19, Springer-Verlag.
49. Shen, J. C., Rideout, W. M. d., and Jones, P. A. (1992) High-frequency mutagenesis by a DNA methyltransferase, *Cell* *71*, 1073–1080.
50. Zingg, J. M., Shen, J. C., and Jones, P. A. (1998) Enzyme-mediated cytosine deamination by the bacterial methyltransferase M.MspI, *Biochem. J.* *332*, 223–230.
51. Zingg, J. M., Shen, J. C., Yang, A. S., Rapoport, H., and Jones, P. A. (1996) Methylation inhibitors can increase the rate of cytosine deamination by (cytosine-5)-DNA methyltransferase, *Nucleic Acids Res.* *24*, 3267–3275.
52. Gabbara, S., Sheluho, D., and Bhagwat, A. S. (1995) Cytosine methyltransferase from *Escherichia coli* in which active site cysteine is replaced with serine is partially active, *Biochemistry* *34*, 8914–8923.
53. O’Gara, M., Klimasauskas, S., Roberts, R. J., and Cheng, X. (1996) Enzymatic C5-cytosine methylation of DNA: mechanistic implications of new crystal structures for HhaI methyltransferase-DNA-AdoHcy complexes, *J. Mol. Biol.* *261*, 634–645.
54. Lau, E. Y., and Bruice, T. C. (1999) Active site dynamics of the HhaI methyltransferase: insights from computer simulation, *J. Mol. Biol.* *293*, 9–18.
55. Fatemi, M., Hermann, A., Pradhan, S., and Jeltsch, A. (2001) The activity of the murine DNA methyltransferase Dnmt1 is controlled by interaction of the catalytic domain with the N-terminal part of the enzyme leading to an allosteric activation of the enzyme after binding to methylated DNA, *J. Mol. Biol.* *309*, 1189–1199.
56. Yokochi, T., and Robertson, K. D. (2002) Preferential methylation of unmethylated DNA by Mammalian de novo DNA methyltransferase Dnmt3a, *J. Biol. Chem.* *277*, 11735–11745.
57. Glickman, J. F., and Reich, N. O. (1994) Baculovirus-mediated high level expression of a mammalian DNA methyltransferase, *Biochem. Biophys. Res. Commun.* *204*, 1003–1008.
58. vanHolde, K. E., Johnson, W. C., and Ho, P. S. (1998) *Principles of Physical Biochemistry*, 1st ed., Prentice Hall.
59. Kumar, S., Horton, J. R., Jones, G. D., Walker, R. T., Roberts, R. J., and Cheng, X. (1997) DNA containing 4’-thio-2’-deoxycytidine inhibits methylation by HhaI methyltransferase, *Nucleic Acids Res.* *25*, 2773–2783.
60. Kumar, S., Cheng, X., Klimasauskas, S., Mi, S., Posfai, J., Roberts, R. J., and Wilson, G. G. (1994) The DNA (cytosine-5) methyltransferases, *Nucleic Acids Res.* *22*, 1–10.

BI050295Z

The Mechanism of Target Base Attack in DNA Cytosine Carbon 5 Methylation[†]Željko M. Svedružić[‡] and Norbert O. Reich*

Department of Chemistry and Biochemistry, University of California, Santa Barbara, California 93106

Received February 12, 2004; Revised Manuscript Received July 1, 2004

ABSTRACT: We measured the tritium exchange reaction on cytosine C⁵ in the presence of AdoMet analogues to investigate the catalytic mechanism of the bacterial DNA cytosine methyltransferase M.HhaI. Poly-(dG-dC) and poly(dI-dC) substrates were used to investigate the function of the active site loop (residues 80–99), stability of the extrahelical base, base flipping mechanism, and processivity on DNA substrates. On the basis of several experimental approaches, we show that methyl transfer is the rate-limiting pre-steady-state step. Further, we show that the active site loop opening contributes to the rate-limiting step during multiple cycles of catalysis. Target base activation and nucleophilic attack by cysteine 81 are fast and readily reversible. Thus, the reaction intermediates involving the activated target base and the extrahelical base are in equilibrium and accumulate prior to the slow methyl transfer step. The stability of the activated target base depends on the active site loop closure, which is dependent on the hydrogen bond between isoleucine 86 and the guanine 5' to the target cytosine. These interactions prevent the premature release of the extrahelical base and uncontrolled solvent access; the latter modulates the exchange reaction and, by implication, the mutagenic deamination reaction. The processive catalysis by M.HhaI is also regulated by the interaction between isoleucine 86 and the DNA substrate. Nucleophilic attack by cysteine 81 is partially rate limiting when the target base is not fully stabilized in the extrahelical position, as observed during the reaction with the Gln²³⁷Trp mutant or in the cytosine C⁵ exchange reaction in the absence of the cofactor.

Enzymatic pyrimidine methylation is essential for diverse biological pathways including gene regulation, DNA and RNA biosynthesis, DNA repair, and protection against foreign DNA (1–3). Not surprisingly, the folate- and *S*-adenosylmethionine-dependent methyltransferases involved in these processes are the targets of antibiotics, cancer chemotherapies, and other drugs (4, 5). Enzymatic activation of the pyrimidine ring occurs by various mechanisms, with the single common feature being formation of a covalent intermediate between the enzyme and the pyrimidine C⁶ position. *S*-Adenosylmethionine-dependent DNA cytosine methyltransferases represent a broad, structurally and mechanistically characterized family of enzymes (4). M.HhaI¹ (methyltransferase *Haemophilus haemolyticus* type I) was the first AdoMet-dependent enzyme to be structurally characterized (6, 7) and provides a paradigm not only for AdoMet-dependent enzymes but for enzymes that induce



FIGURE 1: Four steps leading to methylation or exchange by DNA cytosine methyltransferases. The exchange reaction is proposed to share all steps up to the transfer of a proton in place of a methyl moiety. The equilibrium steps up to and including covalent adduct formation are implied by the results in this work.

dramatic conformational changes within their duplex DNA substrate (8, 9). M.HhaI methylates the underlined cytosine in duplex DNA (GCGC), stabilizing the cytosine into an extrahelical position residing within the active site of the enzyme (Figure 1).

Formation of the ternary M.HhaI·DNA·AdoMet complex is followed by at least three steps leading to product formation, outlined in Figure 1: base flipping, covalent adduct formation, and methyl transfer. We and others have studied this process in detail for M.HhaI (9, 10), as well as other DNA methyltransferases (11, 12). In contrast to the detailed structural information available for M.HhaI (8), little is known about the kinetics of these steps. For example, the flipping and methyl transfer kinetics have been directly measured for M.EcoRI (11–13), an adenine methyltransferase, but other than similar experiments with mismatched DNA (14), no such measurements have been made for M.HhaI. ¹⁹F NMR and gel shifting evidence support the existence of two M.HhaI·DNA intermediates involving an extrahelical cytosine, one of which is stabilized by the presence of the cofactor (15); however, these experiments provide limited mechanistic insights since they represent largely static descriptions and use 5-fluorocytosine, which

[†] This work was supported by NIH Grant GM 463333 and NSF Grant MCB-9983125 to N.O.R.

* To whom correspondence should be addressed: e-mail, reich@chem.ucsb.edu; tel, 805-893-8368; fax, 805-893-4120.

[‡] Current address: School of Molecular Biosciences, Department of Biophysics and Biochemistry, Washington State University, Pullman, WA 99164.

¹ Abbreviations: AdoMet, *S*-adenosyl-L-methionine; AdoHcy, *S*-adenosyl-L-homocysteine; bp, base pair; C⁵, C², C⁴, etc., carbon 5, carbon 2, carbon 4, etc. of the target base ring; ^{5m}C, 5-methyl-2'-deoxycytosine; dCTP, deoxycytosine triphosphate; poly(dG-dC) or dGdC, double-stranded alternating polymer of deoxyguanine and deoxycytosine; dTTP, deoxythymine triphosphate; M.HhaI, methyltransferase *Haemophilus haemolyticus* type I; M.SssI, methyltransferase *Spiroplasma* sp. type I; poly(dI-dC) or dIdC, double-stranded alternating polymer of deoxyinosine and deoxycytosine; pss, pre steady state; ss, steady state; sin, sinefungin; WT, wild type; N-AdoMet, *N*-methyl-AdoMet.

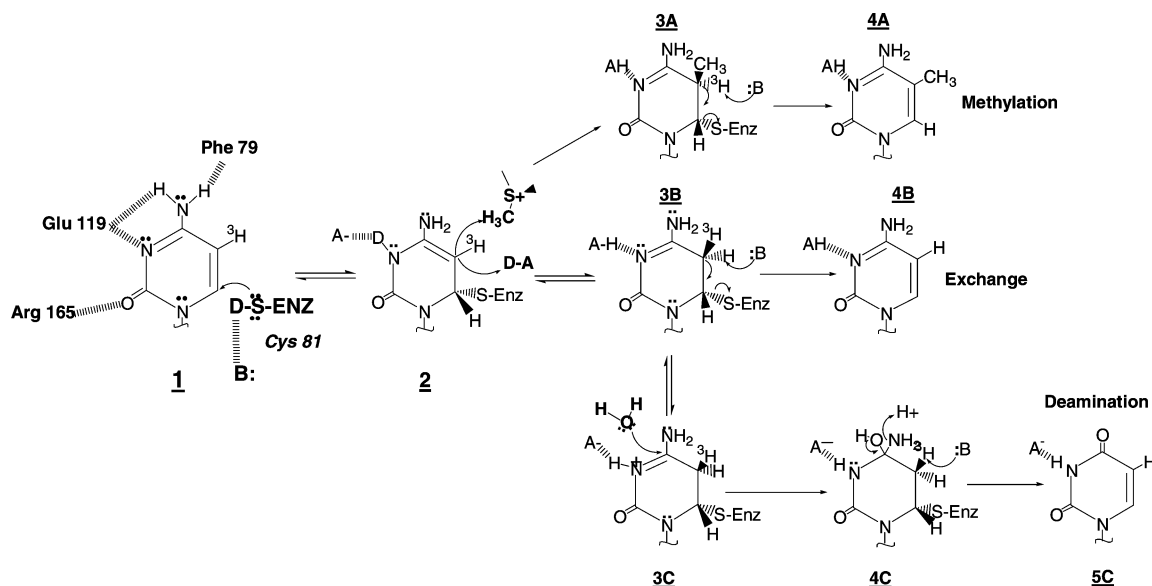


FIGURE 2: Reactions catalyzed by cytosine methyltransferases: methylation (A), ^3H exchange (B), and deamination (C). The extrahelical cytosine interacts with active site amino acids that facilitate cysteine 81 nucleophilic attack at cytosine C^6 (intermediate **1**). Nucleophilic attack disrupts the pyrimidine's aromaticity, forming intermediate **2**. Intermediate **2** can readily undergo electrophilic addition, either through methylation (**3A**) or protonation (**3B**). The 5,6-dihydropyrimidine adduct (**3B**) can lead to the exchange reaction (**4B**) or be attacked by water to form intermediate **4C**, which can lead to elimination of NH_3 and mutagenic deamination (**5C**). Acidic groups are labeled as HA and basic groups as :B. All exchangeable protons that can cause SKIE are shown as D in the intermediates (**1** and **2**). ^3H exchange rates are measured by acid quench; thus the ^3H exchange reaction is detected as soon as intermediate **3A** or **3B** is formed. The methylation reaction is detected as soon as intermediate **3A** is formed. For both reactions the pre steady states are steps that lead to intermediate **3A** (and **3B** for exchange), while the steady-state rates include the subsequent steps (see Methods).

severely perturbs the kinetics of attack and methyl transfer (10). Single-turnover measurements with M.HhaI show that the methyl transfer step, or some prior transition, has a rate constant of $0.14\text{--}0.26\text{ s}^{-1}$ (9, 10), and the methylation reaction shows a pre-steady-state burst, suggesting that methyl transfer is followed by slow product release steps (9, 10).

We refer to the base flipping and covalent adduct formation as the "target base attack" steps which serve to activate the cytosine to displace the electrophilic methylsulfonium on AdoMet (Figure 2). The proposed mechanism in Figure 2 is based largely on three lines of evidence: (1) structural and mechanistic parallels with the well-studied folate-dependent thymidylate synthetase (16), (2) structure–function studies of M.HhaI (7, 17) and other DNA cytosine methyltransferases (8), and (3) theoretical studies (18). However, details involving individual steps, the identity of the functionalities involved, and the relative contribution to rate-limiting steps remain uncertain. For example, Arg¹⁶⁵, Glu¹¹⁹, and Phe⁷⁹ are clearly positioned to interact with the cytosine as shown in Figure 1. Yet, the proposal that the nucleophilic attack by cysteine 81 is assisted by protonation at the cytosine N^3 , rather than the cytosine O^2 (18) (or both), has no experimental support. Similarly, there is little evidence for the existence, identity, or importance of moieties involved in acid- and base-assisted catalysis to facilitate the β -elimination step (Figure 2). Protein engineering efforts to determine the mechanisms of base flipping and stabilization include the interaction between glutamine 237 and the orphan guanosine (19); although the mutants retained function, albeit reduced ~ 50 -fold, the underlying mechanisms were not determined.

M.HhaI catalyzes the exchange of the cytosine C^5 hydrogen (17), which is compelling evidence for the proposed

mechanism and cysteinylcytosine covalent intermediate (Figure 2). Moreover, because this reaction occurs in the absence of cofactors and is inhibited by *S*-adenosylhomocysteine (17), it supports methods of study not suitable for the methylation reaction itself. No evidence for the exchange reaction during AdoMet-dependent steady-state methylation was described for M.HhaI (17) or for M.EcoRII, the only other DCMTase studied by this method (20); rather, M.HhaI simply replaces the C^5 proton with a methyl group (Figure 2). Bacterial DCMTases catalyze the deamination of cytosine to uracil and of 5-methylcytosine to thymine (Figure 2 and refs 21–23). This mutagenic reaction, if catalyzed by human DCMTases, is postulated to account in part for the high level of CG to TG mutations that occur within critical genes in human cancers (24).

We describe pre-steady-state, steady-state, pH, and solvent kinetic isotope effect (SKIE) studies of the methylation and ^3H exchange reactions using structural analogues of the DNA and cofactor, AdoMet. The exchange reaction provides unique opportunities because the mechanistic importance of the cofactor can be readily probed with analogues. We used poly(dI-dC) and poly(dG-dC) in our analysis because (i) these substrates allow a quantitative analysis since every enzyme molecule can bind a recognition site and proceed with catalysis, and (ii) the preparation of DNA substrates containing a single radiolabeled [^3H]cytosine is problematic and provides a less sensitive measure of catalysis (20). Poly(dI-dC) and the Gln²³⁷Trp mutant provide unique opportunities to study the base flipping step and stabilization of the extrahelical cytosine. Pre-steady-state kinetic, pH, and SKIE studies were used to determine the importance of cysteine 81 toward the rate-limiting events during target base attack, methylation, and exchange.

EXPERIMENTAL PROCEDURES

Materials

S-Adenosyl-L-[methyl-¹⁴C]methionine (59 mCi/mmol or 131 cpm/pmol), S-adenosyl-L-[methyl-³H]methionine (66–82 Ci/mmol or 6100–7200 cpm/pmol), deoxy[5-³H]cytidine 5'-triphosphate (19.0 Ci/mmol) ammonium salt, and Sequenase 2.0 were purchased from Amersham Corp. Poly(dI-dC), 1960 bp, dITP, and dCTP were purchased from Pharmacia Biotech. DTT, Trizma, and acid-washed activated charcoal were purchased from Sigma Chemical Co. BSA was purchased from Boehringer Mannheim, and it was DNA free on the basis of the absorbance ratio at 280 and 260 nm. DE81 filters were purchased from Whatman, Inc. Sinefungin was purchased from Sigma Chemical Co. AdoMet (85% pure) was purchased from Sigma Chemical Co. and HPLC purified as described earlier (25). WT M.HhaI and the Gln²³⁷Trp²³⁷ mutant were expressed using *Escherichia coli* strain ER1727 containing plasmids pHSW-5 and pSH0-1, respectively (generously provided by Dr. S. Kumar, New England Biolabs), and purified as previously described (9). The M.HhaI concentration at the end of the preparation was determined by pre-steady-state burst. AdoMet, sinefungin, poly(dI-dC), and poly(dG-dC) concentrations were determined by absorbance at 260 nm. The respective molar absorptivity coefficients are $15.0 \times 10^3 \text{ M}^{-1} \text{ cm}^{-1}$ for AdoMet and its analogues, $6.9 \times 10^3 \text{ M}^{-1} \text{ cm}^{-1}$ for poly(dI-dC) (per bp), and $8.4 \times 10^3 \text{ M}^{-1} \text{ cm}^{-1}$ for poly(dG-dC) (per bp) (Pharmacia Technical Information Sheet).

Methods

Preparation of [5-³H]Cytosine–Poly(dI-dC). Labeling reactions were prepared by incubating 500 μM bp poly(dI-dC) with 100 μM [5-³H]dCTP, 1 mM CTP, 10 mM dITP with 0.62 unit/ μL Sequenase 2.0 in 40 mM Tris-HCl (pH 7.5), 10 mM MgCl₂, 50 mM NaCl, 10 mM DTT, and 1.0 mg/mL BSA. Labeling reactions for [5-³H]cytosine–poly(dG-dC) used the same approach except that poly(dI-dC) was replaced with poly(dG-dC) and 10 mM dITP was replaced by 1 mM dGTP. Reactions were run for 5 h at room temperature. Incorporation of [5-³H]cytosine was followed by spotting the reaction aliquots onto DE81 paper. Spotted papers were washed twice for 5 min in 500 mM KP_i buffer (pH = 6.8) and dried under a heat lamp. The extent of label incorporation was calculated by comparing the counts from unwashed and washed papers. This procedure gives approximately 60% label incorporation. The reaction was stopped by incubating the sample for 5 min at 90 °C followed by slow cooling (2–3 h⁻¹) to room temperature. The cooled sample was centrifuged and the supernatant dialyzed against 10 mM Tris-HCl (pH 8.0) and 10 mM EDTA. The removal of reaction components was determined by comparing the radioactivity from unwashed and washed DE81 papers. The [5-³H]cytosine-labeled poly(dI-dC) and poly(dG-dC) prepared in the described procedure was between 13 and 40 cpm/pmol of base pairs for dIdC, and between 60 and 105 cpm/pmol of base pairs for dGdC.

Methylation Reactions. The methylation reactions were prepared by incubating M.HhaI, DNA substrate, and radioactive AdoMet in 100 mM Tris-HCl (pH 8.0), 10 mM EDTA, 10 mM DTT, and 0.5 mg/mL BSA at 37 °C. The enzyme and DNA concentrations are specific for each assay

and are described in the figure legends. Incorporation of [³H]-methyl groups in the DNA substrate was determined as previously described (25, 26). Briefly, the reaction is followed by spotting reaction aliquots on DE81 paper, leading to the detection of intermediate **3A** and all products resulting from its formation (Figure 2). Thus, the pre-steady-state rates are determined by the steps that lead to intermediate **3A** (Figures 1 and 2), while the steady-state rates are determined by steps that follow formation of intermediate **3A**.

Tritium Exchange Reactions. The tritium exchange reaction was followed essentially as previously described (17). Briefly, tritium exchange is measured by quenching reaction aliquots in an acid suspension (HCl, pH = 2.0–2.5) of activated charcoal. Because **3A** and **3B** (Figure 2) rapidly degrade in acid, their formation can be detected prior to release from the enzyme, thereby allowing the determination of kinetic constants up to and including the formation of **3A** and **3B** as a part of the pre-steady-state rate. The enzyme concentration, DNA concentration, and cofactor concentration are specific for each assay and are described in the figure legends. All reactions were saturated with the cofactor. The reaction buffer was 100 mM Tris-HCl (pH, 8.0), 10 mM EDTA, 10 mM DTT, and 0.5 mg/mL BSA.

Data Analysis. All reaction rates were calculated using Microcal Origin 5.0. All rates were reported as the best fit values \pm standard deviation. The burst profiles were fit to a two-step irreversible mechanism (27):

$$[P](t) = \alpha E_t (1 - e^{-k_{\text{pss}} t}) + E_t k_{\text{ss}} t \quad (1)$$

where $[P](t)$ is the product concentration generated at time t , E_t is the total enzyme concentration, α is the factor that correlates stoichiometry between burst amplitude and enzyme concentration, k_{pss} and k_{ss} are pre-steady-state and steady-state rates, respectively, and t is the time from the start of the reaction. Unless otherwise indicated, all other profiles were analyzed using a linear equation. Each experiment was repeated in several independent measurements until the reproducibility of observed phenomena was established. The presented data show representative examples of analyzed phenomena.

pH Measurements. pH measurements between 6.5 and 7.5 were measured in 100 mM Bis-Tris-HCl ($\text{p}K_a = 6.5$ at 25 °C), EDTA (10 mM), DTT (10 mM), and BSA (0.5 mg/mL). The pH profiles between 7.5 and 9.0 were measured in 100 mM Tris-HCl ($\text{p}K_a = 8.1$ at 25 °C), EDTA (10 mM), DTT (10 mM), and BSA (0.5 mg/mL). The catalytic rates were within 10% when measured in Bis-Tris and Tris at pH 7.5. The pH profiles were analyzed using a single acidic and basic site (28):

$$v = \frac{V_{\text{max}}}{1 + 10^{-\text{pH}}/K_1 + K_2/10^{-\text{pH}}} \quad (2)$$

where V_{max} is the maximal rate observed in the pH profile, K_1 is the acidic constant, and K_2 is the basic constant. The expected SKIE at the given pH and $\text{p}K_a$ for the active site cysteine was calculated using the relations (29):

$$10^{\text{pH}-\text{p}K_a} = [\text{cys-}]/[\text{Hcys}]$$

and

$$2 = \frac{[\text{cys}_{\text{D}^-}]/[\text{Dcys}]}{[\text{cys}_{\text{H}^-}]/[\text{Hcys}]} \quad (3)$$

where [cys-] is the concentration of unprotonated cysteine, [cys_D⁻] and [cys_H⁻] are the concentrations of unprotonated cysteine in D₂O and H₂O buffer, [Dcys] and [Hcys] are the concentrations of protonated cysteine in D₂O and H₂O buffer, and the ratio of unprotonated and protonated cysteine in D₂O is two times higher than the ratio of unprotonated and protonated cysteine in H₂O. The sum of [cys_D⁻] and [Dcys] or [cys_H⁻] and [Hcys] equals the total cysteine concentration.

SKIE Measurements. All experiments in D₂O buffers were measured in parallel with corresponding H₂O experiments, and except for the solvent difference the two reactions are identical. The D₂O buffer was prepared as 10×, and its pH was adjusted, taking into account the pD vs pH correction (29) to be the same as in the corresponding H₂O buffer. Proton inventory profiles were analyzed using different forms of the Gross–Buttler equation (29):

$$k_{\nu}^{\text{D}_2\text{O}} = k^{\text{H}_2\text{O}} \frac{(1 + \nu - \nu\phi^{\text{T}})^n}{(1 + \nu - \nu\phi^{\text{G}})^m} Z^{-\nu} \quad (4)$$

where $k_{\nu}^{\text{D}_2\text{O}}$ is the measured rate at the given fraction of D₂O, $k^{\text{H}_2\text{O}}$ is the rate measured in 100% H₂O, ν is the fraction of D₂O at which the rate was measured (i.e., 0.1, 0.2, 0.3, etc.), ϕ^{T} and ϕ^{G} are deuterium fractionation factors at the transition and the ground state, respectively, and Z is a cumulative fractionation factor for multiple small sites (29). Different forms of eq 4 can be produced by changing the values for parameters n , m , and Z as described in the Results section. Each form of eq 4 represents a unique mechanism with a distinct shape. Accordingly, each proton inventory profile was analyzed using several forms of eq 4, and the best fits were chosen on the basis of error in the best fit parameters, random distribution of the best fit residuals, and resolution between the fit parameters.

RESULTS

Methylation and Proton Exchange Reactions with ³H-Poly-(dG-dC) (Figure 4). We measured the proton exchange rates in the presence of AdoMet and AdoMet analogues and in the absence of cofactors to focus on the catalytic events involving the cytosine C⁵ (Figure 2, conversions **2** → **3A** or **2** → **3B**). The experiments were inspired by previous studies which showed that the cofactor can modulate the exchange (17) and cytosine deamination rates (21–23). The AdoMet analogues used in this study differ only at the position of the active methyl group (Figure 3). The exchange rates vary by over 3 orders of magnitude when measured in the presence of different cofactor analogues or in the absence of the cofactor (Table 1). The exchange rates are low in the presence of AdoMet (Figure 4A) and AdoHcy, intermediate with *N*-methyl-AdoMet, and high with sinefungin and in the absence of the cofactor (Figure 4B, Table 1). The relatively high tritium release rates in the presence of AdoMet result from the methylation reaction (Figure 2, **3A** → **4A**); thus no net exchange occurs with AdoMet (Figure 2, **3B** → **4B**). A stoichiometric proton release during the steady-state methylation reaction was shown before (17). Here we show that

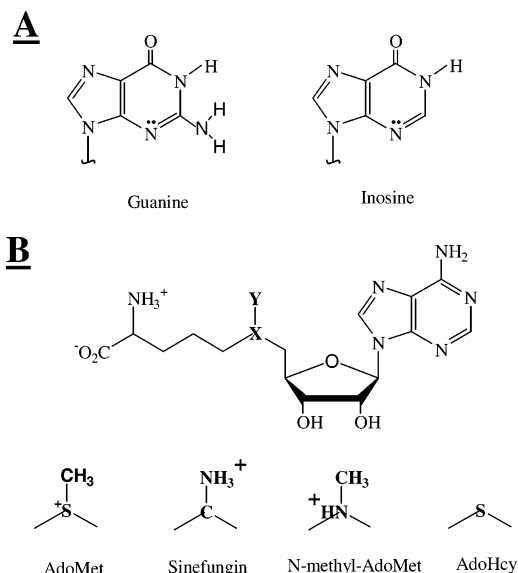


FIGURE 3: Structures of inosine and guanine (A) and AdoMet and its analogues (B).

Table 1: Pre-Steady-State and Steady-State Rate Constants for Methylation and ³H Exchange Reactions^a

	poly(dG-dC)		poly(dI-dC) ^b
	pss	ss	ss
wild type			
methylation (AdoMet)	140 ± 20	40 ± 4	65 ± 8
exchange (AdoMet)	146 ± 15	43 ± 4	230 ± 25
exchange (sinefungin)	500 ± 200	44 ± 3	165 ± 20
exchange (no cofactor)	650 ± 200	105 ± 10	10 ± 1
exchange (N-AdoMet)	33 ± 5	33 ± 5	145 ± 15
exchange (AdoHcy)	0.1 ± 0.02	NM	0.5 ± 0.005
Gln ²³⁷ Trp			
methylation (AdoMet)	1.10 ± 0.05	NM	1.15 ± 0.1
exchange (AdoMet)	1.06 ± 0.04	NM	1.15 ± 0.05
exchange (no cofactor)	0.045 ± 0.008	NM	0.047 ± 0.006
exchange (sinefungin)	0.31 ± 0.02	NM	NM
exchange (N-AdoMet)	0.23 ± 0.03	NM	NM

^a All rates are expressed as h⁻¹ ± best fit error. NM, not measured. All values below the Gln²³⁷Trp row are for this mutant. ^b The reactions with poly(dI-dC) do not show a pre-steady-state (pss) burst, so the rates measured during the first turnover and the subsequent turnovers are all indicated as the steady-state (ss) rates.

the methylation and proton release reactions have identical pre-steady-state rates. Thus, in the presence of AdoMet, intermediate **2** leads exclusively to methyl transfer (Figure 2, **2** → **3A**). A pre-steady-state burst is observed during AdoMet-dependent methylation and exchange (Figure 4A), in the exchange reaction in the presence of sinefungin (Figure 4B), and in the ³H exchange reaction without cofactors (Figure 4B). The relatively large errors for the reported pre-steady-state rates (Table 1) are caused by the fast rates, allowing only for measurements of the burst and later stages of the reaction (Figure 4B). The pre-steady-state burst in the methylation reaction indicates that the steps leading to methyl transfer (Figure 2, **2** → **3A**) are faster than the subsequent steps, while the pre-steady-state burst in the exchange reaction indicates that the proton transfer (Figure 2, **2** → **3B**) at C⁵ is faster than the subsequent steps. In summary, this study shows that the ability of different cofactor analogues to support or inhibit the exchange rates is dependent on the availability of a proton proximal to the C⁵ moiety of the target cytosine (Figure 3).

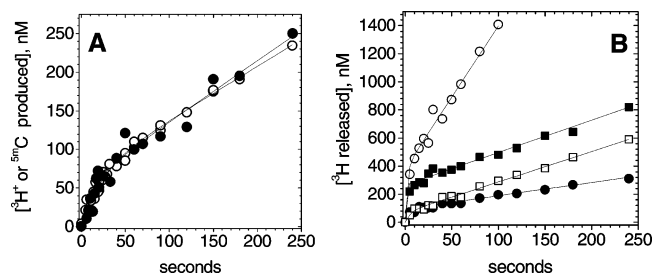


FIGURE 4: ^3H exchange and methylation reaction with ^3H -poly(dG-dC). (A) ^3H exchange (\circ) and methylation rates (\bullet) were measured in parallel by using M.HhaI (75 nM), ^3H -poly(dG-dC) (10 μM bp, 80 cpm/pmol), and ^{14}C -AdoMet (12 μM , 130 cpm/pmol). The rates were calculated using eq 1. (B) All reactions were measured in the presence of M.HhaI (285 nM) and ^3H -poly(dG-dC) (8 μM bp, 88 cpm/pmol). The reactions with sinefungin (10 μM) at pH = 8.0 (\blacksquare) and pH = 6.5 (\bullet) are shown. The reactions in the absence of the cofactor at pH = 8.0 (\circ) and pH = 6.5 (\square) are also shown.

Analysis of pH and Solvent Kinetic Isotope Effects (SKIE) during Methylation and Exchange Reactions with Poly(dG-dC) (Figure 5). Previous studies suggested that nucleophilic attack by the active site Cys⁸¹ is rate limiting during methylation (10, 18). Because cysteine has a unique 2-fold preference for hydrogen vs deuterium (29), pH/SKIE studies can be used to probe if the rate-limiting step in methylation or any of the exchange reactions depends on nucleophilic attack by Cys⁸¹ (30–33). If Cys⁸¹ attacks the target base as the thiolate, the observed reactions will give an inverse SKIE with the ground state ϕ_G close to 0.5 (eq 4 and ref 29). If Cys⁸¹ attacks as the thiol and is deprotonated during nucleophilic attack, the reaction will give a normal SKIE and the transition state ϕ_T will be close to 0.5 (eq 4 and ref 29). Both effects should disappear as the pH increases above the $\text{p}K_a$ for the active site cysteine. We measured the pH profiles for the pre-steady-state rates during methylation and different exchange reactions (e.g., in the absence of cofactors and in the presence of sinefungin) to determine the number

of pH-sensitive steps and the corresponding $\text{p}K_a$ values (Figure 5). In reactions without cofactor analogues and with sinefungin we show that changes in pH affect the intercept in the pre-steady-state burst (Figure 4B), since the pre-steady-state rates were too fast to allow accurate determination of the kinetic constants. The pH profiles were analyzed using eq 2 and can be best described assuming a single protonation site with $\text{p}K_a$ s ranging from 7.4 to 7.8 (Table 2). Interestingly, the pH profiles are similar even though the catalytic rates vary by 3 orders of magnitude, suggesting that a similar residue(s) is (are) critical for the pH-sensitive step. The observed SKIE is specific for each reaction and principally pH-independent, unlike the pH-activity profiles. Thus, the pH and SKIE profiles are at least in part caused by different groups, and it is thus unlikely that a single rate-limiting step is being probed by these methods. We used eq 3 to generate the predicted SKIE profiles for a reaction limited by a nucleophilic cysteine, the medium value for the measured $\text{p}K_a$ range (Table 2), and the known fractionation factor for cysteine $\phi = 0.5$ (29).

The exchange reaction without cofactor has an inverse SKIE, and the SKIE increases with increasing pH (Figure 5B). This pH-induced change in the SKIE indicates that the SKIE is at least in part a result of a pH-sensitive step. If the pH response is controlled by the active site Cys⁸¹, a pH-induced change in the SKIE suggests that conversion between intermediates **1** and **2** contributes to the rate-determining step. The observed pH/SKIE profiles are different from the pH/SKIE profiles expected for a reaction that is primarily controlled by a cysteine nucleophilic attack with the measured $\text{p}K_a$ (Figure 5B, upper panel). However, the observed SKIE may be caused by the nucleophilic cysteine and some other group, which is consistent with dome-shaped proton inventory studies (Figure 10A).

Methylation and Tritium Exchange Reaction with Poly(dI-dC) and AdoMet Analogues (Figures 6 and 7). We

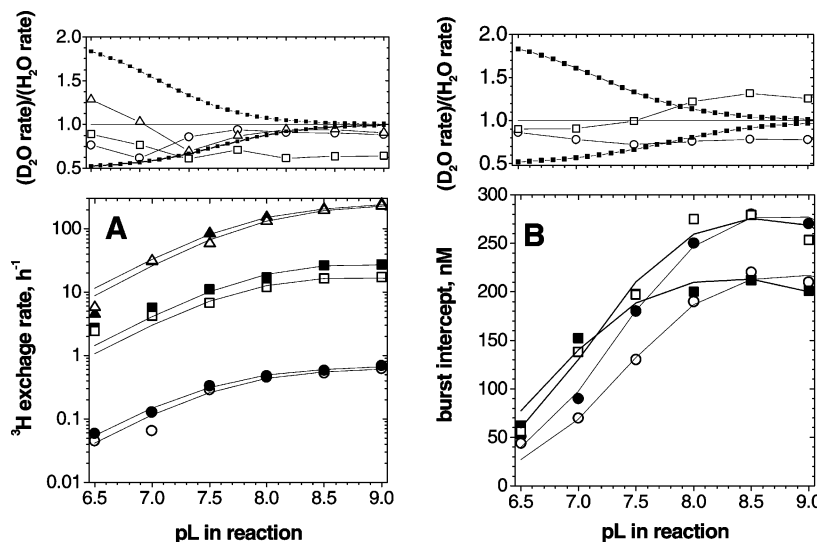


FIGURE 5: pH profiles and SKIE analysis of the ^3H exchange reaction with ^3H -poly(dG-dC). (A) pH profile for the ^3H exchange reaction with AdoMet (\blacktriangle , \triangle), *N*-methyl-AdoMet (\blacksquare , \square), and AdoHcy (\bullet , \circ) in H_2O and D_2O , respectively. Each profile was analyzed using eq 2, and the best fit values are listed in the Table 2. In the upper panel the symbols represent AdoMet (\triangle), *N*-methyl-AdoMet (\square), and AdoHcy (\circ). The dashed line is calculated using eq 3 and shows the expected SKIE if the rate-limiting step is primarily dependent on a nucleophilic cysteine with $\text{p}K_a = 7.5$. (B) pH profile for the burst intercept in the ^3H exchange reaction with sinefungin (\bullet , \circ) and in the absence of the cofactors (\blacksquare , \square) in H_2O and D_2O . Each profile was analyzed using eq 2, and the best fit values are listed in Table 2. In the upper panel the symbols represent sinefungin (\circ) and the reaction in the absence of the cofactor (\square). The dashed line is calculated using eq 3 and represents the expected SKIE if the rate-limiting step is primarily dependent on a nucleophilic cysteine with $\text{p}K_a = 7.5$.

Table 2: Summary of the pH and SKIE Analysis of the Presented Reactions

	apo	sinefungin	AdoMet	N-AdoMet	AdoHcy
Wild Type with ^3H -Poly(dG-dC) Substrate					
SKIE type and shape ^a	inverse and dome shape	normal and bowl shape	none	normal and dome shape	none
ϕ_T	3.2 ± 1	0.42 ± 0.07		0.34 ± 0.04	
ϕ_G	2.1 ± 0.7	1.8 ± 0.2		1.4 ± 0.2	
$\text{p}K_a(\text{H}_2\text{O})$	7.7 ± 0.08	7.3 ± 0.05	7.8 ± 0.06	7.8 ± 0.2	7.5 ± 0.07
$\text{p}K_a(\text{D}_2\text{O})$	7.1 ± 0.08	7.3 ± 0.07	7.9 ± 0.04	7.4 ± 0.3	7.6 ± 0.1
comments				$Z = 1 \pm 0.03$	
Wild Type with ^3H -Poly(dI-dC) Substrate					
SKIE type and shape ^a	inverse and almost linear	normal and bowl shape	normal and linear when reciprocal	normal and linear when reciprocal	none
ϕ_T	3.7 ± 0.5	0.47 ± 0.05	1.08 ± 0.32	0.94 ± 0.33	NM ^b
ϕ_G	1.1 ± 0.2	1.7 ± 0.12	2.04 ± 0.66	2.15 ± 0.7	NM ^b
$\text{p}K_a(\text{H}_2\text{O})$		7.4 ± 0.07	7.6 ± 0.04	7.5 ± 0.08	7.6 ± 0.06
$\text{p}K_a(\text{D}_2\text{O})$		7.5 ± 0.05	7.4 ± 0.06	7.7 ± 0.07	7.5 ± 0.08
comments	no pH response	slower than GC in pss ^c and faster in ss ^c	exchange faster than methylation	5 times faster with IC relative to GC	5 times faster with IC relative to GC
Gln ²³⁷ Trp with ^3H -Poly(dG-dC) Substrate					
SKIE type and shape ^a	inverse and mild dome shape	normal and linear when reciprocal	inverse and mild dome shape	inverse and mild dome shape	
ϕ_T	2.4 ± 0.5	1.1 ± 0.3	2.2 ± 0.8	1.8 ± 0.04	
ϕ_G	1 ± 0.5	2.1 ± 0.6	1.1 ± 0.4	0.96 ± 0.2	
$\text{p}K_a(\text{H}_2\text{O})$	NM ^b	7.3 ± 0.06	7.4 ± 0.12	7.4 ± 0.07	
$\text{p}K_a(\text{D}_2\text{O})$		7.5 ± 0.1	7.5 ± 0.1	7.6 ± 0.1	
comments		SKIE type and shape changes with pH	SKIE changes with the pH	SKIE type and shape changes with pH	

^a To describe the shape, we used the nomenclature described in ref 29; inverse means the reaction is faster in D₂O, and normal means the reaction is slower in D₂O. ^b NM, not measured. ^c pss stands for pre steady state; ss stands for steady state.

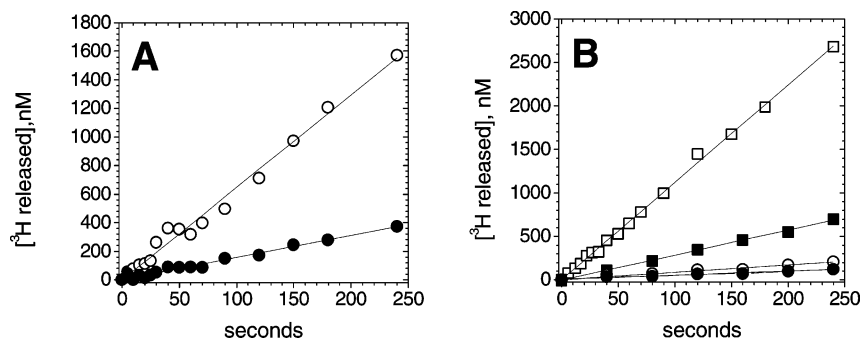


FIGURE 6: ^3H exchange and methylation reaction of ^3H -poly(dI-dC). (A) ^3H exchange (○) and methylation rates (●) were measured in parallel using M.HhaI (100 nM), ^3H -poly(dI-dC) (10 μM bp, 13 cpm/pmol), and ^{14}C -AdoMet (12 μM , 130 cpm/pmol). The rates were calculated by linear regression. (B) ^3H exchange reaction with sinefungin (□, ■) and in the absence of the cofactor (○, ●) at pH = 8.0 and 6.5, respectively. All reactions with ^3H -poly(dI-dC) were analyzed using linear equations.

compared the methylation and proton exchange reactions with ^3H -poly(dG-dC) and ^3H -poly(dI-dC) to understand how enzyme–DNA interactions alter catalysis. Poly(dI-dC) is a good substrate for the methylation and exchange reactions (Table 1 and Figure 6). Except for the exchange reaction in the absence of the cofactor (Table 1), the rate for poly(dI-dC) and the pre-steady-state and steady-state rate for poly(dG-dC) are quite similar. The reaction with poly(dI-dC) is slightly faster with AdoHcy and *N*-methyl-AdoMet and slightly slower with sinefungin (Table 1). The AdoMet-dependent methylation reaction and the sinefungin-dependent exchange reactions have 2-fold slower rates with poly(dI-dC), but the steady-state rates are 4-fold faster than with poly(dG-dC) (Table 1). We observe no burst with poly(dI-dC) during methylation (Figure 4A vs Figure 6A), nor in the exchange reactions with sinefungin (Figure 4B vs Figure 6B), indicating that the product release steps are faster and thus no longer rate limiting. Surprisingly, AdoMet-dependent

methylation with poly(dI-dC) shows exchange rates which are four times faster than the methylation rates (Figure 6A and Table 1). The excess tritium released in the methylation reaction during the first turnover indicates that proton transfer at cytosine C⁵ (Figure 2, **2** → **3B**) occurs prior to methyl transfer (Figure 2, **2** → **3A**). In addition, since a single target base attack can result in only one tritium release (Figure 2, **2** → **3B** → **4B**), the excess tritium released during the multiple catalytic turnovers in the methylation reaction indicates that the enzyme rapidly attacks and releases several target bases before catalyzing methyl transfer from the bound AdoMet. Such a rapid interchange between different bases indicates that there is a dynamic equilibrium between intermediates **1** and **2** (i.e., Figure 2, **1** ↔ **2**) and that the base restacking is fast and in a direct competition with the covalent adduct formation (**1** → **2**, Figure 2) and methyl transfer (**2** → **3A**, Figure 2). Crystallographic studies (34), ^{19}F NMR studies (15), and fluorescent studies (14) showed

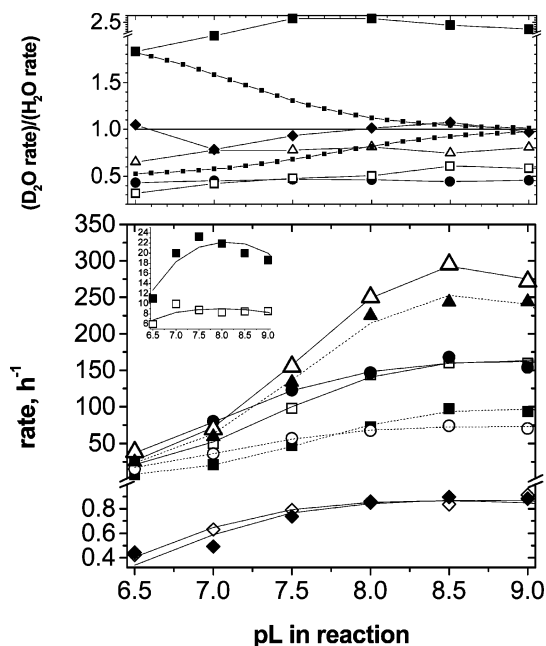


FIGURE 7: pH profile and SKIE analysis of the ^3H exchange reaction with ^3H -poly(dI-dC). The pH profiles for the ^3H exchange reaction with AdoMet (\blacktriangle , \triangle), sinefungin (\bullet , \circ), *N*-methyl-AdoMet (\blacksquare , \square), and AdoHcy (\blacklozenge , \lozenge) in H_2O and D_2O , respectively, are shown. The insert shows the pH profile for the reaction without cofactors (\blacksquare , \square) in D_2O and H_2O , respectively. All profiles were analyzed using eq 2, and the best fit values are listed in the Table 2. The upper panel shows the ratios between the rates measured in D_2O and H_2O in the presence of AdoMet (\circ), sinefungin (\bullet), *N*-methyl-AdoMet (\square), AdoHcy (\triangle), and apoenzyme (\blacksquare). The dashed lines are calculated using eq 3 and show the expected SKIE if the rate-limiting step is primarily dependent on a nucleophilic cysteine with $\text{p}K_a = 7.5$ as described in the text.

that the extrahelical base can exist as a stable and distinct intermediate. Our results show that with poly(dI-dC) the extrahelical base is a short-lived intermediate. Our observation that the exchange rate is much faster with poly(dI-dC) than methylation supports the idea that the methyl transfer step is limiting.

The pH profiles (Figure 7) for the exchange reaction with AdoMet and poly(dI-dC) and different analogues are very similar and closely resemble the profiles in similar reactions with poly(dG-dC) (Table 2 and Figure 5). Thus, any differences between poly(dG-dC) and poly(dI-dC) do not affect the pH-sensitive step. The SKIE for each reaction with poly(dI-dC) is unique and pH-independent. Thus, as with poly(dG-dC), the SKIE and pH profiles are at least in part caused by different phenomena. The most significant distinction between these two substrates is observed in the exchange reaction without cofactor (Figures 6B and 7, insert), with the poly(dI-dC) reaction being 2 orders of magnitude slower, is largely pH-independent, and has a large inverse SKIE. These observations suggest that in the absence of the cofactor the exchange reaction with poly(dI-dC) has a unique rate-limiting step and mechanism.

Processivity on Poly(dG-dC) and Poly(dI-dC) Substrates (Figure 8). To measure the processivity on DNA substrates, we prepared two identical exchange reactions, one containing only labeled DNA (called the *free* reaction) and one having ^3H -labeled DNA plus an *n*-fold excess (usually $n = 10$) of unlabeled DNA (called the *dilute* reaction). Both reactions are started simultaneously by adding equal amounts of enzyme. As expected, the ^3H release rate in the free reaction is *n*-fold higher than in the dilute reaction. By the end of the first turnover (Figure 8, arrow), an aliquot from the free reaction is mixed with an *n*-fold excess of unlabeled DNA (*chase* reaction). If the enzyme is fully processive, addition of the 10-fold excess of unlabeled substrate in the chase reaction will not affect the tritium release rates. If the enzyme is not processive, the ^3H release rates in the chase reaction will be immediately identical to the tritium release rates in the dilute reaction. A partially processive enzyme in which only a fraction of the enzyme molecules stay on the original substrate will result in the ^3H release rates in the chase reaction being between the tritium release rates for the free and dilute reactions. The rate will gradually decrease with each turnover until the chase and dilute reactions become

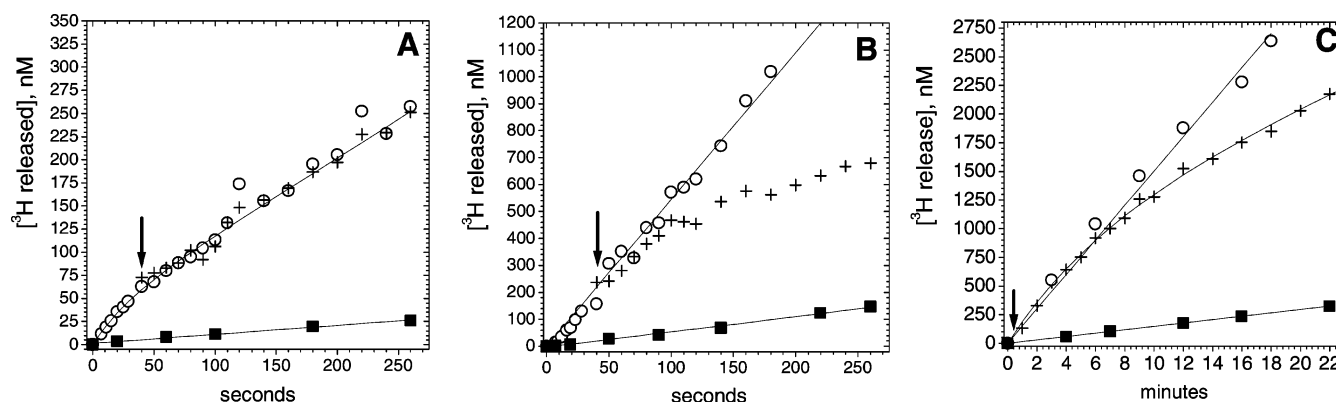


FIGURE 8: Chase processivity assay with M.HhaI and ^3H -poly(dG-dC) (A) or ^3H -poly(dI-dC) (B) and M.SssI with ^3H -poly(dI-dC) (C). (A) The free (\circ) reaction had M.HhaI (50 nM), ^3H -poly(dG-dC) (8 μM bp, 102 cpm/pmol), and AdoMet (10 μM). The dilute reaction (\blacksquare) was prepared from a free reaction aliquot by adding a 10-fold excess of unlabeled poly(dG-dC). Free and dilute reactions were started simultaneously; the chase reaction ($+$) was started 40 s later (after the first turnover) by adding unlabeled poly(dG-dC) (80 μM bp) to the free reaction aliquot. (B) The free (\circ) reaction had M.HhaI (100 nM), AdoMet (10 μM), and ^3H -poly(dI-dC) (8 μM bp, 24 cpm/pmol). The dilute reaction (\blacksquare) was prepared from a free reaction aliquot by adding a 10-fold excess of unlabeled poly(dI-dC). Free and dilute reactions were started simultaneously; the chase reaction ($+$) was started 45 s after the free reaction (after the second turnover) by adding unlabeled poly(dI-dC) (100 μM bp) to the free reaction aliquot. (C) The free (\circ) reaction had M.SssI (30 nM), ^3H -poly(dI-dC) (10 μM bp, 24 cpm/pmol), and AdoMet (10 μM). The dilute reaction (\blacksquare) was prepared from a free reaction aliquot by adding a 10-fold excess of unlabeled poly(dI-dC). The chase reaction ($+$) was started 45 s after the free reaction by adding 100 μM bp unlabeled poly(dI-dC) to a free reaction aliquot.

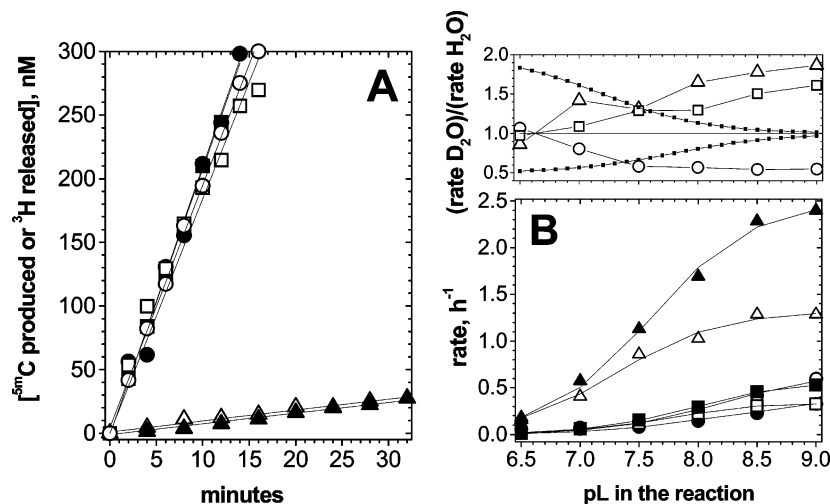


FIGURE 9: (A) Gln²³⁷Trp mutant exchange and methylation reactions with ³H-poly(dG-dC) and ³H-poly(dI-dC) and (B) pH/SKIE profiles in the reaction with ³H-poly(dG-dC). (A) Methylation and the ³H exchange rates with the Gln²³⁷Trp mutant (1000 nM) were measured in parallel using ¹⁴C-AdoMet (12 μM, 131 cpm/pmol) and ³H-poly(dG-dC) (12 μM bp, 88 cpm/pmol) or ³H-poly(dI-dC) (12 μM bp, 25 cpm/pmol). The symbols represent the ³H exchange (○, □) and methylation (●, ■) reaction with ³H-poly(dG-dC) and ³H-poly(dI-dC), respectively, and the ³H exchange reaction without cofactor and ³H-poly(dG-dC) (▲) and ³H-poly(dI-dC) (△). All profiles were analyzed using a linear equation, and the best fit values are listed in the Table 1. (B) The lower panel shows pH profiles for exchange reactions measured with AdoMet (▲, △), sinefungin (○, ●), and *N*-methyl-AdoMet (■, □) in D₂O and H₂O, respectively. The pH profiles were analyzed using eq 2, and the best fit values are given in Table 2. The upper panel shows the ratios between the rates measured in D₂O and H₂O in the presence of AdoMet (△), sinefungin (●), and *N*-methyl-AdoMet (□) in D₂O and H₂O, respectively. The dashed lines are calculated according to eq 3 and represent the expected SKIE for a reaction that is primarily limited by cysteine nucleophilic attack with $\text{pK}_a = 7.5$ as described in the text.

identical. We find that M.HhaI is fully processive for five turnovers in the methylation reaction with poly(dG-dC) substrate. M.HhaI is only partially processive in the methylation reaction with the poly(dI-dC) substrate for about three to four turnovers. Since processivity experiments measure tritium release rates rather than the methyl transfer rates, the small processivity on poly(dI-dC) substrates can be attributed to excess tritium released during the methylation reaction with the poly(dI-dC) substrate (Figure 6A). A positive control was included in the form of M.SssI since this enzyme was previously shown to be processive (35). Here we show that M.SssI catalyzes 30 turnovers on the same DNA molecule.

Exchange Reaction with the Gln²³⁷Trp Mutant (Figure 9). Gln²³⁷ interacts with the amino group on the C² of the orphan guanine; this interaction forms part of the network of hydrogen bonds that stabilize intermediates **1** and **2** (Figure 2 and ref 36). The Gln²³⁷Trp mutant is one of the least active Gln²³⁷ mutants (19). We were interested in using the kinetic analyses presented for the wild-type M.HhaI to identify which step(s) during catalysis is (are) significantly altered in the mutant. The Gln²³⁷Trp mutant has methylation and exchange rates with poly(dG-dC) and poly(dI-dC) that are more than 10-fold slower than those of the wild-type enzyme (Table 1). The exchange rates are slowest in the absence of the cofactor, and there is little difference in catalytic rates with AdoMet, sinefungin, and *N*-methyl-AdoMet. Unlike the WT enzyme, we observe identical rates for the methylation and tritium release kinetics during AdoMet-dependent methylation of poly(dI-dC) (Figure 9A), and the mutant shows identical methylation and exchange kinetics for the two DNA substrates (Figure 9A).

The pH profiles with the mutant (Figure 9B) closely resemble the pH profiles in similar reactions with the WT enzyme (Figure 5 and Table 2). Since reactions with the mutant and the WT enzyme show very different rates, the

observed similarity in the pH profiles further supports the idea that the ionization state of similar residues carries out similar functions in the two proteins. The mutant and the wild-type enzymes show distinct SKIE (Figures 5, 7, and 9B). For example, all reactions with the mutant show pH-dependent changes in the SKIE (Figure 9B); thus, the SKIE is at least in part caused by the pH-sensitive step.

Proton Inventory Experiments (Figure 10). Proton inventory profiles are measured at varying ratios of D₂O and H₂O (29). This approach represents a sensitive strategy to describe and compare the rate-limiting step in enzyme-catalyzed reactions (29). We measured proton inventories with the exchange reactions to determine if different reactions share similar intermediates and rate-limiting steps. For those reactions showing a pre-steady-state burst, the proton inventories were measured in the pre steady state; reactions showing linear profiles were measured in the first and subsequent turnovers. Proton inventories are usually described according to their shape and fractionation factors, i.e., ϕ_{T} and ϕ_{G} (29). The shape of the proton inventory profile indicates the number of steps or groups controlling the SKIE and whether the observed SKIE is caused in the ground state, transition state, or both (29). The fractionation factors can help to identify the group that causes the SKIE (i.e., $\phi = 0.5$ – 0.6 indicates cysteine) and also to compare proton inventory profiles from different reactions. The proton inventory profile is fit by using different forms of eq 4 involving different values and combinations of the n , m , and Z parameters. We used eq 4 to identify the simplest form that describes the proton inventory profiles based on the following options and parameters: (i) two SKIE-sensitive steps in the transition state ($n = 2$, $m = 0$, $Z = 1$); (ii) two SKIE-sensitive steps in the ground state ($n = 0$, $m = 2$, $Z = 1$); (iii) one SKIE-sensitive step in the ground state and one in the transition state ($v = 1$, $v = 1$, $Z = 1$). We also

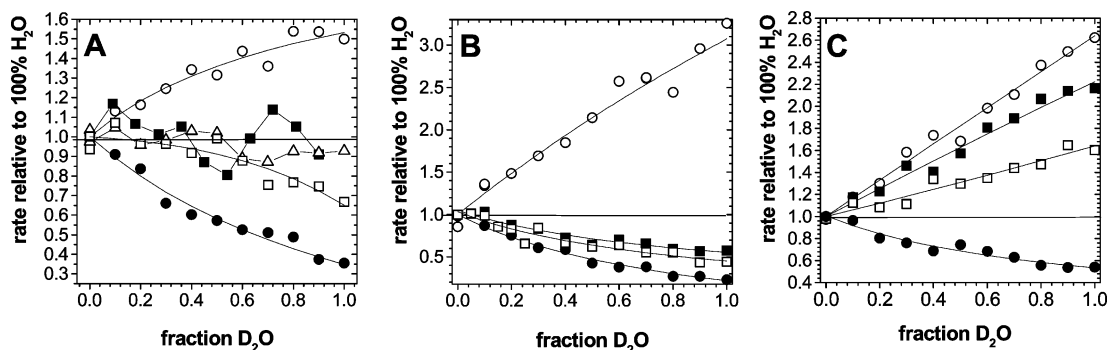


FIGURE 10: Proton inventory for the ^3H exchange reaction with (A) ^3H -poly(dG-dC), (B) ^3H -poly(dI-dC), and (C) the Gln²³⁷Trp mutant and ^3H -poly(dG-dC). In all three panels the symbols indicate proton inventory profiles for reaction without cofactors (○), AdoMet (■), *N*-methyl-AdoMet (□), and sinefungin (●). Panel A also has data for AdoHcy (△). The profiles represent rates measured in the pre steady state or in the steady state as described in the text. All profiles were analyzed using the Gross–Butler equation (eq 4), and the best fit values are given in the Table 2.

considered a situation involving contributions from multiple sites; i.e., the *Z* factor was allowed to float and $n = 1$, $m = 0$ or $n = 0$, $m = 1$. On the basis of the best fit residuals, the proton inventory profiles are best described as one SKIE-sensitive step in the transition state and one in the ground state (i.e., $n = 1$, $m = 1$, $Z = 1$). The calculated best fit fractionation factors are summarized in Table 2, and the best fit profiles are presented in Figure 10.

Different proton inventory profiles are observed during methylation with poly(dG-dC), methylation with poly(dI-dC), and methylation with the Gln²³⁷Trp mutant. Therefore, these reactions depend on different relative contributions from several steps, implicating distinct mechanisms. In contrast, the proton inventories and fractionation factors for the exchange reactions with sinefungin and poly(dG-dC) or poly(dI-dC) are within experimental error identical (Table 2), indicating that they have very similar mechanisms. All reactions with the wild-type enzyme have a ground state fractionation factor (ϕ_G) between 1.8 and 2, while the transition state fractionation factor ϕ_T is unique for each reaction (Table 2). The proton inventory analysis shows that the exchange reactions with both DNA substrates in the absence of cofactor are similar to the reactions catalyzed by the Gln²³⁷Trp mutant (Table 2): an inverse SKIE, an increase in SKIE with an increasing pH, and a transition state fractionation factor ϕ_T close to 2 (Table 2). The dome-shaped proton inventory profiles for the proton exchange reaction without cofactor (Figure 10A) suggest that the SKIE and multiple steps are rate limiting and determine the SKIE (29).

DISCUSSION

Despite a wealth of information regarding DNA cytosine methyltransferases, and in particular *M.HhaI*, there is little experimental evidence regarding three fundamental aspects of enzyme catalysis: the identity and roles of critical active site groups other than Cys⁸¹, the identity and roles of reaction intermediates, and the rate constants associated with their interconversion (Figure 2). Our goals were to (1) understand which steps are rate limiting (Figure 2), (2) characterize the relative stabilities of intermediates **1** and **2**, (3) characterize the interconversion kinetics involving intermediates **1** and **2**, (4) investigate the extent to which solvent molecules gain access to intermediate **2**, and (5) characterize how protein–DNA interactions alter the stability of intermediates **1** and

2. Our approach uses both base and cofactor analogues (Figure 3) in conjunction with several kinetic strategies.

Stabilization of the extrahelical cytosine (base flipping, Figure 1) within the enzyme's active site (Figure 2, intermediate **1**) has been proposed to activate the ring for nucleophilic attack at the C⁶ position by protonation at N³ (Figure 2, **1**, and refs 18 and 37). Nucleophilic attack to form the covalent intermediate (Figure 2, **2**) is an essential feature of all DNA cytosine methyltransferases, including the enzymes involved in epigenetic regulation in humans (38). Indeed, nucleophilic attack at the pyrimidine C⁶ position is core to all C⁵ pyrimidine methyltransferases and the basis of drug action for several clinically used mechanism-based cancer treatments (5, 39). Formation of intermediate **2** disrupts the aromaticity of the pyrimidine, while the insertion of electron density deriving from the thiolate enables the normally unreactive pyrimidine to attack a proximal electrophile. Experiments demonstrating that *M.HhaI* catalyzes the exchange of tritium placed at the cytosine C⁵ position provided the first definitive evidence for the formation of intermediate **2** (17). This cytosine C⁵ exchange reaction provides a unique opportunity to expand our ability to analyze the target base attack beyond the limitations of routine methylation assays. Like methylation, the exchange reaction requires that the enzyme forms a covalent adduct with the target base. Both reactions are the result of electrophilic addition at the cytosine C⁵, and both reactions end with the β elimination involving proton removal at the cytosine C⁵ position (Figure 2, **3A** \rightarrow **4A** and **3B** \rightarrow **4B**).

In this study we find that the tritium exchange rates vary by 3 orders of magnitude when measured in the presence of different cofactor analogues or in the absence of the cofactor (Table 1). The AdoMet analogues used in this study differ only at the position of active methyl group (Figure 3), and the analogues' ability to support the exchange reaction correlates with the proton presence at the position of the active methyl group (Figure 3). Possible mechanisms by which AdoMet and AdoHcy can inhibit the exchange reaction were previously described (17, 20, 40). Briefly, AdoMet and AdoHcy can inhibit the exchange reaction (i) by controlling the stereochemistry of the β elimination step (Figure 2, **3B** \rightarrow **4B**), (ii) by affecting the enzyme's ability to form intermediates **1** or **2**, or (iii) by affecting proton access at the C⁵ of the activated target base (Figure 2, **2** \rightarrow

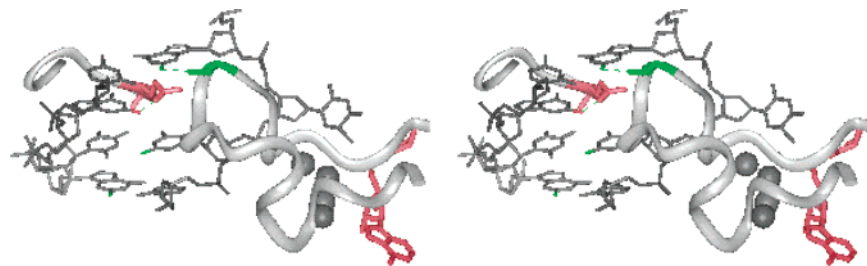


FIGURE 11: Structure of the active site loop, the Gln²³⁷ site, and the GCGC recognition sequence with an extrahelical base (7). DNA is shown in thin gray lines. The gray ribbon in the front represents the active site loop (amino acids 80–99) in the closed position when Ile⁸⁶ (green) can make a hydrogen bond with the C² amino group (green) on guanine that is in the 5' position relative to target cytosine. The background gray ribbon represents the peptide backbone with Gln²³⁷ (red) which makes a hydrogen bond with the C² amino group (red) on the orphan guanine. The cofactor is shown in red in the lower right corner, while the four solvent molecules near the target base are shown as gray spheres. The C² amino groups (green) on two of guanine residues are exposed to solvent and make no contacts with enzyme.

3B). Our exchange assay detects tritium exchange upon delivery of the proton to the cytosine C⁵ position (Figure 2, **3A**) and the pre-steady-state rates do not depend on the stereochemistry of proton release (Figure 2, **3B** → **4B**). Thus, stereochemical control of the proton release step by the different analogues seems unlikely. It is equally unlikely that the analogues interfere with enzyme's ability to form intermediates **1** and **2** because (i) we observe different exchange rates with poly(dG-dC) and poly(dI-dC) in the presence of AdoMet (Figures 4A and 6A), (ii) AdoMet does not support the exchange reaction with poly(dG-dC) (Figure 4A), (iii) our pH/SKIE studies (Figures 5 and 8) are inconsistent with a rate-limiting step involving nucleophilic attack by Cys⁸¹, and (iv) the subtle structural differences within the different cofactor analogues would seem unlikely to cause such dramatic changes in the enzyme's ability to form intermediate **2**, since high exchange rates in the absence of any cofactor involving well-studied and large conformational changes in the enzyme (7) have minimal effects on the exchange process.

The observed pattern in modulation of the exchange rates by AdoMet analogues and the crystal structures of M.HhaI (7, 40, 41) suggest that the exchange rates depend on the proton access to the C⁵ of the target base. The four analogues (Figure 3) are likely to bind the active site in the same fashion since the cocrystal structures of the two most diverse forms involving AdoMet (41) and AdoHcy (7) reveal similar cofactor binding orientations. We suggest that the most likely candidate for the proton donor is the cofactor and/or the solvent molecules that are frequently observed in the active site (Figure 11 and ref 42). The high exchange rates in the absence of the cofactor can be attributed to solvent which has ready access to the C⁵ on the activated target base [$pK_a = 18$ (18)]. The low exchange rates in the presence of AdoMet and AdoHcy are to be expected since their proximity to the cytosine C⁵ (7, 18, 40) can block solvent access. Although sinefungin and *N*-methyl-AdoMet can also block solvent access to the cytosine C⁵ position, the relatively high exchange rates may derive from the proximal amino groups found within these analogues. The exchange rates are higher with sinefungin than *N*-methyl-AdoMet, since sinefungin's three protons are most likely closer to the cytosine C⁵.

In summary, our study of AdoMet analogues and the exchange reaction extends the previous study (17) which showed that AdoMet and AdoHcy inhibit the exchange reaction when compared to the same reaction without cofactors. We show that the ability of the cofactors to support

the exchange reaction correlates with the proton access and proximity (Figure 3) at the C⁵ on the target base. These insights allow us to describe the catalytic events following the formation of the covalent intermediate **2** (Figure 2, **2** → **3A** → **4A** and **2** → **3B** → **4B**) and the rate limiting step as described further in the text. Furthermore, the exchange reaction shows a similar cofactor dependency as was previously reported for the mutagenic deamination reaction (23). The similar trends are reasonable since C⁵ protonation is known to increase deamination rates by at least 4 orders of magnitude (37). Because the deamination reaction is difficult to study mechanistically, the exchange reaction provides a convenient mechanistic probe of the common features of these reactions. For example, the exchange reaction could be used to investigate the extent to which eukaryotic cytosine methyltransferases (e.g., Dnmt1) support the deamination reaction² or to investigate the basis for any differences in the deamination kinetics observed with different bacterial enzymes (22).

pH/SKIE Studies. We used pH and SKIE studies (Figures 5 and 7) to probe if the rate-limiting step in methylation or any of the exchange reactions depends on nucleophilic attack by Cys⁸¹ involving the transition between intermediates **1** and **2** (Figure 2). Based on theoretical studies (18), nucleophilic attack by Cys⁸¹ is thought to be rate limiting during methylation (10, 42). Our pH/SKIE analysis showed no evidence that the cysteine nucleophilic attack is rate limiting during methylation or any of the exchange reactions in the presence of the cofactor. Interestingly, we find that even though the relative exchange rates vary by orders of magnitude (Table 1), all exchange reactions have very similar pH profiles (Table 2), and in the majority of the reactions the SKIE (ratio between the rates measured in D₂O and H₂O) is pH-independent and unique for each reaction (Figures 5 and 7). To understand how the conversion between intermediates **1** and **2** (Figure 2) might affect catalytic rates, it is necessary to realize that this conversion is in principle reversible and that reversion back to intermediate **1** is expected if methyl transfer (**2** → **3A**) or proton transfer (**2** → **3B**) is relatively slow. If the rate of reversal (**2** → **1**) is at least severalfold faster than the specific catalytic process at cytosine C⁵, intermediates **1** and **2** will be in equilibrium (i.e., Figure 2, **1** → **2**, and Figure 1). Several experimental observations support a rapid equilibrium between intermediates **1** and **2**. First we observe an excess release of tritium

² Ž. M. Svedružić and N. O. Reich, manuscript in preparation.

during the methylation reaction involving poly(dI-dC) (Figure 6A). Second, the pre-steady-state exchange kinetics with sinefungin and poly(dG-dC) (Table 1) show that the conversion between intermediates **1** and **2** can be severalfold faster than the subsequent methyl transfer step. Finally, the results of the pH/SKIE studies (Figures 5 and 7) are also compatible with the rapid equilibrium proposal. A decrease in pH results in protonation of Cys⁸¹ and a shift in the equilibrium between **1** and **2** in favor of intermediate **1**, which leads to a decrease in the catalytic rates. We observe that solvent changes (e.g., replacement of H₂O with D₂O) have little effect on the pK_a of Cys⁸¹ (43) but do affect hydrogen-bonding interactions and proton transfer steps that lead to the exchange reaction. Hence, pH/SKIE studies (Figures 5 and 7) reveal that a change in the pH does affect catalytic rates, while the SKIE is pH-independent and specific for the particular mechanism of the proton transfer at the C⁵ on the target base. In summary, the most important consequence of our proposed rapid equilibrium mechanism is that the catalytic rates are dependent on the steps that control the concentration of intermediate **2** and the steps that control the conversion to intermediate **3A** (Figure 2, **2** → **3A**) or **3B** (Figure 2, **2** → **3B**); this is in contrast to the circumstance in which only the formation of intermediate **2** is rate limiting (Figure 2, **1** → **2**).

The exchange reaction in the absence of the cofactor is unique in several features. High exchange rates without cofactors in the presence of poly(dG-dC) (Figure 4B and ref 17) indicate that conformational changes associated with the cofactor binding are not necessary for a successful target base attack (Table 1). An increased SKIE with increasing pH suggests that nucleophilic attack by Cys⁸¹ (Figure 2, **1** → **2**, and Figure 5) is at least partially rate limiting in the exchange reaction. Once intermediate **2** is formed, the proton transfer to cytosine C⁵ is likely to be relatively efficient since the target base is fully accessible to solvent molecules in the absence of bound cofactor (Figure 11 and ref 42). Thus, it appears unlikely that intermediates **1** and **2** are in rapid equilibrium in the absence of cofactor and that proton transfer at cytosine C⁵ is rate limiting. Further support for these conclusions is presented below in the exchange reaction with poly(dI-dC), in our studies with the Gln²³⁷Trp mutant and in the analysis of various M.HhaI structures. The cofactor binding increases the enzyme's affinity for DNA by orders of magnitude (9). Cofactor binding is believed to induce active site loop movement (amino acids 80–99 (7)) and extensive conformational changes in protein structure (7).

Methylation and Exchange with Poly(dI-dC). Crystallographic studies with different DNA sequences (8), theoretical analysis (36), and various M.HhaI mutants (10, 19, 44) suggest how M.HhaI:DNA interactions can affect DNA binding, target sequence recognition, and the base flipping process. Investigation of various proposed mechanisms requires suitable assays, and we sought to apply our exchange assays to this end. Poly(dI-dC) has several unique features that provide an opportunity to probe the importance of the active site loop (residues 80–99, Figure 11, and ref 7), the base flipping mechanism, and the functional distinctions between M.HhaI and the more complex mammalian enzyme Dnmt1.² Poly(dI-dC) cannot form a hydrogen bond with Ile⁸⁶ within the active site loop. Closure of this loop appears to be crucial for the stabilization of the extrahelical base (Figure

11 and ref 7); however, its dynamics and precise function cannot be completely understood from the static crystal structures. Poly(dI-dC) is a unique probe for interactions between the active site loop and Ile⁸⁶ since the hydrogen bond is between the C² amino group on guanine and the protein backbone (Figure 11 and ref 7). We also used poly(dI-dC) as a probe of the interactions that may contribute to the base flipping process since, in contrast to the G·C pair, the I·C base pair has only two hydrogen bonds (Figure 3 and ref 45). Finally, the studies with poly(dI-dC) provide a basis for investigating the mammalian enzyme, Dnmt1, which has a strong preference for poly(dI-dC) (26).²

Poly(dG-dC) and poly(dI-dC) substrates show similar methylation and exchange rates (Table 1), and methylation rates with poly(dG-dC) and poly(dI-dC) are similar to the catalytic rates previously reported with different DNA substrates (9, 10, 17, 44). The similar catalytic rates (Table 1) indicate that any structural differences between poly(dG-dC) and poly(dI-dC), or other DNA substrates used in the past, have negligible impacts on the enzyme's ability to form intermediates **3A** and **3B** (Figure 2, **1** → **2** → **3A** or **1** → **2** → **3B**). This is consistent with the available structures of M.HhaI complexed to DNA, which show that the majority of the M.HhaI·DNA interactions involve the phosphate backbone (ref 7 and Figure 11) and numerous base contacts involve the major groove. Poly(dG-dC) and poly(dI-dC) have identical functional groups in the major groove (Figure 3), and the I·C and G·C base pairs share the same conformation (45).

The poly(dI-dC) substrate revealed insightful changes in the stability of intermediates **1** and **2** (Figures 4A and 6A), in the partitioning of intermediate **2** toward proton or methyl transfer (Figures 4A and 6A), and in catalytic processivity (Figure 8A,B). The main difference between poly(dG-dC) and poly(dI-dC) is in the potential hydrogen-bonding interactions involving Gln²³⁷ or Ile⁸⁶ (ref 7 and Figure 11). The hydrogen bonds involving Gln²³⁷ and Ile⁸⁶ are most likely important for different steps in the target base attack (refs 7 and 36 and Figure 11). Gln²³⁷ interacts with the orphan guanine and is thought to regulate the early steps in the base flipping process and the formation of intermediates **1** and **2** (7, 36). Thus, alterations in interactions involving Gln²³⁷ may affect steps leading to intermediates **3A** and **3B** (Figure 2). Our observation that the pre-steady-state methylation rates with poly(dI-dC) are 2-fold slower than with poly(dG-dC) may therefore result from this missing hydrogen bond between Gln²³⁷ and the orphan inosine. In contrast, the enzyme–DNA interactions at Ile⁸⁶ require that the active site loop is closed (ref 7 and Figure 11) with the cytosine positioned in the active site (i.e., intermediates **1** and **2** are formed (ref 7 and Figure 11)). Thus, a lack of interaction with Ile⁸⁶ should not affect the steps leading to intermediates **3A** and **3B** but rather the stability of this active site loop in the closed position. The release of the active site loop is part of the product release process and the accompanying proton elimination steps (Figure 2, **3A** → **4A** and **3B** → **4B**). Thus, loop opening before methyl transfer may lead to uncontrolled solvent access to intermediate **2** (Figure 11 and ref 42) and/or premature release of intermediates **1** and **2**. The excess tritium released during the methylation reaction with poly(dI-dC) (Figure 6A) is fully consistent with this scenario. The premature loop release prior to methyl transfer

can lead to uncontrolled protonation of intermediate **2**, and/or premature release of intermediates **1** and **2**, without the methyl transfer step. Similarly, loop release and uncontrolled solvent access to intermediate **2** are likely causes of the faster exchange rates with poly(dI-dC) in the presence of AdoHcy and *N*-methyl-AdoMet relative to poly(dG-dC) (Table 1). In summary, comparison of poly(dG-dC) and poly(dI-dC) substrates is consistent with the stabilization of the active site loop through a hydrogen bond between Ile⁸⁶ and guanine (ref 7 and Figure 11). Since intermediates **1** and **2** tend to accumulate prior to the slow methyl transfer step, the closure of the active site loop prevents premature release of the target base and uncontrolled solvent access at the reactive intermediate **2** (Figure 2). Blocking uncontrolled solvent access to intermediate **2** is important for minimizing both the exchange reaction and the mutagenic deamination (Figure 2, **1** → **2** → **3B** → **4B**).

The reactions with the poly(dI-dC) substrate also indicate that the loop closure can contribute to the slow steady-state step and to the early steps in target base recognition. The faster steady-state rates with no pre-steady-state burst in the reaction with poly(dI-dC) relative to poly(dG-dC) (Figure 4A vs Figure 6A and Figure 4B vs Figure 6B) are most likely caused by unstable active site loop, leading to faster product release (ref 7 and Figure 11). Moreover, the differences between poly(dG-dC) and poly(dI-dC) during processive catalysis (Figure 8A) suggest that the active site loop is partially closed with poly(dG-dC) after AdoHcy release, retaining the enzyme on the DNA. This is somewhat surprising since structural studies (ref 7 and Figure 11) suggest that the loop closure is primarily dependent on cofactor binding. In contrast, the relative instability of the loop and thus the M.HhaI-DNA complex with poly(dI-dC) results in the enzyme leaving prematurely and is thus less processive. Similarly, the large difference between poly(dG-dC) and poly(dI-dC) in the exchange rates in the absence of the cofactor is in a sharp contrast to the similar exchange rates in the presence of the cofactor (Table 1). We suggest that the low exchange rates with poly(dI-dC) in the absence of cofactor are due to the lack of both factors that control the closure of the active site loop: interaction at the Ile⁸⁶ site and the cofactor binding (ref 7 and Figure 11).

Finally, these studies with poly(dG-dC) and poly(dI-dC) substrates offer some insights into the enzyme's role in the base flipping process (8, 15, 34). A passive mechanism involves the protein simply stabilizing the extrahelical target base which spontaneously becomes unstacked from the duplex DNA, while an active mechanism invokes participation of the enzyme in the unstacking process itself. The loss of one of the three hydrogen bonds per base pair in poly(dI-dC) should result in faster formation of intermediate **1** and **2**, if these intermediates are formed largely by a passive mechanism. Our observation of similar rates with poly(dI-dC) and poly(dG-dC) argues against a passive mechanism. Interestingly, we find the reverse is true with the mammalian enzyme (Dnmt1), which shows at least 10-fold higher catalytic rates with poly(dI-dC) than poly(dG-dC).²

Methylation and Exchange with the Gln²³⁷Trp Mutant. Gln²³⁷ makes hydrogen bonds that are considered to be crucial for the base flipping process and stabilization of the extrahelical cytosine (Figure 11 and refs 7 and 36). Earlier analysis (19) of 19 different Gln²³⁷ mutants showed that the

methylation rates can be 2–33-fold slower than wild-type M.HhaI. The Gln²³⁷Trp mutant is one of the least active (19), and based on the crystal structures (Figure 11 and refs 7 and 36) these substitutions are thought to impact the enzyme's ability to form intermediate **1**. We were interested to see if the exchange reactions could be used to probe this prediction. We find that, similar to the exchange reaction in the absence of the cofactor (Figure 5B), the mutant clearly shows a pH-dependent change in SKIE. This is expected if the pH profiles and the measured pK_a are caused by the active site Cys⁸¹, and if the reactions are limited by the cysteine nucleophilic attack and the conversion between intermediates **1** and **2**. None of the reactions with the mutant show a pH/SKIE response expected for a reaction that is primarily limited by the cysteine nucleophilic attack with the measured pK_a (dashed line, upper panel, in Figures 5, 7, and 9B). This is understandable since the conversion between intermediates **1** and **2** depends on a specific set of hydrogen bonds (Figure 2 and refs 7 and 18) which may contribute to the SKIE (46). In summary, our results with the Gln²³⁷ mutant support our proposal that the pH/SKIE studies can be used to study the relationship between base flipping and catalysis. For a comparison, crystallographic (34) and fluorescence studies (14) reveal the extent of DNA deformation but do not monitor catalysis by Cys⁸¹. ¹⁹F NMR studies (15) do provide insights into intermediates **1** and **2** (Figure 2); however, the methyl transfer step at 5-fluorocytosine is exceptionally slow, which obscures the actual rates of conversion between intermediates. The pH/SKIE studies can be measured with any DNA substrate using routine methyltransferase assays.

In contrast to the wild-type enzyme, the exchange reaction with the mutant shows a notably decreased dependence on the cofactor analogues (Table 1). Thus, the mutation affects not only interactions with the orphan guanine but also interactions between intermediate **2** and the cofactor that take place in the active site. Since the enzyme's active site is 15 Å away from Gln²³⁷ (Figure 11), substitutions of Gln²³⁷ indirectly alter the network of hydrogen bonds (36) that position intermediates **1** and **2** in the active site. The results with the mutant also support our conclusions from poly(dI-dC) studies using the wild-type enzyme. The mutant shows no difference between the poly(dI-dC) and poly(dG-dC) substrates (Table 1 and Figure 9A), and both substrates show identical methylation and accompanying tritium release rates. As suggested above, the excess tritium release which occurs with the wild-type enzyme (Figure 6A) results from the destabilization of the active site loop and increased solvent access to reactive intermediate **2** (Figure 2) that accumulates prior to the slow methyl transfer step. Accumulation of intermediates **1** and **2** does not occur with the mutant since formation of intermediates **1** and **2** is the slow step (Figure 1).

Proton Inventory Studies. We used proton inventory analysis (Figure 10) in an attempt to further determine if different reactions share similar rate-limiting steps and catalytic intermediates. Proton inventory profiles are usually described according to their shape and calculated fractionation factors (eq 4 and ref 29). The overall shape can indicate the number of steps controlling the rate-limiting step and SKIE and whether the SKIE is caused in the ground state, transition state, or both. The fractionation factors provide insights into functionalities causing the SKIE and can support

a comparison of different proton inventory profiles with numerical precision. While proton inventory results can be difficult to interpret precisely, we are primarily interested in their application to determine if the exchange reaction under different conditions follows similar mechanisms.

The proton inventory results support our earlier proposal that the methylation reactions with poly(dG-dC), poly(dI-dC), and Gln²³⁷Trp depend on different rate-limiting steps. The pre-steady-state methylation rates with poly(dG-dC) depend on the methyl transfer step (Figure 2, **2** → **3A**), and no SKIE is observed (Figure 10A). The proton inventory for the methylation reaction with poly(dI-dC) (Figures 10B and 6A) results from the combined steps of methyl and proton transfer (Figure 2, **2** → **3A** and **2** → **3B**). The methylation reactions with the Gln²³⁷Trp mutant and the wild-type enzyme without cofactor show similar proton inventory profiles, consistent with our earlier proposal that in both reactions the rate-limiting step is the nucleophilic attack by Cys⁸¹ (Figure 2, **1** → **2**).

The proton inventory profiles for the exchange reaction with sinefungin and poly(dI-dC) and poly(dG-dC) appear to be identical (Figure 10A,B and Table 2), indicating that the rate-limiting steps and catalytic mechanism are similar for these two reactions. The ϕ_T measured with sinefungin (Table 2) can be found in reactions where the rate-limiting step involves a proton bridge (N-H-C) in the transition state (ref 29, pp 85 and 86). This is consistent with our proposal that the exchange reaction with sinefungin and both DNA substrates involves a direct interaction between the amino group on the cofactor and the C⁵ on the target base. Moreover, similar proton inventory profiles are observed in the same reaction with Dnmt1,² indicating that M.HhaI and Dnmt1 follow very similar mechanisms with sinefungin.

The ϕ_T is similar in magnitude for the exchange reaction with *N*-methyl-AdoMet and sinefungin with poly(dG-dC) but not with poly(dI-dC) (Table 2). This is consistent with our proposal that the slow exchange reaction with *N*-methyl-AdoMet and poly(dG-dC) depends on the cofactor amino moiety, while the high exchange rates in the reaction with poly(dI-dC) and *N*-methyl-AdoMet (Table 1) result in part from the premature release of the active site loop, exposing intermediate **2** (Figure 2) to solvent molecules. The similar proton inventory profiles for the exchange reactions with AdoMet and *N*-methyl-AdoMet with poly(dI-dC) (Table 2) suggest that both reactions result from uncontrolled solvent access to intermediate **2**, caused by premature active site loop release. In summary, the proton inventory results support the proposed mechanism that tritium release by sinefungin and *N*-methyl-AdoMet is controlled by the cofactor and the active site loop.

The proton inventory profiles in the exchange reaction without cofactor and poly(dG-dC) and the exchange reactions with the Gln²³⁷Trp mutant are dome shaped at pH 6.5 (data not shown) and partially curved (Figure 10C) at pH 8.0. Dome-shaped proton inventories which change with pH (Figures 5B and 9B) suggest that more than one step determines the rate-limiting step in those reactions (29), and that at least one is pH sensitive. This is consistent with our suggestion that nucleophilic attack by Cys⁸¹ is partially rate limiting in these reactions. If the pH-sensitive component of the SKIE is cysteine nucleophilic attack, the increase in SKIE caused by the increase in pH suggests that the

nucleophilic cysteine is deprotonated in the transition state during the conversion between intermediates **1** → **2** (eq 4, ϕ_T , $n = 1$, $m = 0$). Thus, deprotonation of Cys⁸¹ occurs during the attack step, not prior. The pH-independent component of the SKIE shows an inverse SKIE which may involve one or more of the hydrogen bonds which activate intermediate **1** (46), since none of the functionalities on intermediates **1** and **2** are likely to cause such a fractionation factor when present alone (29). Finally, the reactions proposed to be limited by the **1** → **2** transition (Figure 10C), and reaction without cofactor and with poly(dG-dC), show an inverse SKIE and an apparent transition state fractionation factor (ϕ_T) of about 2 (Table 2). The reactions that are limited by proton transfer at intermediate **2** (**2** → **3B**) show a ground state fractionation factor ϕ_G around 2 (Figure 10A,B).

ACKNOWLEDGMENT

We gratefully acknowledge Ben Hopkins and Stephen Fiacco for their excellent help in these experiments and Drs. R. J. Roberts and S. Kumar from New England Biolabs for their generous gift of mutant M.HhaI plasmids.

REFERENCES

- Jones, P. A., and Laird, P. W. (1999) Cancer epigenetics comes of age, *Nat. Genet.* **21**, 163–167.
- Jones, P. A., and Takai, D. (2001) The role of dna methylation in mammalian epigenetics, *Science* **293**, 1068–1070.
- Robertson, K. D., and Jones, P. A. (2000) DNA methylation: past, present and future directions, *Carcinogenesis* **21**, 461–467.
- Cheng, X., and Blumhethal, R. M. (1999) *S-Adenosylmethionine-Dependent Methyltransferases: Structures and Functions*, pp 1–400, World Scientific, Singapore, New Jersey, London, and Hong Kong.
- Douglas, K. T. (1987) The thymidylate synthesis cycle and anticancer drugs, *Med. Res. Rev.* **7**, 441–475.
- Cheng, X., Kumar, S., Posfai, J., Pflugrath, J. W., and Roberts, R. J. (1993) Crystal structure of the HhaI DNA methyltransferase complexed with S-adenosyl-L-methionine, *Cell* **74**, 299–307.
- Klimasauskas, S., Kumar, S., Roberts, R. J., and Cheng, X. (1994) HhaI methyltransferase flips its target base out of the DNA helix, *Cell* **76**, 357–369.
- Cheng, X., and Roberts, R. J. (2001) AdoMet-dependent methylation, DNA methyltransferases and base flipping, *Nucleic Acids Res.* **29**, 3784–3795.
- Lindstrom, W. M., Jr., Flynn, J., and Reich, N. O. (2000) Reconciling structure and function in HhaI DNA cytosine-C-5 methyltransferase, *J. Biol. Chem.* **275**, 4912–4919.
- Vilkaitis, G., Merkiene, E., Serva, S., Weinhold, E., and Klimasauskas, S. (2001) The mechanism of DNA cytosine-5 methylation. kinetic and mutational dissection of HhaI methyltransferase, *J. Biol. Chem.* **276**, 20924–20934.
- Allan, B. W., Beechem, J. M., Lindstrom, W. M., and Reich, N. O. (1998) Direct real time observation of base flipping by the EcoRI DNA methyltransferase, *J. Biol. Chem.* **273**, 2368–2373.
- Allan, B. W., and Reich, N. O. (1996) Targeted base stacking disruption by the EcoRI DNA methyltransferase, *Biochemistry* **35**, 14757–14762.
- Allan, B. W., Garcia, R., Maegley, K., Mort, J., Wong, D., Lindstrom, W., Beechem, J. M., and Reich, N. O. (1999) DNA bending by EcoRI DNA methyltransferase accelerates base flipping but compromises specificity, *J. Biol. Chem.* **274**, 19269–19275.
- Holz, B., Klimasauskas, S., Serva, S., and Weinhold, E. (1998) 2-Aminopurine as a fluorescent probe for DNA base flipping by methyltransferases, *Nucleic Acids Res.* **26**, 1076–1083.
- Klimasauskas, S., Szyperski, T., Serva, S., and Wuthrich, K. (1998) Dynamic modes of the flipped-out cytosine during HhaI methyltransferase-DNA interactions in solution, *EMBO J.* **17**, 317–324.
- Finer-Moore, J. S., Santi, D. V., and Stroud, R. M. (2003) Lessons and conclusions from dissecting the mechanism of a bisubstrate

- enzyme: thymidylate synthase mutagenesis, function, and structure, *Biochemistry* 42, 248–256.
17. Wu, J. C., and Santi, D. V. (1987) Kinetic and catalytic mechanism of HhaI methyltransferase, *J. Biol. Chem.* 262, 4778–4786.
 18. Perakyla, M. (1998) A model study of the enzyme-catalyzed cytosine methylation using ab initio quantum mechanical and density functional theory calculations: pK_a of the cytosine N3 in the intermediates and transition states of the reaction, *J. Am. Chem. Soc.* 120, 12895–12902.
 19. Mi, S., Alonso, D., and Roberts, R. J. (1995) Functional analysis of Gln-237 mutants of HhaI methyltransferase, *Nucleic Acids Res.* 23, 620–627.
 20. Gabbara, S., Sheluho, D., and Bhagwat, A. S. (1995) Cytosine methyltransferase from *Escherichia coli* in which active site cysteine is replaced with serine is partially active, *Biochemistry* 34, 8914–8923.
 21. Shen, J. C., Rideout, W. M. d., and Jones, P. A. (1992) High-frequency mutagenesis by a DNA methyltransferase, *Cell* 71, 1073–1080.
 22. Zingg, J. M., Shen, J. C., and Jones, P. A. (1998) Enzyme-mediated cytosine deamination by the bacterial methyltransferase M.MspI, *Biochem. J.* 332, 223–230.
 23. Zingg, J. M., Shen, J. C., Yang, A. S., Rapoport, H., and Jones, P. A. (1996) Methylation inhibitors can increase the rate of cytosine deamination by (cytosine-5)-DNA methyltransferase, *Nucleic Acids Res.* 24, 3267–3275.
 24. Pfeifer, G. P., Tang, M., and Denisenko, M. F. (2000) in *DNA Methylation and Cancer* (Johns, P. A., and Vogt, P. K., Eds.) pp 1–19, Springer-Verlag, Berlin.
 25. Reich, N. O., and Mashhoon, N. (1991) Kinetic mechanism of the EcoRI DNA methyltransferase, *Biochemistry* 30, 2933–2939.
 26. Flynn, J., Glickman, J. F., and Reich, N. O. (1996) Murine DNA cytosine-C5 methyltransferase: pre-steady- and steady-state kinetic analysis with regulatory DNA sequences, *Biochemistry* 35, 7308–7315.
 27. Johnson, K. A. (1992) in *The Enzymes* (Boyer, P. A., Ed.) Academic Press, New York.
 28. Cornish-Bowden, A. (1999) *Fundamentals of Enzyme Kinetics*, Portland Press, Colchester, U.K.
 29. Quinn, D. M., and Sutton, L. D. (1991) in *Enzyme Mechanism from Isotope Effects* (Cook, P. F., Ed.) pp 73–126, CRC Press, Boca Raton, FL.
 30. Born, T. L., and Blanchard, J. S. (1999) Enzyme-catalyzed acylation of homoserine: mechanistic characterization of the *Escherichia coli* metA-encoded homoserine transsuccinylase, *Biochemistry* 38, 14416–14423.
 31. Brocklehurst, K., Kowlessur, D., Patel, G., Templeton, W., Quigley, K., Thomas, E. W., Wharton, C. W., Willenbrock, F., and Szawelski, R. J. (1988) Consequences of molecular recognition in the S1-S2 intersubsite region of papain for catalytic-site chemistry. Change in pH-dependence characteristics and generation of an inverse solvent kinetic isotope effect by introduction of a P1–P2 amide bond into a two-protonic-state reactivity probe, *Biochem. J.* 250, 761–772.
 32. Kinch, L. N., and Phillips, M. A. (2000) Single-turnover kinetic analysis of *Trypanosoma cruzi* S-adenosylmethionine decarboxylase, *Biochemistry* 39, 3336–3343.
 33. Scheuring, J., and Schramm, V. L. (1997) Pertussis toxin: transition state analysis for ADP-ribosylation of G-protein peptide alpha13C20, *Biochemistry* 36, 8215–8223.
 34. O’Gara, M., Horton, J. R., Roberts, R. J., and Cheng, X. (1998) Structures of HhaI methyltransferase complexed with substrates containing mismatches at the target base, *Nat. Struct. Biol.* 5, 872–877.
 35. Renbaum, P., and Razin, A. (1992) Mode of action of the *Spiroplasma* CpG methylase M.SssI, *FEBS Lett.* 313, 243–247.
 36. Huang, N., Banavali, N. K., and MacKerell, A. D., Jr. (2003) Protein-facilitated base flipping in DNA by cytosine-5-methyltransferase, *Proc. Natl. Acad. Sci. U.S.A.* 100, 68–73.
 37. Ivanetich, K. M., and Santi, D. V. (1992) 5,6-dihydropyrimidine adducts in the reactions and interactions of pyrimidines with proteins, *Prog. Nucleic Acid Res. Mol. Biol.* 42, 127–156.
 38. Yoder, J. A., Soman, N. S., Verdine, G. L., and Bestor, T. H. (1997) DNA (cytosine-5)-methyltransferases in mouse cells and tissues. Studies with a mechanism-based probe, *J. Mol. Biol.* 270, 385–395.
 39. Szyf, M. (1996) The DNA methylation machinery as a target for anticancer therapy, *Pharmacol. Ther.* 70, 1–37.
 40. O’Gara, M., Klimasauskas, S., Roberts, R. J., and Cheng, X. (1996) Enzymatic C5-cytosine methylation of DNA: mechanistic implications of new crystal structures for HhaI methyltransferase-DNA-AdoHcy complexes, *J. Mol. Biol.* 261, 634–645.
 41. O’Gara, M., Zhang, X., Roberts, R. J., and Cheng, X. (1999) Structure of a binary complex of HhaI methyltransferase with S-adenosyl-L-methionine formed in the presence of a short nonspecific DNA oligonucleotide, *J. Mol. Biol.* 287, 201–209.
 42. Lau, E. Y., and Bruce, T. C. (1999) Active site dynamics of the HhaI methyltransferase: insights from computer simulation, *J. Mol. Biol.* 293, 9–18.
 43. Schowen, R. L. (1977) Isotope effects on enzyme-catalyzed reactions, in *Proceedings of the Sixth Annual Harry Steenbock Symposium* (Cleland, W. W., Northrop, D. B., and O’Leary, M. H., Eds.) Madison, WI, June 4 and 5, 1976, pp 64–99, University Park Press, Baltimore, MD.
 44. Vilkaitis, G., Dong, A., Weinhold, E., Cheng, X., and Klimasauskas, S. (2000) Functional roles of the conserved threonine 250 in the target recognition domain of HhaI DNA methyltransferase, *J. Biol. Chem.* 275, 38722–38730.
 45. Kumar, V. D., Harrison, R. W., Andrews, L. C., and Weber, I. T. (1992) Crystal structure at 1.5-Å resolution of d(CGICICG), an octanucleotide containing inosine, and its comparison with d(CGCG) and d(CGCGCG) structures, *Biochemistry* 31, 1541–1550.
 46. Cleland, W. W. (1992) Low-barrier hydrogen bonds and low fractionation factor bases in enzymatic reactions, *Biochemistry* 31, 317–319.

BI0496743